Numerical Analysis of Frictional Wear Contact Problems Computational Model and Applications

C. Agelet de Saracibar
M. Chiumenti

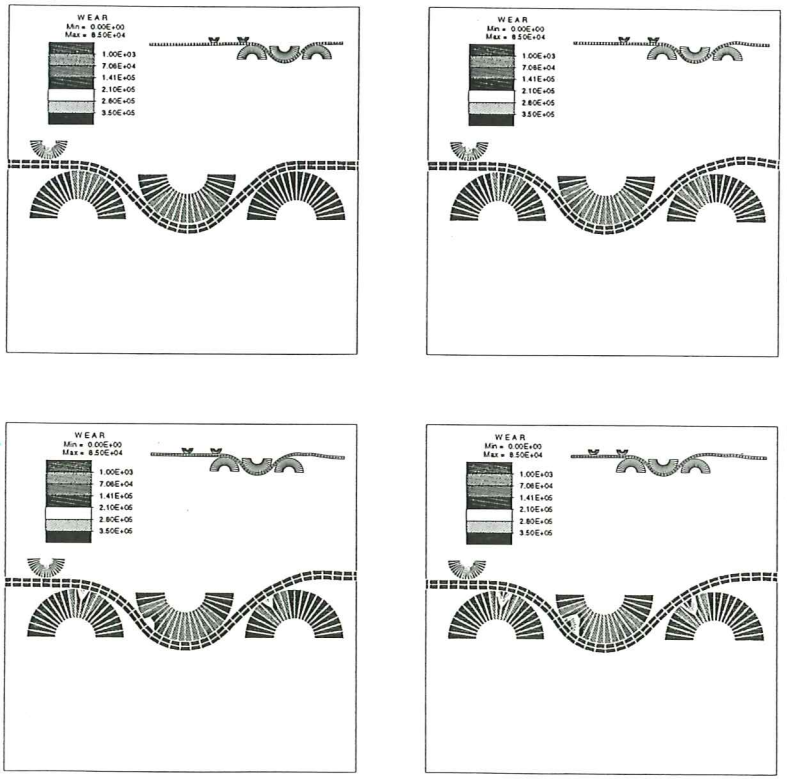

Publication CIMNE Nº 70, Septiembre 1995

Numerical Analysis of Frictional Wear Contact Problems Computational Model and Applications

C. Agelet de Saracibar
M. Chiumenti

Publication CIMNE Nº 70, Septiembre 1995

Submitted to:
International Journal for Numerical Methods in Engineering

International Center for Numerical Methods in Engineering
Gran Capitán s/n, 08034 Barcelona, Spain

Numerical Analysis of Frictional Wear Contact Problems Computational Model and Applications

C. AGELET DE SARACIBAR & M. CHIUMENTI

ETS Ingenieros de Caminos, Canales y Puertos
Universitat Politècnica de Catalunya
Barcelona, Spain

Submitted to
International Journal for Numerical Methods in Engineering

Revised, September 25, 1995

Table of Contents

Numerical Analysis of Frictional Wear Contact Problems Computational Model and Applications

C. AGELET DE SARACIBAR & M. CHIUMENTI

ETS Ingenieros de Caminos, Canales y Puertos
Universitat Politècnica de Catalunya
Barcelona, Spain

Abstract

In this paper a numerical model for the analysis of multi-body frictional wear contact problems at finite deformations is presented. Wear phenomena are analysed and the main wear mechanisms are identified. Archard's wear law provides an estimate of the amount of wear volume produced during forming operations. Wear phenomena are incorporated into the Coulomb frictional model by considering a friction coefficient as a function of an internal variable to be defined as the frictional dissipation or the slip amount.

Within the context of a displacement-driven formulation of frictional contact problems, i.e. penalty or augmented Lagrangian methods, and exploiting the computational framework developed for plasticity, two methods are considered for the time integration of the constrained frictional evolution problem: the lowest Backward Difference (BD) method, Backward Euler (BE) algorithm, and an Implicit Runge-Kutta (IRK) method, the generalized Projected Mid-Point (PMP) algorithm. The constrained frictional algebraic problem arising from the application of these time integration algorithms to the constrained frictional evolution problem, is amenable to exact linearization leading to an assymptotic quadratic rate of convergence when used within a Newton-Raphson solution scheme.

The numerical model has been implemented into an enhanced version of the computational finite element program FEAP. Numerical examples and simulation of industrial metal forming processes show the performance of the numerical model in the analysis of frictional wear contact problems.

1. Introduction. Motivation and Goals.

Numerical analysis of frictional contact problems has been one of the research topics of main interest over the last years. Frictional contact problems arises in many application fields such as metal forming processes, crashworthiness and projectile impact, among others. In spite of important progresses achieved in the computational mechanics, the large scale numerical simulation of these topics continuous to be nowadays a very complex task due mainly to the highly nonlinear nature of the problem, usually involving nonlinear kinematics, large deformations, large inelastic strains, nonlinear boundary conditions, frictional contact interaction, wear phenomena, large slips and in many cases coupled thermomechanical effects. During the last decade, a growing interest on these and related topics, has been shown by many industrial companies, such as automotive and aeronautical, motivated by the need to get high quality final products and to reduce manufacturing costs. The phenomena related to wear have an important impact on the economy of industrial metal forming processes. Statistical results show that wear is the dominating die failure mechanism for both bulk and sheet forming operations and has therefore an important influence on the production costs of formed products. Methodologies currently used

are based mainly on designers intuition and experience, which are not the most adequate when considering the complexity of the problem. Experts claim that a more quantitative approach to die design would improve service life considerably, leading to an important reduction of manufacturing costs for forging and stamping production. To enhance available decision support systems used in industrial design and optimization practice, taking into account complex phenomena such as wear effects, is one of the goals to be achieved in the up-coming years.

The phenomena of wear are extremely complex and an attempt to understand and quantify the mechanisms involved requires fundamental studies at the micromechanical level. The aim of these studies has been to develop appropriate micromechanical models to be able to estimate and to model wear effects in terms of slip amount, slip velocity, contact pressure, frictional dissipation and temperature for given tribological conditions such as surface hardness, surface roughness, lubricant film thickness, etc. The computer implementation of numerical models characterizing wear effects derived from micromechanical models and laboratory tests, is necessary to estimate and to model with enhanced accuracy, complex frictional contact phenomena arising in metal forming operations. An analysis of wear phenomena, as the dominant die failure mechanism in bulk and sheet forming operations, is presented in Section 2. Also, the main wear mechanisms for hot forging and sheet forming processes are identified and Archard's wear law is considered as an estimate of, both adhesive and abrasive, wear volume amount produced in the forming operations.

Mathematically, the numerical analysis of frictional contact problems amounts to finding the solution of an Initial Boundary Value Problem (IBVP) within a constrained solution space. Consideration of the weak form of momentum balance equations induces limitations on admissible variations in the tangent solution space, imposed by the physical constraints, leading to variational inequalities. See, for example, KIKUCHI & ODEN [1988] and DUVAUT & LIONS [1972]. A regularization of the frictional contact constraints, using for instance penalty or augmented Lagrangian methods, allows to bypass the need to find a solution within a constrained solution space and provides a very convenient displacement-driven frictional contact formulation. The penalty method has been used by ODEN & PIRES [1984], CHENG & KIKUCHI [1985], HALLQUIST, GOUDREAU & BENSON [1985], SIMO, WRIGGERS & TAYLOR [1985], CURNIER & ALART [1988], WRIGGERS, VU VAN & STEIN [1990], BELYTSCHKO & NEAL [1991], LAURSEN [1992] and LAURSEN & SIMO [1992,1993] among others. On the other hand, the augmented Lagrangian method has been used, for example, by LAURSEN [1992], SIMO & LAURSEN [1992], LAURSEN & SIMO [1992,1994] and LAURSEN & GOVINDJEE [1994]. Furthermore, the displacement-driven formulation of frictional contact problems, allows to widely exploit the framework developed for computational plasticity. See, for example, SIMO & HUGHES [1994] and SIMO [1994], for an excellent presentation of current topics and last developments in computational plasticity. In particular, return mapping algorithms developed for plasticity can be applied to integrate the frictional traction. Frictional return mapping algorithms have been used by GIANNAKOPOULOS [1989], WRIGGERS, VU VAN & STEIN [1990] and LAURSEN & SIMO [1993,1994], among others. Enhanced Coulomb frictional models, using a non-constant friction coefficient have been used, for example, by WRIGGERS [1987] and OWEN

et al. [1995]. Numerical models for coupled thermomechanical frictional contact problems have been used by WRIGGERS & MIEHE [1992], among others. A fully nonlinear kinematics formulation of frictionless contact problems, including the derivation of the algorithmic contact operators, was developed by WRIGGERS & SIMO [1985] for 2D linear surface elements and by PARISH [1989] for 3D linear surface elements. An extension to frictional contact problems for 2D linear surface elements was provided by WRIGGERS [1987]. A general fully nonlinear kinematics formulation of multi-body frictional contact problems at finite strain was first developed on a continuum setting for 3D and 2D contact surfaces, by LAURSEN & SIMO [1993]. A new frictional time integration algorithm for large slip multi-body frictional contact problems at finite deformations has been recently proposed by AGELET DE SARACIBAR [1995].

The remaining of the paper is as follows. Section 3, deals with the numerical analysis of frictional wear contact problems. The multi-body frictional contact formulation proposed by LAURSEN & SIMO [1993,1994], fully developed on a continuum setting, has been extended to accomodate wear phenomena, throughout the introduction of an internal variable, to be defined as the frictional dissipation or the slip amount. Then the Coulomb frictional model has been modified to incorporate a friction coefficient as a function of this internal variable.

In Section 4, the discretization of the initial boundary value problem including frictional wear contact constraints is presented. The focuss has been placed on the time integration of the constrained frictional evolution problem. Two time integration algorithms are presented. First, the lower Backward-Difference (BD) method, the Backward-Euler (BE) algorithm. Second, within the Implicit Runge-Kutta (IRK) methods, the generalized Projected Mid-Point (PMP) algorithm. This algorithm was first proposed, within a J2 plasticity context, by SIMO [1994]. See also AGELET DE SARACIBAR [1995]. Both algorithms are amenable to exact linearization and the algorithmic frictional wear contact tangent operators are derived.

The frictional wear contact model has been implemented into an enhanced version of the computational finite element program FEAP developed by R.L. Taylor and J.C. Simo and described in ZIENKIEWICZ & TAYLOR [1991]. Numerical examples and metal forming simulations are provided in Section 5. Finally some concluding remarks are included.

2. Wear Model.

Wear phenomena are the dominanting failure mechanism of dies in both sheet and bulk metal forming operations. When considering wear in forming process attention should be focussed on the following items: type of die failure, choice of die material, surface treatment and lubrication, process parameters such as temperature and forming speed and predominant wear mechanisms. The life-time of a die, is usually expressed by the number of parts that can be produced before the dimensions of the parts exceed the given tolerances or serious damage of the die occur. To be able to estimate, to predict and to incorporate into a numerical model the complex wear phenomena will improve considerably the life of dies in metal forming operations.

(A) *Wear mechanisms in hot forging processes.* Statistical results show that wear is up to a $60-70\%$, the dominating failure mechanism for hot forging dies, and has therefore an important influence on the production costs of forged products. Critical regions in a forging die are places exposed to a very high pressure, internal corners with a notch effect, areas that reach a very high temperature and finally regions with large slip amounts on the die. Statistical investigations of the type of die failure which have the greatest influence on the scrapping of forging dies, show that the primary reason for scrapping a die are wear phenomena at external corners or at roundings. In order to describe wear as the main reason for the scrapping of forging tools it is important to determine which are the main mechanisms that causes wear. It is generally agreed that the most important wear mechanism in hot forging is three body abrasive wear caused by hard scale particles embedded in the surface of the work piece. Experimental results show that the amount and type of scale, the adhesion of the scale to the surface of the work piece and the hardness (chemical structure) of the scale are the determining factors for tool wear. Wear is also found to be proportional to the hardness of the work piece material and inversely proportional to the hardness of the die material at the maximum temperature reached by the surface during the forging process.

(B) *Wear mechanisms in sheet metal forming processes.* In sheet metal forming processes, it has been found that 65% of tool failure is caused by adhesive and abrasive wear in the drawbead and die radius regions. Due to the surface roughness and asperities, when two surfaces are pressed together, the real contact area will be much smaller that the apparent one. The pressure on these asperities will be sufficiently high to cause plastic deformations on the asperities. Also the sliding of the sheet over the tool surface leads to heating due to frictional dissipation. The high surface pressure combined with the heat generation due to frictional dissipation leads to welding of the asperities of the tool and sheet surfaces. The break off of these welded asperities can scratch the tool surface.

(C) *Wear model.* The two most important mechanisms of wear in forming processes have been identified as adhesive and abrasive wear.

(C1) *Adhesive wear.* During relative sliding between two surfaces, the lubricant film may thin out and break down, allowing the two materials to cold weld at the asperities contact. Further relative sliding will break either in the cold welded contact or in one of the materials. This process does not produce any free wear particles but could possibly transfer a small amount of material from one surface to another. On the other hand, by continuous sliding a free wear particle can be formed by two mechanisms: (a) Adhesion of particles takes place under high pressure. Continuous sliding relieves the pressure in the contact and the particle may break off. (b) Due to chemical changes in the particle when is transferred from one surface to another, the particle may oxidize and thus adhere poorly to the new surface. The free wear particles and the accumulation of material formed by adhesive wear will often cause abrasive wear.

Assuming circular contacting asperities of the same size, ARCHARD [1953] proposed a model for adhesive wear with the following assumptions: it is proportional to the local sliding length and to the normal pressure, it is inversely proportional to the local hardness of the surface (the yield stress of a deformed asperity) and it is dependent of a wear

constant (to be determined experimentally and ranging from 0 to 1), which indicates the probability of the formation of a particle in an asperity contact. This constant will depend on the work piece and die material, the tendency to cold weld, and the interface conditions (surface films, lubricant film, temperature, etc.). Then Archard's law for adhesive wear can be written (in rate form) as

$$\dot{Z} = K_{adh} \, [q \, \dot{s}/H] \tag{2.1}$$

where Z is the (adhesive) wear volume per unit area, q is the local normal pressure, s is the local sliding length, H is the local hardness of the material, K_{adh} is the adhesive wear constant and the superposed dot means material time derivation.

(C2) *Abrasive wear.* The term abrasive covers the situations of two-body and three-body abrasive wear. In two-body abrasive wear an asperity from the harder material ploughs a furrow in the softer material during the relative sliding. In three-body abrasive wear the furrow is ploughed by a hard particle. In two-body abrasive wear, normally only the softer surface is subjected to wear and if the harder surface is sufficiently smooth, it is possible to eliminate the two-body abrasive wear totally. The three-body abrasive wear is much more difficult to eliminate as it is very difficult to avoid impurities, including hard particles, between the two surfaces in contact. Hard particles that can cause abrasion are for instance, dust, wear particles from adhesive wear that are very hard after severe plastic deformations, particles formed by corrosion of the surface (i.e. scale in hot forging), etc.

Assuming a number of isolated and uniform asperity contacts, it is possible to derive a simplified model for abrasive wear, similar to the Archard's model for adhesive wear. Here the law for abrasive wear can be written (in rate form) as

$$\dot{Z} = K_{abr} \, [q \, \dot{s}/H] \tag{2.2}$$

where Z is the (abrasive) wear volume per unit area and K_{abr} is the abrasive wear constant. The abrasive wear law states that (instantaneuous) abrasive wear is proportional to the local sliding length and normal pressure, inversely proportional to the local hardness of the surface and depends of an abrasive wear constant (to be determined experimentally and ranging from 0 to 1), now dependent on the surface topography, the presence of hard abrasive particles, lubricant, etc.

From (2.1) and (2.2) a unified law for adhesive and abrasive wear can be written (in rate form) as

$$\boxed{\dot{Z} = K_{wear} \, [q \, \dot{s}/H]} \tag{2.3}$$

where Z is the (adhesive/abrasive) wear volume per unit area and K_{wear} is a wear constant to be determined experimentally (ranging from 0 to 1), which for adhesive wear mechanisms will depend mainly on the material combination, interface conditions, lubricant and temperature, and for abrasive wear mechanisms will depend mainly on surface topology, hard particles between surfaces and lubricant.

The local hardness of the die surface is a strong function of the local temperature of the die surface and a fully coupled thermomechanical model would be necessary. The

sliding length, which is the amount of material passing a specific point on the die surface, is considered to be the most important parameter in the wear estimation, due to its strong influence on the heat generation by frictional dissipation.

In the time discrete setting, within a typical time sub-interval $[t_n, t_{n+1}] \subset [0, T]$ of the time interval of interest and using for instance a BE algorithm, time integration of wear volume rate per unit area given by (2.3), leads to the discrete adhesive and abrasive wear algorithmic expression

$$\boxed{Z_{n+1} = Z_n + K_{wear}\,[q_{n+1}\,(s_{n+1} - s_n)/H_{n+1}]} \tag{2.4}$$

where $(\cdot)_n$ and $(\cdot)_{n+1}$ denote the algorithmic approximation to their exact values at times t_n and t_{n+1}, respectively.

REMARK 2.1. Under some simplified assumptions, i.e. constant surface material hardness, the wear evolution estimate can be integrated in closed-form leading to an explicit wear function of the (accumulated) frictional dissipation.

Lets consider, as a simple model problem, a Coulomb frictional model with a friction coefficient defined as a function of the frictional dissipation rate. Then, the frictional dissipation evolution equation takes the form:

$$\mathcal{D}_{fric} := \dot{\alpha} := \mu(\alpha)\; q\; \dot{s} \tag{2.5}$$

Using (2.3) and (2.5) the following expression can be derived

$$\dot{Z} = \frac{K_{wear}}{H}\;\frac{\dot{\alpha}}{\mu(\alpha)} \tag{2.6}$$

Lets consider now two simple cases: friction coefficient as a linear function of frictional dissipation and constant friction coefficient.

i. *Linear friction coefficient.* Assume a friction coefficient described by a linear function of the frictional dissipation

$$\mu(\alpha) := \mu_0 + \mu_1\;\alpha \tag{2.7}$$

Substituting (2.7) into (2.6) and integrating leads to the following logarithmic closed-form expression for the wear estimate

$$\boxed{Z = \frac{K_{wear}}{\mu_1\;H}\;\log\,[\frac{\mu(\alpha)}{\mu_0}]} \tag{2.8}$$

ii. *Constant friction coefficient.* Assume a constant friction coefficient

$$\mu(\alpha) := \mu_0 \tag{2.9}$$

Substituting (2.9) into (2.6) and integrating leads to the following linear closed-form expression for the wear estimate

$$\boxed{Z = \frac{K_{wear}}{\mu_0 \, H} \, \alpha} \tag{2.10}$$

3. Formulation of the Multi-Body Frictional Wear Contact Problem.

In this section we present the *continuum* formulation of the multi-body frictional wear contact problem.

3.1. Notation.

Let $2 \leq n_{dim} \leq 3$ be the space dimension and $I := [0,T] \subset \mathbb{R}_+$ the time interval of interest. Let the open sets $\Omega^{(1)} \subset \mathbb{R}^{n_{dim}}$ and $\Omega^{(2)} \subset \mathbb{R}^{n_{dim}}$ with smooth boundaries $\partial\Omega^{(1)}$ and $\partial\Omega^{(2)}$ and closures $\bar{\Omega}^{(1)} := \Omega^{(1)} \cup \partial\Omega^{(1)}$ and $\bar{\Omega}^{(2)} := \Omega^{(2)} \cup \partial\Omega^{(2)}$, be the reference placement of two continuum bodies $\mathcal{B}^{(1)}$ and $\mathcal{B}^{(2)}$, with material particles labeled $\boldsymbol{X} \in \bar{\Omega}^{(1)}$ and $\boldsymbol{Y} \in \bar{\Omega}^{(2)}$ respectively.

Denote by $\varphi^{(i)} : \bar{\Omega}^{(i)} \times I \to \mathbb{R}^{n_{dim}}$ the orientation preserving deformation map of the body $\mathcal{B}^{(i)}$, with material velocities $\boldsymbol{V}^{(i)} := \partial_t \varphi^{(i)}$ and deformation gradients $\boldsymbol{F}^{(i)} := D\varphi^{(i)}$. For each time $t \in I$, the mapping $t \in I \mapsto \varphi_t^{(i)} := \varphi^{(i)}(\cdot, t)$ represents a one-parameter family of configurations indexed by time t, which maps the reference placement of body $\mathcal{B}^{(i)}$ onto its current placement $\mathcal{S}_t^{(i)} : \varphi_t^{(i)}(\mathcal{B}^{(i)}) \subset \mathbb{R}^{n_{dim}}$.

We will assume that no contact forces are present between the two bodies at the reference configuration. Subsequent configurations cause the two bodies to physically contact and produce interactive forces during some portion of $I = [0,T]$.

We will denote as the *contact surface* $\Gamma^{(i)} \subset \partial\Omega^{(i)}$ the part of the boundary of the body $\mathcal{B}^{(i)}$ such that all material points where contact will occur at any time $t \in I$ are included. The current placement of the contact surface $\Gamma^{(i)}$ is given by $\gamma^{(i)} := \varphi_t^{(i)}(\Gamma^{(i)})$.

Attention will be focussed to material points on these surfaces denoted as $\boldsymbol{X} \in \Gamma^{(1)}$ and $\boldsymbol{Y} \in \Gamma^{(2)}$. Current placement of these particles is given by $\boldsymbol{x} = \varphi_t^{(1)}(\boldsymbol{X}) \in \gamma^{(1)}$ and $\boldsymbol{y} = \varphi_t^{(2)}(\boldsymbol{Y}) \in \gamma^{(2)}$. See FIGURE 3.1 for an illustration of the notation to be used.

(A) *Parametrization of the contact surfaces.* Let $\mathcal{A}^{(i)} \subset \mathbb{R}^{n_{dim}-1}$ be a parent domain for the contact surface of body $\mathcal{B}^{(i)}$. A parametrization of the contact surface for each body $\mathcal{B}^{(i)}$ is introduced by a family of (orientation preserving) one-parameter mappings indexed by time, $\psi_t^{(i)} : \mathcal{A}^{(i)} \subset \mathbb{R}^{n_{dim}-1} \to \mathbb{R}^{n_{dim}}$ such that $\Gamma^{(i)} := \psi_0^{(i)}(\mathcal{A}^{(i)})$ and $\gamma^{(i)} := \psi_t^{(i)}(\mathcal{A}^{(i)})$. Using the mapping composition rule, it also follows that $\psi_t^{(i)} = \varphi_t^{(i)} \circ \psi_0^{(i)}$.

In particular, for any material point $\boldsymbol{Y} \in \Gamma^{(2)}$ with current placement $\boldsymbol{y} \in \gamma^{(2)}$, there exist some point $\boldsymbol{\xi} \in \mathcal{A}^{(2)}$ such that $\boldsymbol{Y} := \psi_0^{(2)}(\boldsymbol{\xi})$ and $\boldsymbol{y} := \psi_t^{(2)}(\boldsymbol{\xi})$. It will be assumed in what follows that these parametrizations have the required smoothness conditions. FIGURE 3.2 shows the parametrization map of reference and current placement of a contact surface.

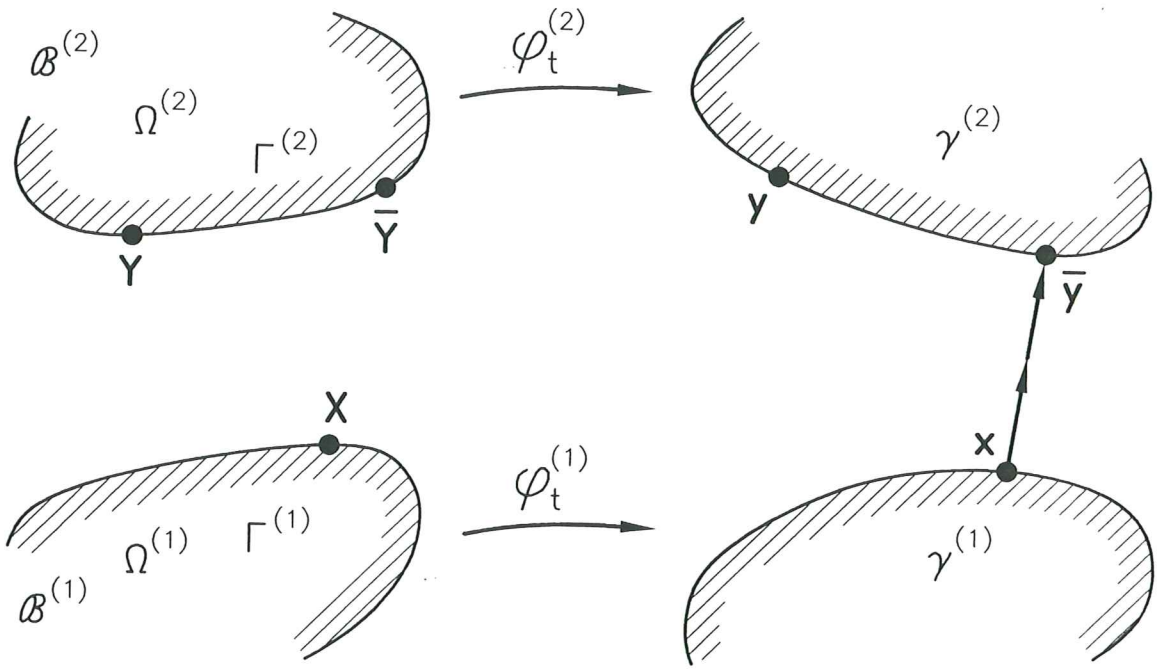

FIGURE 3.1. Schematic description of two interacting bodies at reference and current placements. Reference and current placement of contact surfaces.

3.2. Frictional contact constraints

Using a standard notation in contact mechanics we will assign to each pair of contact surfaces involved in the problem, the roles of *slave* and *master* surface. In particular, let $\Gamma^{(1)}$ be the *slave surface* and $\Gamma^{(2)}$ be the *master surface.* Additionally, we will denote *slave particles* and *master particles* to the material points of the slave and master surfaces, respectively. With this notation in hand, we will require that any slave particle may not penetrate the master surface, at any time $t \in I$.

Although in the continuum setting the slave-master notation plays no role, in the discrete setting this choice becomes important.

(A) *Closest-point projection of a slave particle onto a master surface.* Attention is focussed to any slave particle $\boldsymbol{X} \in \Gamma^{(1)}$ with current placement $\boldsymbol{x} := \varphi_t^{(1)}(\boldsymbol{X}) \in \gamma^{(1)}$ and to the master surface $\Gamma^{(2)}$, with particles $\boldsymbol{Y} \in \Gamma^{(2)}$ and current placement $\boldsymbol{y} := \varphi_t^{(2)}(\boldsymbol{Y}) \in \gamma^{(2)}$.

Let $\bar{\boldsymbol{y}}(\boldsymbol{X},t) \in \gamma^{(2)}$ be the closest-point projection of the current position of the slave particle $\boldsymbol{X}$ onto the current placement of the master surface $\Gamma^{(2)}$, defined as

$$\bar{\boldsymbol{Y}}(\boldsymbol{X},t) := \arg \min_{\boldsymbol{Y} \in \Gamma^{(2)}} \{\|\varphi_t^{(1)}(\boldsymbol{X}) - \varphi_t^{(2)}(\boldsymbol{Y})\|\} \tag{3.1}$$

$$\bar{\boldsymbol{y}}(\boldsymbol{X},t) := \varphi_t^{(2)}(\bar{\boldsymbol{Y}}) \tag{3.2}$$

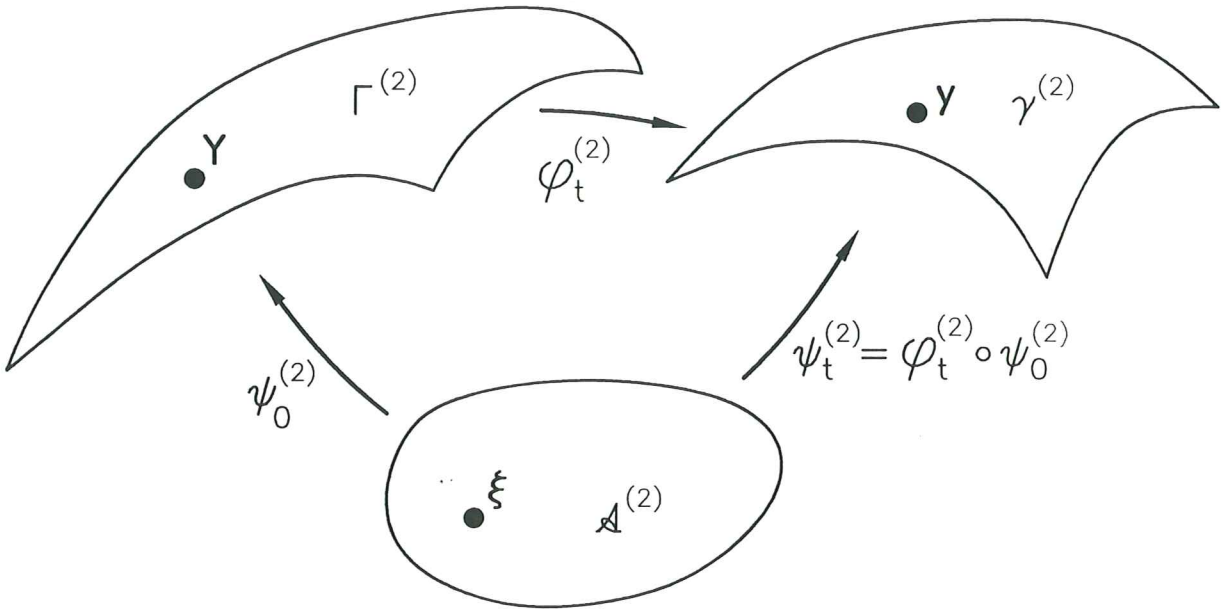

FIGURE 3.2. Contact surfaces parametrization. Parametrization map of reference and current placement of a contact surface.

The definition of the closest-point projection allows us to define the distance between any slave particle and the master surface at any time $t \in I$.

Let $g_N(\boldsymbol{X},t)$ be the gap function defined for any slave particle $\boldsymbol{X} \in \Gamma^{(1)}$ and for any time $t \in I$ as (minus) the distance of the current placement of this particle to the current placement of the master surface $\gamma^{(2)} := \varphi_t^{(2)}(\Gamma^{(2)})$. Using the definition of the closest-point projection stated above, the gap function $g_N(\boldsymbol{X},t)$ may be defined as

$$\boxed{g_N(\boldsymbol{X},t) := -[\varphi_t^{(1)}(\boldsymbol{X}) - \varphi_t^{(2)}(\bar{\boldsymbol{Y}}(\boldsymbol{X},t))] \cdot \boldsymbol{\nu}} \tag{3.3}$$

where $\boldsymbol{\nu} : \gamma^{(2)} \to S^2$ is the unit outward normal field to the current placement of the master surface particularized at the closest-point projection $\bar{\boldsymbol{y}}(\boldsymbol{X},t) \in \gamma^{(2)}$. Here S^2 denotes the unit sphere defined as

$$S^2 := \{\boldsymbol{\nu} \in \mathbb{R}^{n_{dim}} \ : \ \|\boldsymbol{\nu}\| = 1\} \tag{3.4}$$

(B) *Contact pressure.* Let $\boldsymbol{P}^{(1)}(\boldsymbol{X},t)$ be the first Piola-Kirchhoff stress tensor and $\boldsymbol{N}^{(1)}(\boldsymbol{X})$ the unit outward normal to the slave surface $\Gamma^{(1)}$ in the reference configuration. The nominal (Piola) frictional contact traction at $\boldsymbol{X} \in \Gamma^{(1)}$ is given as

$$\boldsymbol{t}^{(1)}(\boldsymbol{X},t) = \boldsymbol{P}^{(1)}(\boldsymbol{X},t) \cdot \boldsymbol{N}^{(1)}(\boldsymbol{X}) \tag{3.5}$$

Additionally one defines the contact pressure $t_N(\boldsymbol{X},t)$ as minus the projection of the nominal frictional contact traction $\boldsymbol{t}^{(1)}$ onto the unit outward normal to the current placement of the slave surface $\boldsymbol{n}^{(1)}(\boldsymbol{X},t)$. Then we can split the nominal frictional contact as

$$\boldsymbol{t}^{(1)}(\boldsymbol{X},t) = -t_N(\boldsymbol{X},t)\ \boldsymbol{n}^{(1)}(\boldsymbol{X},t) + \mathbb{P}_{n^{(1)}}\boldsymbol{t}^{(1)}(\boldsymbol{X},t) \tag{3.6}$$

where $\mathbb{P}_{n^{(1)}}\boldsymbol{t}^{(1)}$ is the projection of $\boldsymbol{t}^{(1)}$ onto the associated tangent plane.

With the required surface smoothness conditions, when the slave particle $\boldsymbol{X}$ comes into contact with the master surface, the following relation holds

$$\boldsymbol{\nu} = \boldsymbol{n}^{(2)}(\bar{\boldsymbol{Y}}(\boldsymbol{X},t),t) = -\boldsymbol{n}^{(1)}(\boldsymbol{X},t) \tag{3.7}$$

Here $\boldsymbol{n}^{(1)}$ is the unit outward normal to the slave surface at the point $\boldsymbol{x} = \boldsymbol{\varphi}_t^{(1)}(\boldsymbol{X})$ and $\boldsymbol{\nu} := \boldsymbol{n}^{(2)}$ is the unit outward normal to the the master surface at the point $\bar{\boldsymbol{y}} = \boldsymbol{\varphi}_t^{(2)}(\bar{\boldsymbol{Y}})$.

Then an equivalent expression for the nominal frictional contact traction split is given as

$$\boxed{\boldsymbol{t}^{(1)}(\boldsymbol{X},t) = t_N(\boldsymbol{X},t)\ \boldsymbol{\nu}(\bar{\boldsymbol{Y}}(\boldsymbol{X},t),t) + \mathbb{P}_{\nu}\boldsymbol{t}^{(1)}(\boldsymbol{X},t)} \tag{3.8}$$

(C) *Contact normal constraints.* With the preceding definitions for the gap function $g_N(\boldsymbol{X},t)$ and the contact pressure $t_N(\boldsymbol{X},t)$ we can introduce the normal constraints induced by the frictionless contact problem.

i. *Impenetrability kinematic constraint.* The kinematic constraint induced by the impenetrability requirement can be expressed in terms of the gap function $g_N(\boldsymbol{X},t)$ as

$$g_N(\boldsymbol{X},t) \leq 0 \tag{3.9}$$

ii. *Non-adhesion constraint.* The non-adhesion constraint implies that the contact pressure must be non-negative. Mathematically, this condition can be expressed as

$$\begin{aligned} t_N(\boldsymbol{X},t) &\geq 0 \quad \text{if} \quad g_N(\boldsymbol{X},t) = 0 \\ t_N(\boldsymbol{X},t) &= 0 \quad \text{if} \quad g_N(\boldsymbol{X},t) < 0 \end{aligned} \tag{3.10}$$

iii. *Contact persistency condition.* This condition implies the requirement that the rate of separation at the contact points must be zero for positive contact pressure. Mathematically, this persistency condition takes the form

$$t_N(\boldsymbol{X},t)\ \dot{g}_N(\boldsymbol{X},t) = 0 \tag{3.11}$$

The above constraints set of impenetrability, non-adherence and contact persistency, can be expressed as Kuhn-Tucker complementarity conditions as

$$\boxed{\begin{aligned} g_N(\boldsymbol{X},t) &\leq 0 \\ t_N(\boldsymbol{X},t) &\geq 0 \\ t_N(\boldsymbol{X},t)\ g_N(\boldsymbol{X},t) &= 0 \\ t_N(\boldsymbol{X},t)\ \dot{g}_N(\boldsymbol{X},t) &= 0 \end{aligned}} \tag{3.12}$$

(D) *Convected basis on the master surface.* Exploiting the geometric structure induced by the impenetrability constraint through the definition of the gap function $g_N(\boldsymbol{X},t)$, we introduce an associated convected basis, suitable for definition of the frictional constraints. The definitions of the convected frames emanate from the differentiation of the contact surfaces with respect to the convected coordinates. Along with the convected basis, dual or reciprocal convected basis are defined following a standard procedure. Attention in what follows will be restricted to $n_{dim} = 3$. Particularization for $n_{dim} = 2$ is trivial once the three-dimensional case has been considered.

Using the parametrization of the contact surfaces introduced above we consider a point $\boldsymbol{\xi} := (\xi^1, \xi^2) \in \mathcal{A}^{(2)}$ of the parent domain, such that

$$\boldsymbol{Y} := \boldsymbol{\psi}_0^{(2)}(\boldsymbol{\xi}) \ , \qquad \boldsymbol{y} := \boldsymbol{\psi}_t^{(2)}(\boldsymbol{\xi}) \tag{3.13}$$

Attached to each master particle $\boldsymbol{Y} \in \Gamma^{(2)}$ we introduce the convected surface basis $\boldsymbol{E}_\alpha(\boldsymbol{\xi})$ and $\boldsymbol{e}_\alpha(\boldsymbol{\xi})$, $\alpha = 1,2$ on the reference and current configurations, respectively, as

$$\boldsymbol{E}_\alpha(\boldsymbol{\xi}) := \boldsymbol{\psi}_{0,\alpha}^{(2)}(\boldsymbol{\xi}) \ , \qquad \boldsymbol{e}_\alpha(\boldsymbol{\xi}) := \boldsymbol{\psi}_{t,\alpha}^{(2)}(\boldsymbol{\xi}) \tag{3.14}$$

where $(\cdot)_{,\alpha}$ denotes partial derivative with respect to ξ^α. Using the composition map $\boldsymbol{\psi}_t^{(2)} = \boldsymbol{\varphi}_t^{(2)} \circ \boldsymbol{\psi}_0^{(2)}$ the following relation holds

$$\boldsymbol{e}_\alpha(\boldsymbol{\xi}) = \boldsymbol{F}_t^{(2)}(\boldsymbol{\psi}_0^{(2)}(\boldsymbol{\xi})) \cdot \boldsymbol{E}_\alpha(\boldsymbol{\xi}) \tag{3.15}$$

where $\boldsymbol{F}_t^{(2)} := D\boldsymbol{\varphi}_t^{(2)}$ is the deformation gradient.

Let consider now for any slave particle $\boldsymbol{X} \in \Gamma^{(1)}$ the master particle $\bar{\boldsymbol{Y}}(\boldsymbol{X},t) \in \Gamma^{(2)}$ such that satisfies the closest-point projection minimization condition given by (3.1). Then for some point $\bar{\boldsymbol{\xi}} := (\bar{\xi}^1, \bar{\xi}^2) \in \mathcal{A}^{(2)}$ of the parent domain we have

$$\bar{\boldsymbol{Y}}(\boldsymbol{X},t) := \boldsymbol{\psi}_0^{(2)}(\bar{\boldsymbol{\xi}}(\boldsymbol{X},t)) \ , \qquad \bar{\boldsymbol{y}}(\boldsymbol{X},t) := \boldsymbol{\psi}_t^{(2)}(\bar{\boldsymbol{\xi}}(\boldsymbol{X},t)) \tag{3.16}$$

Attached to the master particle $\bar{\boldsymbol{Y}}(\boldsymbol{X},t) \in \Gamma^{(2)}$ we define the convected surface basis on the reference and current configurations, respectively, as

$$\boxed{\boldsymbol{\tau}_\alpha^{ref}(\boldsymbol{X},t) := \boldsymbol{E}_\alpha(\bar{\boldsymbol{\xi}}(\boldsymbol{X},t)) \ , \qquad \boldsymbol{\tau}_\alpha(\boldsymbol{X},t) := \boldsymbol{e}_\alpha(\bar{\boldsymbol{\xi}}(\boldsymbol{X},t))} \tag{3.17}$$

Using the composition map $\boldsymbol{\psi}_t^{(2)} = \boldsymbol{\varphi}_t^{(2)} \circ \boldsymbol{\psi}_0^{(2)}$ the following relation holds

$$\boldsymbol{\tau}_\alpha = \boldsymbol{F}_t^{(2)}(\boldsymbol{\psi}_0^{(2)}(\bar{\boldsymbol{\xi}})) \cdot \boldsymbol{\tau}_\alpha^{ref} \tag{3.18}$$

showing that the surface basis vectors $\boldsymbol{\tau}_\alpha^{ref}$ and $\boldsymbol{\tau}_\alpha$ are convected through the deformation gradient map $\boldsymbol{F}_t^{(2)}$ at the master particle $\bar{\boldsymbol{Y}}(\boldsymbol{X},t)$.

Additionaly, the unit outward normals $\boldsymbol{\nu}^{ref} \in S^2$ and $\boldsymbol{\nu} \in S^2$ at the master particle $\bar{\boldsymbol{Y}}(\boldsymbol{X},t)$ on the reference and current configurations, respectively, can be defined as

$$\boldsymbol{\nu}^{ref} := \frac{\boldsymbol{\tau}_1^{ref} \times \boldsymbol{\tau}_2^{ref}}{\|\boldsymbol{\tau}_1^{ref} \times \boldsymbol{\tau}_2^{ref}\|} , \qquad \boldsymbol{\nu} := \frac{\boldsymbol{\tau}_1 \times \boldsymbol{\tau}_2}{\|\boldsymbol{\tau}_1 \times \boldsymbol{\tau}_2\|} \tag{3.19}$$

The vectors $\boldsymbol{\tau}_\alpha^{ref} \in T_{\nu^{ref}} S^2$ and $\boldsymbol{\tau}_\alpha \in T_\nu S^2$, $\alpha = 1,2$ span the tangent spaces $T_{\nu^{ref}} S^2$ and $T_\nu S^2$ to the S^2 unit sphere at $\boldsymbol{\nu}^{ref}$ and $\boldsymbol{\nu}$, respectively. Here the tangent space to the S^2 unit sphere at $\boldsymbol{\nu} \in S^2$ is defined as

$$T_\nu S^2 := \{\delta\boldsymbol{\nu} \in \mathbb{R}^{n_{dim}} \ : \ \delta\boldsymbol{\nu} \cdot \boldsymbol{\nu} = 0\} \tag{3.20}$$

The convected surface basis vectors $\boldsymbol{\tau}_\alpha^{ref}$ and $\boldsymbol{\tau}_\alpha$, $\alpha = 1,2$, augmented with the unit outward normals $\boldsymbol{\nu}^{ref}$ and $\boldsymbol{\nu}$, provides local spatial frames at the master particle $\bar{\boldsymbol{Y}}(\boldsymbol{X},t)$ on the reference and current configurations, respectively.

(E) *Surface metric and curvature on the reference and current configurations.* The convected surface basis vectors $\boldsymbol{\tau}_\alpha^{ref}$ and $\boldsymbol{\tau}_\alpha$, $\alpha = 1,2$, induces a surface metric or first fundamental form on the reference and current configurations, defined respectively as

$$\boxed{M_{\alpha\beta} := \boldsymbol{\tau}_\alpha^{ref} \cdot \boldsymbol{\tau}_\beta^{ref} , \qquad m_{\alpha\beta} := \boldsymbol{\tau}_\alpha \cdot \boldsymbol{\tau}_\beta} \tag{3.21}$$

Inverse surface metrics $M^{\alpha\beta}$ and $m^{\alpha\beta}$ are defined in the usual manner. Additionally, dual surface basis on the reference and current configurations are straightforward defined respectively as

$$\boldsymbol{\tau}_{ref}^\alpha := M^{\alpha\beta} \boldsymbol{\tau}_\beta^{ref} , \qquad \boldsymbol{\tau}^\alpha := m^{\alpha\beta} \boldsymbol{\tau}_\beta \tag{3.22}$$

The variation of the convected surface basis along the convected coordinates, together with the unit normal, induces the second fundamental form or surface curvature defined, on the reference and current configurations, as

$$\boxed{\kappa_{\alpha\beta}^{ref} := \boldsymbol{E}_{\alpha,\beta}(\bar{\boldsymbol{\xi}}) \cdot \boldsymbol{\nu}^{ref} , \qquad \kappa_{\alpha\beta} := \boldsymbol{e}_{\alpha,\beta}(\bar{\boldsymbol{\xi}}) \cdot \boldsymbol{\nu}} \tag{3.23}$$

(F) *Relative slip velocity on the convected description.* We introduce the relative slip velocity on the convected (reference) configuration defined as

$$\boldsymbol{v}_T^{ref}(\boldsymbol{X},t) := \dot{\bar{\boldsymbol{Y}}}(\boldsymbol{X},t) \tag{3.24}$$

The relative velocity on the convected description can be expressed in terms of the rate of the parent coordinates, using the map $(3.16)_1$, the convected surface basis on the reference configuration given by $(3.17)_1$ and applying the chain rule derivation, as

$$\boldsymbol{v}_T^{ref}(\boldsymbol{X},t) := \dot{\bar{\xi}}^\alpha \boldsymbol{\tau}_\alpha^{ref} \tag{3.25}$$

As expected, the convected relative slip velocity defined by (3.24) or (3.25) lies in the tangent plane to the master surface at the master point $\bar{\boldsymbol{Y}}(\boldsymbol{X},t)$.

The relative velocity on the current configuration can be defined as the push-forward of the relative velocity in the convected description with the deformation gradient $\boldsymbol{F}_t^{(2)}$, as

$$\boldsymbol{v}_T(\boldsymbol{X},t) := \boldsymbol{F}_t^{(2)}(\bar{\boldsymbol{\xi}}(\boldsymbol{X},t)) \cdot \boldsymbol{v}_T^{ref}(\boldsymbol{X},t) \tag{3.26}$$

The one-form associated to the relative velocity in the convected description is defined as

$$\boldsymbol{v}_T^{\flat ref}(\boldsymbol{X},t) := \dot{\bar{\xi}}^{\alpha} M_{\alpha\beta} \tau_{ref}^{\beta} \tag{3.27}$$

while the one-form associated to the relative velocity in the current configuration is defined as the push-forward of the corresponding one-form in the convected description, as

$$\boxed{\boldsymbol{v}_T^{\flat}(\boldsymbol{X},t) := \dot{\bar{\xi}}^{\alpha} M_{\alpha\beta} \boldsymbol{\tau}^{\beta}} \tag{3.28}$$

REMARK 3.1. The definition of $\boldsymbol{v}_T^{\flat}(\boldsymbol{X},t)$ is *frame indifferent*, despite the fact that the material and spatial velocity fields are not. This crucial property arises because the definition of $\boldsymbol{v}_T^{\flat}(\boldsymbol{X},t)$ uses the convected basis. □

REMARK 3.2. We note that the definition of the one-form associated to the relative velocity involves the metric $M_{\alpha\beta}$ at the point $\bar{\boldsymbol{Y}}(\boldsymbol{X},t)$ in the reference configuration, and *not* the metric $m_{\alpha\beta}$ in the current configuration. This is because we define $\boldsymbol{v}_T^{\flat}$ as the push-forward of the corresponding one-form in the convected description and not as the one-form associated to the spatial vector $\boldsymbol{v}_T$ in the current configuration. This last definition leads to an increase in the computational cost, due to the complexities involved in the linearization of the frictional integration algorithm. □

(G) *Frictional traction.* We define the nominal frictional tangent traction $\boldsymbol{t}_T(\boldsymbol{X},t)$ as (minus) the projection of the nominal frictional contact traction $\boldsymbol{t}^{(1)}(\boldsymbol{X},t)$ onto the unit normal $\boldsymbol{\nu}$, as

$$\boldsymbol{t}_T(\boldsymbol{X},t) := -\mathbb{P}_{\nu} \boldsymbol{t}^{(1)}(\boldsymbol{X},t) = t_T^{\alpha}(\boldsymbol{X},t)\ \boldsymbol{\tau}_{\alpha} \tag{3.29}$$

Additionally the one-form associated to this object is defined as

$$\boxed{\boldsymbol{t}_T^{\flat}(\boldsymbol{X},t) := -\mathbb{P}_{\nu} \boldsymbol{t}^{\flat(1)}(\boldsymbol{X},t) = t_{T_{\alpha}}(\boldsymbol{X},t)\ \boldsymbol{\tau}^{\alpha}} \tag{3.30}$$

(H) *Frictional constraints.* With the preceding definitions for the relative slip velocity and frictional traction, the frictional constraints are introduced as follows:

i. *Slip function. Admissible traction space.* We define a *slip function* $\Phi : T_{\nu}S^2 \times \mathbb{R}_+ \times \mathbb{R}_+ \to \mathbb{R}$ such that the states $(\boldsymbol{t}_T^{\flat}, t_N) \in T_{\nu}S^2 \times \mathbb{R}_+$ in the traction space and the internal variable $\alpha \in \mathbb{R}_+$ are constrained to lie in the closed set of admissible states defined as

$$\mathbb{E}_t := \{(\boldsymbol{t}_T^{\flat}, t_N, \alpha) \in T_{\nu}S^2 \times \mathbb{R}_+ \times \mathbb{R}_+ \ :\ \Phi(\boldsymbol{t}_T^{\flat}, t_N, \alpha) \leq 0\} \tag{3.31}$$

In particular, the classical friction Coulomb law can be extended to accomodate wear effects using a friction coefficient defined as a function of an internal variable α, such as the frictional dissipation or the slip amount. Then the admissible states space is defined by the slip function:

$$\Phi(\boldsymbol{t}_T^\flat, t_N, \alpha) := \|\boldsymbol{t}_T^\flat\| - \mu(\alpha) t_N \tag{3.32}$$

where $\|\cdot\|$ denotes the norm of its argument and $\mu(\alpha)$ is the Coulomb friction coefficient.

ii. *Slip rule and internal evolution equation.* The slip rule is defined as follows

$$\begin{aligned} \boldsymbol{v}_T^\flat(\boldsymbol{X}, t) &:= 0 \qquad \text{if} \quad \Phi(\boldsymbol{t}_T^\flat, t_N, \alpha) < 0 \\ \boldsymbol{v}_T^\flat(\boldsymbol{X}, t) &:= \gamma\, \boldsymbol{p}_T^\flat \qquad \text{if} \quad \Phi(\boldsymbol{t}_T^\flat, t_N, \alpha) = 0 \end{aligned} \tag{3.33}$$

where $\boldsymbol{p}_T^\flat := \partial_{\boldsymbol{t}_T^\flat} \Phi(\boldsymbol{t}_T^\flat, t_N, \alpha)$ and $\gamma \in \mathbb{R}_+$ is the non-negative slip consistency factor. For the frictional Coulomb law $\boldsymbol{p}_T^\flat$ is the normalized one-form frictional traction defined as $\boldsymbol{p}_T^\flat := \boldsymbol{t}_T^\flat / \|\boldsymbol{t}_T^\flat\|$.

Additionally one needs to define an evolution equation for the internal variable α. As stated above, one may define α as the slip amount leading to the following evolution equation:

$$\begin{aligned} \dot{\alpha}(\boldsymbol{X}, t) &:= 0 \qquad \text{if} \quad \Phi(\boldsymbol{t}_T^\flat, t_N, \alpha) < 0 \\ \dot{\alpha}(\boldsymbol{X}, t) &:= \gamma \qquad \text{if} \quad \Phi(\boldsymbol{t}_T^\flat, t_N, \alpha) = 0 \end{aligned} \tag{3.34}$$

or, alternatively, one may define α as the frictional dissipation, leading to the following evolution equation:

$$\begin{aligned} \dot{\alpha}(\boldsymbol{X}, t) &:= 0 \qquad\qquad\qquad\quad \text{if} \quad \Phi(\boldsymbol{t}_T^\flat, t_N, \alpha) < 0 \\ \dot{\alpha}(\boldsymbol{X}, t) &:= \boldsymbol{t}_T^\flat \cdot \boldsymbol{v}_T^\flat = \gamma\, \|\boldsymbol{t}_T^\flat\| \qquad \text{if} \quad \Phi(\boldsymbol{t}_T^\flat, t_N, \alpha) = 0 \end{aligned} \tag{3.35}$$

where the last expression in $(3.35)_2$ comes out using the slip rule (3.33).

These two alternative definitions can be easily accomodated into a single expression in the form:

$$\begin{aligned} \dot{\alpha}(\boldsymbol{X}, t) &:= 0 \qquad\qquad\qquad\quad \text{if} \quad \Phi(\boldsymbol{t}_T^\flat, t_N, \alpha) < 0 \\ \dot{\alpha}(\boldsymbol{X}, t) &:= \gamma\, [(1 - w) + w \|\boldsymbol{t}_T^\flat\|] \qquad \text{if} \quad \Phi(\boldsymbol{t}_T^\flat, t_N, \alpha) = 0 \end{aligned} \tag{3.36}$$

where $w \in [0, 1]$ is a constant such that, for $w = 0$ one recovers (3.34) and α is defined as the slip amount, for $w = 1$ one recovers (3.35) and α is defined as the frictional dissipation, and additionally for $w \in (0, 1)$ α is defined as a linear combination of slip amount and frictional dissipation. In what follows, we will use this single expression for the evolution equation of α, allowing to easily recover both alternative definitions as a particular case.

iii. *Slip consistency condition.* The slip consistency condition states that the rate of change of the slip function must be zero for positive values of the slip consistency factor. Mathematically this condition is expressed as

$$\gamma\, \dot{\Phi}(\boldsymbol{t}_T^\flat, t_N, \alpha) = 0 \tag{3.37}$$

The above expressions lead to a constrained evolution problem defined by the evolution equations

$$\boxed{\begin{aligned} \boldsymbol{v}_T^\flat(\boldsymbol{X},t) &= \gamma\ \boldsymbol{p}_T^\flat \\ \dot{\alpha}(\boldsymbol{X},t) &= \gamma\ [(1-w)+w\|\boldsymbol{t}_T^\flat\|] \end{aligned}} \tag{3.38}$$

subjected to the constraints, expressed as Kuhn-Tucker complementarity conditions as,

$$\boxed{\begin{aligned} \Phi(\boldsymbol{t}_T^\flat, t_N, \alpha) &\leq 0 \\ \gamma &\geq 0 \\ \gamma\ \Phi(\boldsymbol{t}_T^\flat, t_N, \alpha) &= 0 \\ \gamma\ \dot{\Phi}(\boldsymbol{t}_T^\flat, t_N, \alpha) &= 0 \end{aligned}} \tag{3.39}$$

3.3. Regularized frictional contact constraints

As discussed in KIKUCHI & ODEN [1988], for instance, solution of initial boundary value problems (IBVP) subject to constraints such as (3.12) and (3.39) amounts to finding a solution within a constrained solution space. Consideration of corresponding weak forms induces limitations on admissible variations in the tangent solution space, imposed by the physical constraints, leading to variational inequalities. See, for example, KIKUCHI & ODEN [1988] or DUVAUT & LIONS [1972].

Different methods have been used to bypass the need to find a solution within a constrained configuration solution space:

i. *Penalization.* In the *penalty* method the configuration solution space turns out to be unconstrained. The penalty method leads to a very convenient *displacement-driven* formulation of the frictional contact problem. See, for example, LAURSEN & SIMO [1991-1994], WRIGGERS & MIEHE [1992] or WRIGGERS, VU VAN & STEIN [1990]. Furthermore, the constraints induced by the frictional contact problem, can be viewed as *constitutive equations* of a *constrained evolution problem*, exactly as the constitutive equations for plasticity. Thus, all the well established algorithms developed for the time integration evolution equations of inelasticity, such as return mapping algorithms, can be applied. See WRIGGERS [1987], GIANNAKOPOULOS [1989], WRIGGERS, VU VAN & STEIN [1990] and LAURSEN & SIMO [1991-1994] among others. As a drawback of the penalty method, the constraints are exactly satisfied for infinite values of the penalty parameters only, leading to an infinite ill-conditioning of the tangent operator. On the other hand the use of too small values for the penalty parameters, leads to unacceptable violations of the kinematic constraints. Then, the choice of an appropiate value for the penalty parameters, must rely in a compromise between acceptable violations of the constraints and an enough small condition number of the tangent operator. The main drawback is the high sensitivity to the choice of the penalty parameters.

ii. *Lagrange Multipliers.* In the *Lagrange Multipliers* method the configuration solution space turns out to be unconstrained, but a *new* and *constrained* solution space, for

the multipliers, is introduced. This will leads to an increase in the number of equations to be solved. Furthermore, the resulting tangent operator is indefinite (zero diagonal block associated to the multipliers) and special care must be taken in the solution procedure. On the other hand the constraints are satisfied exactly. Lagrange multipliers method has been used, for example, by BATHE & CHAUDHARY [1985] and GALLEGO & ANZA [1989].

iii. *Perturbed Lagrange Multipliers.* The *Perturbed Lagrange Multipliers* method can be viewed as a regularization of the classical Lagrange Multipliers, leading to a definite tangent operator, through the introduction of a perturbation parameter. Within this approach, both the penalty and classical Lagrange Multipliers can be formulated in an unified manner. When the perturbation parameter goes to infinity, the classical Lagrange Multipliers method is recovered. On the other hand, solving for the multipliers the penalty method can be recovered. A perturbed Lagrange multipliers frictional contact formulation has been used by SIMO, WRIGGERS & TAYLOR [1985], JU & TAYLOR [1988].

iv. *Augmented Lagrangian.* In the *Augmented Lagrangian* method the constraints are exactly satisfied at *finite* values of the penalty parameters. This overcomes the main problems associated with the penalty method: choice of penalty parameters and ill-conditioning of the tangent operator. Furthermore, used in conjunction with Uzawa's algorithm, no increase of the number of equations to be solved is produced and the multipliers are simply updated after each converged equilibrium step (nested Uzawa's algorithm) or after each equilibrium iteration (simultaneous Uzawa's algorithm). In the nested augmentation algorithm an outer extra loop to perform the augmentations is needed, but the quadratic rate of convergence of Newton-Raphson method is preserved. On the other hand, in the simultaneous augmentation algorithm no extra loops are needed, but the update of the multipliers destroys the quadratic rate of convergence typical of Newton-Raphson iteration procedure. Augmented Lagrangian formulations for frictional contact problems have been used by SIMO & LAURSEN [1992], LAURSEN & SIMO [1992,1994] and LAURSEN & GOVINDJEE [1994].

Here we will use the *penalty* method to remove the restrictions associated to the constrained solution space and enforce the constraints through the introduction of constituve equations for the frictional contact traction.

(A) *Regularization of normal constraints.* The normal constraints induced by the contact problem are regularized introducing a *normal penalty* parameter ϵ_N and substituting the Kuhn-Tucker complementarity conditions defined in (3.12) with the following constitutive-like equation for the contact pressure

$$\boxed{t_N(\boldsymbol{X},t) := \epsilon_N \langle g_N(\boldsymbol{X},t) \rangle} \tag{3.40}$$

where $\langle \cdot \rangle$ is the Macauley bracket, representing the positive part of its operand. Expression (3.40) can be viewed as a Yosida regularization of the Kuhn-Tucker complementarity conditions given by (3.12), providing a constitutive-like equation for the contact pressure and leading to a convenient displacement-driven formulation.

Comparison of (3.40) with (3.12) reveals that now a (hopefully small) violation of the constraints (3.12) is allowed, and that the constraints will be exactly satisfied as $\epsilon_N \to \infty$.

(B) *Regularization of frictional constraints.* The regularization of the constrained frictional evolution problem defined by (3.38) and (3.39) is performed introducing a *tangential penalty* parameter ϵ_T playing the role of constitutive parameter in the relative slip velocity evolution equation. Then the regularized constrained frictional evolution problem takes the form:

$$\boxed{\begin{aligned} \boldsymbol{v}_T^\flat(\boldsymbol{X},t) &= \gamma\ \boldsymbol{p}_T^\flat + \frac{1}{\epsilon_T}\mathcal{L}_{v_T}\boldsymbol{t}_T^\flat \\ \dot{\alpha}(\boldsymbol{X},t) &= \gamma\ [(1-w) + w\|\boldsymbol{t}_T^\flat\|] \end{aligned}} \tag{3.41}$$

subjected to the following constraints

$$\boxed{\begin{aligned} \Phi(\boldsymbol{t}_T^\flat, t_N, \alpha) &\leq 0 \\ \gamma &\geq 0 \\ \gamma\ \Phi(\boldsymbol{t}_T^\flat, t_N, \alpha) &= 0 \\ \gamma\ \dot{\Phi}(\boldsymbol{t}_T^\flat, t_N, \alpha) &= 0 \end{aligned}} \tag{3.42}$$

where $\mathcal{L}_{v_T}\boldsymbol{t}_T^\flat$ is the Lie derivative of the frictional tangent traction along the flow induced by the relative slip velocity $\boldsymbol{v}_T$, defined as

$$\mathcal{L}_{v_T}\boldsymbol{t}_T^\flat := \dot{t}_{T\alpha}\boldsymbol{\tau}^\alpha \tag{3.43}$$

Comparison of (3.41) and (3.42) with (3.38) and (3.39), reveals that the frictional constraints are exactly satisfied as $\epsilon_T \to \infty$, in which case the (plastic) slip rate γ is equal to the norm of the relative slip velocity $\boldsymbol{v}_T^\flat$. Otherwise, it is assumed that the relative slip velocity can be decomposed into an elastic or recoverable part and a plastic or irreversible part. Introduction of the Lie derivative in the regularized relative slip velocity, maintains frame indifference of the frictional evolution equations.

Using the definition of the one-form relative slip velocity given by (3.28) and the Lie derivative of the frictional tangent traction along the flow induced by the relative slip velocity given by (3.43), the component form of the frictional tangent traction evolution equation $(3.41)_1$, along with the internal variable evolution equation, takes the form

$$\begin{aligned} \dot{t}_{T\alpha} &= \epsilon_T\ (M_{\alpha\beta}\dot{\bar{\xi}}^\beta - \gamma\ p_{T\alpha}) \\ \dot{\alpha} &= \gamma\ [(1-w) + w\|\boldsymbol{t}_T^\flat\|] \end{aligned} \tag{3.44}$$

(C) *Frictional operator split.* As we have seen above, the regularization of the frictional constraint problem leads to the following frictional constrained evolution problem

$$\begin{aligned} \mathcal{L}_{v_T}\boldsymbol{t}_T^\flat &= \epsilon_T\ [\boldsymbol{v}_T^\flat - \gamma\ \partial_{t_T^\flat}\Phi(\boldsymbol{t}_T^\flat, t_N, \alpha)] \\ \dot{\alpha} &= \gamma\ [(1-w) + w\|\boldsymbol{t}_T^\flat\|] \\ \Phi(\boldsymbol{t}_T^\flat, t_N, \alpha) \leq 0, \quad \gamma \geq 0, \quad \gamma\ \Phi(\boldsymbol{t}_T^\flat, t_N, \alpha) &= 0 \\ \gamma\ \dot{\Phi}(\boldsymbol{t}_T^\flat, t_N, \alpha) &= 0 \end{aligned} \tag{3.45}$$

Within the context of the product formula algorithms, a frictional operator split of the constrained evolution problem can be introduced by means of a *trial state*, defined by freezing the irreversible (plastic) slip response, i.e. setting $\gamma = 0$, as follows

Trial state *Return mapping*

$$\left\{\begin{array}{l} \mathcal{L}_{v_T} \boldsymbol{t}_T^\flat := \epsilon_T \, \boldsymbol{v}_T^\flat \\ \dot{\alpha} := 0 \\ \text{unconstrained} \end{array}\right\} \quad \left\{\begin{array}{l} \mathcal{L}_{v_T} \boldsymbol{t}_T^\flat := -\epsilon_T \, \gamma \, \partial_{t_T^\flat} \Phi(\boldsymbol{t}_T^\flat, t_N, \alpha) \\ \dot{\alpha} := \gamma \, [(1-w) + w \|\boldsymbol{t}_T^\flat\|] \\ \Phi(\boldsymbol{t}_T^\flat, t_N, \alpha) \leq 0, \; \gamma \geq 0, \; \gamma \, \Phi(\boldsymbol{t}_T^\flat, t_N, \alpha) = 0 \end{array}\right\} \tag{3.46}$$

REMARK 3.3. We point out that here only the regularization of the slip rule has been performed and (3.41) and (3.42) can be viewed as the governing equations of a *rate-independent* constrained frictional evolution problem. On the other hand, a Yosida regularization of the complementary Kuhn-Tucker frictional conditions (3.39), analogously to the regularization of the complementary Kuhn-Tucker contact normal conditions (3.12), would lead to a *rate-dependent* frictional evolution equations. □

3.4. Local form of the IBVP including frictional contact constraints

To formulate the Initial Boundary Value Problem (IBVP) including frictional contact constraints, we must introduce the local momentum balance equations, boundary conditions and initial conditions. No assumptions will be made on the constitutive equations and we will assume that the frictional contact tractions are related with corresponding kinematical fields through constitutive-like equations, within the framework of the penalty method. Additionally, the equilibrium of forces on the contact interfaces provides the link between the frictional tractions at the contact surfaces on the interacting bodies.

i. *Local form of momentum balance equations.* The local material form of the momentum balance equations for the body $\mathcal{B}^{(i)}$ can be written in conservation form as

$$\left.\begin{array}{l} \rho_0^{(i)} \dot{\boldsymbol{\varphi}}^{(i)} = \rho_0^{(i)} \boldsymbol{V}^{(i)} \\ \rho_0^{(i)} \dot{\boldsymbol{V}}^{(i)} = \mathrm{DIV}[\boldsymbol{P}^{(i)}] + \boldsymbol{B}^{(i)} \end{array}\right\} \quad \text{in} \quad \bar{\Omega}^{(i)} \times I \tag{3.47}$$

where $\rho_0^{(i)} : \bar{\Omega}^{(i)} \to \mathbb{R}_+$ is the reference density, $\boldsymbol{B}^{(i)} : \bar{\Omega}^{(i)} \times I \to \mathbb{R}^{n_{dim}}$ the reference body forces, DIV[·] the reference divergence operator and $\boldsymbol{P}^{(i)}$ the non-symmetric nominal or first Piola-Kirchhoff stress tensor.

ii. *Boundary conditions.* We will assume that the deformation $\boldsymbol{\varphi}^{(i)}$ is prescribed on $\Gamma_\varphi^{(i)} \subset \partial\Omega^{(i)}$ while the nominal traction $\boldsymbol{t}^{(i)}$ is prescribed on the part of the boundary $\Gamma_\sigma^{(i)} \subset \partial\Omega^{(i)}$, with unit outward normal field $\boldsymbol{N}^{(i)} : \Gamma_\sigma^{(i)} \to S^2$ as

$$\left.\begin{array}{lll} \boldsymbol{\varphi}^{(i)} = \bar{\boldsymbol{\varphi}}^{(i)} & \text{on} & \Gamma_\varphi^{(i)} \times I \\ \boldsymbol{t}^{(i)} = \boldsymbol{P}^{(i)} \cdot \boldsymbol{N}^{(i)} = \bar{\boldsymbol{t}}^{(i)} & \text{on} & \Gamma_\sigma^{(i)} \times I \end{array}\right\} \tag{3.48}$$

where $\bar{\varphi}^{(i)} : \Gamma_{\varphi}^{(i)} \times I \rightarrow \mathbb{R}^{n_{dim}}$ and $\bar{t}^{(i)} : \Gamma_{\sigma}^{(i)} \times I \rightarrow \mathbb{R}^{n_{dim}}$ are prescribed deformation and nominal traction maps. As usual it is assumed that the following conditions hold

$$\left.\begin{aligned} \Gamma_{\varphi}^{(i)} \cup \Gamma_{\sigma}^{(i)} \cup \Gamma^{(i)} &= \partial\Omega^{(i)} \\ \Gamma_{\varphi}^{(i)} \cap \Gamma_{\sigma}^{(i)} = \Gamma_{\varphi}^{(i)} \cap \Gamma^{(i)} &= \Gamma_{\sigma}^{(i)} \cap \Gamma^{(i)} = \emptyset \end{aligned}\right\} \tag{3.49}$$

iii. *Initial conditions.* Additionally, we will assume the following initial conditions

$$\left.\begin{aligned} \varphi^{(i)}(\cdot,t)|_{t=0} &= \bar{\varphi}_0^{(i)}(\cdot) \\ \boldsymbol{V}^{(i)}(\cdot,t)|_{t=0} &= \bar{\boldsymbol{V}}_0^{(i)}(\cdot) \end{aligned}\right\} \quad \text{in} \quad \bar{\Omega}^{(i)} \tag{3.50}$$

iv. *Equilibrium condition on the contact interface.* For each material point $\boldsymbol{X} \in \Gamma^{(1)}$ at any time $t \in I$, we require that the (differential) frictional contact force induced on body $\mathcal{B}^{(2)}$ at the material point $\bar{\boldsymbol{Y}}(\boldsymbol{X},t)$ be *equal* and *opposite* to that produced on body $\mathcal{B}^{(1)}$ at $\boldsymbol{X}$. Mathematically, this equilibrium condition takes the form

$$\boldsymbol{t}^{(1)}(\boldsymbol{X},t)\, d\Gamma^{(1)} + \boldsymbol{t}^{(2)}(\bar{\boldsymbol{Y}}(\boldsymbol{X},t),t)\, d\Gamma^{(2)} = 0 \tag{3.51}$$

3.5. Variational formulation. Weak form of the IBVP including frictional contact constraints

(A) *Configuration space.* Let the configuration space for the body $\mathcal{B}^{(i)}$ be defined as the set

$$\mathcal{C}^{(i)} := \{\varphi^{(i)} \in W^{1,p}(\Omega^{(i)})^{n_{dim}} : \det[D\varphi^{(i)}] > 0 \text{ in } \Omega^{(i)} \quad \text{and} \quad \varphi^{(i)}|_{\Gamma_{\varphi}^{(i)}} = \bar{\varphi}^{(i)}\} \tag{3.52}$$

where $W^{1,p}(\Omega^{(i)})$ is the Sobolev space of order $(1,p)$ for some p such that $2 \leq p < \infty$.

(B) *Admissible variations space.* We define the (time independent) set of (material) admissible variations or trial functions as the fixed linear space

$$\mathcal{V}_0^{(i)} := \{\boldsymbol{\eta}_0^{(i)} : \bar{\Omega}^{(i)} \rightarrow \mathbb{R}^{n_{dim}} \mid \boldsymbol{\eta}_0^{(i)}|_{\Gamma_{\varphi}^{(i)}} = 0\} \tag{3.53}$$

The admissible variations span the tangent space to the configuration manifold at the reference configuration.

(C) *Weak form of the IBVP.* Using standard procedures, the weak form of the momentum balance equations can be formally justified by taking the L_2–inner product of (3.47) with any $\boldsymbol{\eta}_0^{(i)} \in \mathcal{V}_0^{(i)}$ and using the divergence theorem. The result can be written as

$$\begin{aligned} \langle \rho_0^{(i)} \dot{\boldsymbol{\varphi}}^{(i)}, \boldsymbol{\eta}_0^{(i)} \rangle &= \langle \rho_0^{(i)} \boldsymbol{V}^{(i)}, \boldsymbol{\eta}_0^{(i)} \rangle \\ \langle \rho_0^{(i)} \dot{\boldsymbol{V}}^{(i)}, \boldsymbol{\eta}_0^{(i)} \rangle + \langle \boldsymbol{P}^{(i)}, \mathrm{GRAD}[\boldsymbol{\eta}_0^{(i)}] \rangle &= \langle \boldsymbol{B}^{(i)}, \boldsymbol{\eta}_0^{(i)} \rangle + \langle \bar{\boldsymbol{t}}^{(i)}, \boldsymbol{\eta}_0^{(i)} \rangle_{\Gamma_{\sigma}^{(i)}} + \langle \boldsymbol{t}^{(i)}, \boldsymbol{\eta}_0^{(i)} \rangle_{\Gamma^{(i)}} \end{aligned} \tag{3.54}$$

which must hold for any (material) test function $\boldsymbol{\eta}_0^{(i)} \in \mathcal{V}_0^{(i)}$. Here $\langle \cdot, \cdot \rangle$ denotes the $L_2(\Omega^{(i)})$–inner product and with a slight abuse in notation $\langle \cdot, \cdot \rangle_{\Gamma_\sigma^{(i)}}$ and $\langle \cdot, \cdot \rangle_{\Gamma^{(i)}}$ denotes the $L_2(\Gamma_\sigma^{(i)})$ and $L_2(\Gamma^{(i)})$–inner products on the boundaries $\Gamma_\sigma^{(i)}$ and $\Gamma^{(i)}$, respectively.

Denoting by $G_{dyn}^{(i)}(\boldsymbol{V}^{(i)}, \boldsymbol{P}^{(i)}; \boldsymbol{\eta}_0^{(i)})$ and $G_{stat}^{(i)}(\boldsymbol{P}^{(i)}; \boldsymbol{\eta}_0^{(i)})$ the dynamic and quasi-static weak forms of the momentum balance equations, respectively, excluding frictional contact contributions, and by $G_c^{(i)}(\boldsymbol{P}^{(i)}; \boldsymbol{\eta}_0^{(i)})$ the frictional contact contribution to the weak form of the momentum balance equations, respectively defined as

$$\begin{aligned} G_{dyn}^{(i)}(\boldsymbol{V}^{(i)}, \boldsymbol{P}^{(i)}; \boldsymbol{\eta}_0^{(i)}) &:= \langle \rho_0^{(i)} \dot{\boldsymbol{V}}^{(i)}, \boldsymbol{\eta}_0^{(i)} \rangle + G_{stat}^{(i)}(\boldsymbol{P}^{(i)}; \boldsymbol{\eta}_0^{(i)}) \\ G_{stat}^{(i)}(\boldsymbol{P}^{(i)}; \boldsymbol{\eta}_0^{(i)}) &:= \langle \boldsymbol{P}^{(i)}, \mathrm{GRAD}[\boldsymbol{\eta}_0^{(i)}] \rangle - \langle \boldsymbol{B}^{(i)}, \boldsymbol{\eta}_0^{(i)} \rangle - \langle \bar{\boldsymbol{t}}^{(i)}, \boldsymbol{\eta}_0^{(i)} \rangle_{\Gamma_\sigma^{(i)}} \\ G_c^{(i)}(\boldsymbol{P}^{(i)}; \boldsymbol{\eta}_0^{(i)}) &:= -\langle \boldsymbol{t}^{(i)}, \boldsymbol{\eta}_0^{(i)} \rangle_{\Gamma^{(i)}} = -\langle \boldsymbol{P}^{(i)} \cdot \boldsymbol{N}^{(i)}, \boldsymbol{\eta}_0^{(i)} \rangle_{\Gamma^{(i)}} \end{aligned} \tag{3.55}$$

the weak form of the momentum balance equations for body $\mathcal{B}^{(i)}$ can be expressed in short hand notation as

$$\left.\begin{aligned} \langle \rho_0^{(i)} (\dot{\boldsymbol{\varphi}}^{(i)} - \boldsymbol{V}^{(i)}), \boldsymbol{\eta}_0^{(i)} \rangle = 0 \\ G_{dyn}^{(i)}(\boldsymbol{V}^{(i)}, \boldsymbol{P}^{(i)}; \boldsymbol{\eta}_0^{(i)}) + G_c^{(i)}(\boldsymbol{P}^{(i)}; \boldsymbol{\eta}_0^{(i)}) = 0 \end{aligned}\right\} \quad \forall\, \boldsymbol{\eta}_0^{(i)} \in \mathcal{V}_0^{(i)} \tag{3.56}$$

For the multi-body dynamics system, we can write the momentum balance equations as

$$\left.\begin{aligned} \sum_{i=1}^{n} \langle \rho_0^{(i)} (\dot{\boldsymbol{\varphi}}^{(i)} - \boldsymbol{V}^{(i)}), \boldsymbol{\eta}_0^{(i)} \rangle = 0 \\ \sum_{i=1}^{n} G_{dyn}^{(i)}(\boldsymbol{V}^{(i)}, \boldsymbol{P}^{(i)}; \boldsymbol{\eta}_0^{(i)}) + \sum_{i=1}^{n} G_c^{(i)}(\boldsymbol{P}^{(i)}; \boldsymbol{\eta}_0^{(i)}) = 0 \end{aligned}\right\} \quad \forall\, \boldsymbol{\eta}_0^{(i)} \in \mathcal{V}_0^{(i)} \tag{3.57}$$

In particular, for two intertacting bodies $\mathcal{B}^{(1)}$ and $\mathcal{B}^{(2)}$, the frictional contact contribution to the weak form of the momentum balance equations, at the material contact points $\boldsymbol{X} \in \Gamma^{(1)}$ and $\bar{\boldsymbol{Y}}(\boldsymbol{X}, t) \in \Gamma^{(2)}$, at any time $t \in I$, takes the form

$$\hat{G}_c^{(1,2)}(\boldsymbol{P}^{(1)}, \boldsymbol{P}^{(2)}; \boldsymbol{\eta}_0^{(1)}, \boldsymbol{\eta}_0^{(2)}) := G_c^{(1)}(\boldsymbol{P}^{(1)}; \boldsymbol{\eta}_0^{(1)}) + G_c^{(2)}(\boldsymbol{P}^{(2)}; \boldsymbol{\eta}_0^{(2)}) \tag{3.58}$$

The weak form of the equilibrium condition at the contact interface given by (3.51), can be expressed as

$$\langle \boldsymbol{t}^{(1)}, \boldsymbol{\eta}_0^{(2)} \rangle_{\Gamma^{(1)}} + \langle \boldsymbol{t}^{(2)}, \boldsymbol{\eta}_0^{(2)} \rangle_{\Gamma^{(2)}} = 0 \tag{3.59}$$

Using (3.55), (3.58) and (3.59) the frictional contact contribution to the weak form of the momentum balance equations, at the material contact points $\boldsymbol{X} \in \Gamma^{(1)}$ and $\bar{\boldsymbol{Y}}(\boldsymbol{X}, t) \in \Gamma^{(2)}$, at any time $t \in I$, takes the form

$$\boxed{G_c^{(1,2)}(\boldsymbol{P}^{(1)}; \boldsymbol{\eta}_0^{(1)}, \boldsymbol{\eta}_0^{(2)}) := -\langle \boldsymbol{t}^{(1)}, \boldsymbol{\eta}_0^{(1)} - \boldsymbol{\eta}_0^{(2)} \rangle_{\Gamma^{(1)}}} \tag{3.60}$$

where the relation $\boldsymbol{t}^{(1)} := \boldsymbol{P}^{(1)} \cdot \boldsymbol{N}^{(1)}$, and the arguments in $\boldsymbol{t}^{(1)}(\boldsymbol{X},t)$, $\boldsymbol{\eta}_0^{(1)}(\boldsymbol{X})$ and $\boldsymbol{\eta}_0^{(2)}(\bar{\boldsymbol{Y}}(\boldsymbol{X},t))$ have been implicitly considered.

3.6. Linearization of the frictional contact kinematics

(A) *Directional derivative.* Given the configurations $\boldsymbol{\varphi}^{(i)}$ and the admissible variations $\boldsymbol{\eta}_0^{(i)}$, for the bodies $\mathcal{B}^{(i)}$, $i = 1,2$, we define the perturbed configurations $\boldsymbol{\varphi}_\epsilon^{(i)}$ as

$$\boldsymbol{\varphi}_\epsilon^{(i)} := \boldsymbol{\varphi}^{(i)} + \epsilon\, \boldsymbol{\eta}_0^{(i)} \tag{3.61}$$

where the ϵ is a scalar perturbation parameter (not to be confused with the penalty parameters ϵ_N and ϵ_T).

Then, for an arbitrary field $A(\boldsymbol{X},\boldsymbol{\varphi}^{(1)},\boldsymbol{\varphi}^{(2)})$ given for any $\boldsymbol{X} \in \Gamma^{(1)}$, the linearized variation $\delta A(\boldsymbol{X},\boldsymbol{\varphi}^{(1)},\boldsymbol{\varphi}^{(2)})$ is defined through the use of the directional derivative, as

$$\delta A(\boldsymbol{X},\boldsymbol{\varphi}^{(1)},\boldsymbol{\varphi}^{(2)}) := \left.\frac{d}{d\epsilon}\right|_{\epsilon=0} A(\boldsymbol{X},\boldsymbol{\varphi}_\epsilon^{(1)},\boldsymbol{\varphi}_\epsilon^{(2)}) \tag{3.62}$$

(B) *Linearized variation of the gap function g_N.* Using the definition of the gap function $g_N(\boldsymbol{X},t)$ given by (3.3) and exploiting the definition of directional derivative (3.62), the linearized variation of the gap function $g_N(\boldsymbol{X},t)$ takes the form

$$\begin{aligned} \delta g_N = &- [\boldsymbol{\eta}_0^{(1)}(\boldsymbol{X}) - \boldsymbol{\eta}_0^{(2)}(\bar{\boldsymbol{Y}}(\boldsymbol{X},t)) - \boldsymbol{\tau}_\alpha(\bar{\boldsymbol{Y}}(\boldsymbol{X},t),t)\ \delta\bar{\xi}^\alpha(\boldsymbol{X},t)] \cdot \boldsymbol{\nu} \\ &- [\boldsymbol{\varphi}^{(1)}(\boldsymbol{X},t) - \boldsymbol{\varphi}^{(2)}(\bar{\boldsymbol{Y}}(\boldsymbol{X},t),t)] \cdot \delta\boldsymbol{\nu} \end{aligned} \tag{3.63}$$

Using the relation $\boldsymbol{\tau}_\alpha \in T_\nu S^2$ along with (3.3) and the constraint $\delta\boldsymbol{\nu} \in T_\nu S^2$ the directional derivative (3.63) can be written as

$$\boxed{\delta g_N = -[\boldsymbol{\eta}_0^{(1)}(\boldsymbol{X}) - \boldsymbol{\eta}_0^{(2)}(\bar{\boldsymbol{Y}}(\boldsymbol{X},t))] \cdot \boldsymbol{\nu}} \tag{3.64}$$

(C) *Linearized variation of the contact parent coordinate $\bar{\boldsymbol{\xi}}(\boldsymbol{X},t)$.* The linearized variation of the contact parent coordinate $\bar{\boldsymbol{\xi}}(\boldsymbol{X},t)$ can be obtained in the following way. Using the definition of closest-point projection, the following normality condition holds for $\alpha = 1,2$,

$$[\boldsymbol{\varphi}^{(1)}(\boldsymbol{X},t) - \boldsymbol{\varphi}^{(2)}(\bar{\boldsymbol{Y}}(\boldsymbol{X},t),t)] \cdot \boldsymbol{\tau}_\alpha = 0 \tag{3.65}$$

The directional derivative of (3.65) leads to the following key expression

$$A_{\alpha\beta}\delta\bar{\xi}^\beta = [\boldsymbol{\eta}_0^{(1)}(\boldsymbol{X}) - \boldsymbol{\eta}_0^{(2)}(\bar{\boldsymbol{Y}}(\boldsymbol{X},t))] \cdot \boldsymbol{\tau}_\alpha - g_N(\boldsymbol{X},t)\ \boldsymbol{\nu} \cdot \boldsymbol{\eta}_{0,\alpha}^{(2)}(\bar{\boldsymbol{Y}}(\boldsymbol{X},t)) \tag{3.66}$$

where

$$A_{\alpha\beta} = m_{\alpha\beta} + g_N\ \kappa_{\alpha\beta} \tag{3.67}$$

Determination of $\delta\bar{\xi}^\alpha$ thus, will requires inversion of a two by two symmetric matrix $\boldsymbol{A} = [A_{\alpha\beta}]$, with components $A_{\alpha\beta}$ defined by (3.67). Denoting by $A^{\alpha\beta}$ the components of the inverse matrix $\boldsymbol{A}^{-1} = [A^{\alpha\beta}]$ the linearized variation $\delta\bar{\xi}^\alpha$ takes the form

$$\boxed{\delta\bar{\xi}^\alpha = A^{\alpha\beta}\{[\eta_0^{(1)}(\boldsymbol{X}) - \eta_0^{(2)}(\bar{\boldsymbol{Y}}(\boldsymbol{X},t))]\cdot\boldsymbol{\tau}_\beta - g_N(\boldsymbol{X},t)\,\boldsymbol{\nu}\cdot\boldsymbol{\eta}_{0,\beta}^{(2)}(\bar{\boldsymbol{Y}}(\boldsymbol{X},t))\}} \tag{3.68}$$

When $g_N = 0$ then $A_{\alpha\beta} = m_{\alpha\beta}$, $A^{\alpha\beta} = m^{\alpha\beta}$ and (3.64) simplifies to

$$\boxed{\delta\bar{\xi}^\alpha|_{g_N=0} = [\eta_0^{(1)}(\boldsymbol{X}) - \eta_0^{(2)}(\bar{\boldsymbol{Y}}(\boldsymbol{X},t))]\cdot\boldsymbol{\tau}^\alpha} \tag{3.69}$$

(D) *Linearized variation of* δg_N. Following a standard use of the directional derivative and after a reasonable amount of algebra, the linearization of δg_N given by (3.64), leads to

$$\boxed{\begin{aligned}\Delta(\delta g_N) = {} & g_N\,(\boldsymbol{\nu}\cdot\boldsymbol{\eta}_{0,\alpha}^{(2)} + \kappa_{\alpha\gamma}\,\delta\bar{\xi}^\gamma)\,m^{\alpha\beta}(\boldsymbol{\nu}\cdot\Delta\boldsymbol{\varphi}_{,\beta}^{(2)} + \kappa_{\beta\delta}\Delta\bar{\xi}^\delta) \\ & + \boldsymbol{\nu}\cdot(\delta\bar{\xi}^\alpha\Delta\boldsymbol{\varphi}_{,\alpha}^{(2)} + \Delta\bar{\xi}^\alpha\boldsymbol{\eta}_{0,\alpha}^{(2)}) + \kappa_{\alpha\beta}\,\delta\bar{\xi}^\alpha\Delta\bar{\xi}^\beta\end{aligned}} \tag{3.70}$$

(E) *Linearized variation of* $\delta\bar{\xi}^\alpha$. The linearized variation of $\delta\bar{\xi}^\alpha$ must be computed implicitly, by computing the directional derivative of (3.66). Since the calculation is quite lengthy we merely state the result, which is:

$$\boxed{\begin{aligned}A_{\alpha\beta}\Delta(\delta\bar{\xi}^\beta) = {} & -(\boldsymbol{\tau}_\alpha\cdot\boldsymbol{\eta}_{0,\beta}^{(2)} + g_N\,\boldsymbol{\nu}\cdot\boldsymbol{\eta}_{0,\alpha\beta}^{(2)})\,\Delta\bar{\xi}^\beta \\ & - (\boldsymbol{\tau}_\alpha\cdot\Delta\boldsymbol{\varphi}_{,\beta}^{(2)} + g_N\,\boldsymbol{\nu}\cdot\Delta\boldsymbol{\varphi}_{,\alpha\beta}^{(2)})\,\delta\bar{\xi}^\beta \\ & + (\boldsymbol{\eta}_0^{(1)} - \boldsymbol{\eta}_0^{(2)} - \delta\bar{\xi}^\gamma\boldsymbol{\tau}_\gamma)\cdot(\Delta\boldsymbol{\varphi}_{,\alpha}^{(2)} + \boldsymbol{e}_{\alpha,\beta}(\bar{\boldsymbol{\xi}})\,\Delta\bar{\xi}^\beta) \\ & + (\Delta\boldsymbol{\varphi}^{(1)} - \Delta\boldsymbol{\varphi}^{(2)} - \Delta\bar{\xi}^\gamma\boldsymbol{\tau}_\gamma)\cdot(\boldsymbol{\eta}_{0,\alpha}^{(2)} + \boldsymbol{e}_{\alpha,\beta}(\bar{\boldsymbol{\xi}})\,\delta\bar{\xi}^\beta) \\ & - [\boldsymbol{\tau}_\alpha\cdot\boldsymbol{e}_{\beta,\gamma}(\bar{\boldsymbol{\xi}}) + g_N\boldsymbol{\nu}\cdot\boldsymbol{e}_{\alpha,\beta\gamma}(\bar{\boldsymbol{\xi}})]\delta\bar{\xi}^\beta\Delta\bar{\xi}^\gamma\end{aligned}} \tag{3.71}$$

Particularizing (3.71) for $g_N = 0$, after some algebraic manipulation and using (3.23) and (3.64), the linearized variation of $\delta\bar{\xi}^\alpha$ at $g_N = 0$, takes the form:

$$\boxed{\begin{aligned}m_{\alpha\beta}\Delta(\delta\bar{\xi}^\beta) = {} & -(\boldsymbol{\tau}_\alpha\cdot\boldsymbol{\eta}_{0,\beta}^{(2)}\,\Delta\bar{\xi}^\beta|_{g_N=0} + \boldsymbol{\tau}_\alpha\cdot\Delta\boldsymbol{\varphi}_{,\beta}^{(2)}\,\delta\bar{\xi}^\beta|_{g_N=0} \\ & - \delta g_N(\Delta\boldsymbol{\varphi}_{,\alpha}^{(2)}\cdot\boldsymbol{\nu} + \kappa_{\alpha\beta}\Delta\bar{\xi}^\beta|_{g_N=0}) \\ & - \Delta g_N(\boldsymbol{\eta}_{0,\alpha}^{(2)}\cdot\boldsymbol{\nu} + \kappa_{\alpha\beta}\delta\bar{\xi}^\beta|_{g_N=0}) \\ & - \boldsymbol{\tau}_\alpha\cdot\boldsymbol{e}_{\beta,\gamma}(\bar{\boldsymbol{\xi}})\,\delta\bar{\xi}^\beta|_{g_N=0}\Delta\bar{\xi}^\gamma|_{g_N=0}\end{aligned}} \tag{3.72}$$

3.7. Frictional contact contribution to the weak form

Starting with the expression for the frictional contact contribution given by (3.60), using the split of the frictional contact traction (3.8) and (3.30), and the linearized variations (3.64) and (3.68), the frictional contact contribution to the weak form can be conveniently expressed as

$$\boxed{G_c(\varphi,\eta_0) := \langle t_N, \delta g_N\rangle_{\Gamma^{(1)}} + \langle t_{T\alpha}, \delta\bar{\xi}^{\alpha}\rangle_{\Gamma^{(1)}}} \tag{3.73}$$

where a short hand notation has been introduced, denoting as $\varphi \in \mathcal{C}$ and $\eta_0 \in \mathcal{V}_0$ the collection of mappings $\varphi^{(i)} \in \mathcal{C}^{(i)}$ and $\eta_0^{(i)} \in \mathcal{V}_0^{(i)}$, $i = 1,2$, such that the restriction of each of the maps φ and η_0 to the domain $\bar{\Omega}^{(i)}$ gives identically $\varphi^{(i)}$ and $\eta_0^{(i)}$, respectively.

4. The Discrete Initial Boundary Value Problem Including Frictional Contact Constraints

The numerical solution of the IBVP including frictional contact constraints at finite strains involves the transformation of an infinite dimensional dynamical system, governed by a system of quasi-linear partial differential equations into a sequence of discrete nonlinear algebraic problems by means of the following two steps:

Step **1.** The infinite dimensional phase space $Z = \mathcal{C} \times \mathcal{V}_0$ is approximated by a finite dimensional phase space $Z^h \subset Z$ via a Galerkin finite element projection. The projection in space of the dynamic weak form of the momentum equations leads to a nonlinear coupled system of ordinary differential equations (ODE's) which describe the time evolution of nodal degrees of freedom in the time interval of interest I.

Step **2.** The coupled system of nonlinear ordinary differential equations describes the time evolution in the time interval I of interest, of the nodal degrees of freedom and the internal variables associated with the finite element Galerkin projection. A time discretization of this problem involves a partition $I = \cup_{n=0}^{N}[t_n, t_{n+1}]$ of the time interval I. Within a typical time subinterval $[t_n, t_{n+1}]$, a time marching scheme for the advancement of the configuration and velocity fields in Z^h together with a return mapping algorithm for the advancement of the internal variables results in a nonlinear algebraic problem which is solved iteratively.

4.1. Spatial discretization: The Galerkin Projection.

Consider a spatial discretization $\Omega^{(i)} = \cup_{e=1}^{n_{elem}}\Omega_e^{(i)}$ of the reference configuration $\Omega^{(i)} \subset \mathbb{R}^{n_{dim}}$, generically refered as the triangularization and denoted by $\mathcal{T}^{(i)h}$ in what follows, into a disjoint collection of non-overlapping subsets $\Omega_e^{(i)}$, $i = 1,2$. We will refer to a typical subset $\Omega_e^{(i)}$ as a finite element and denote by $h > 0$ the characteristic size of an element in a given triangularization.

Associated with the triangularization $\mathcal{T}^{(i)h}$ one introduces a finite dimensional approximation $\mathcal{C}^{(i)h} \subset \mathcal{C}^{(i)}$ to the configuration manifold $\mathcal{C}^{(i)}$, defined as

$$\mathcal{C}^{(i)h} := \{\varphi^{(i)h} \in \mathcal{C}^{(i)} \;:\; \varphi^{(i)h} \in [C^0(\Omega^{(i)})]^{n_{dim}} \quad \text{and} \quad \varphi^{(i)h}|_{\Omega_e^{(i)}} \in [P^k(\Omega_e^{(i)})]^{n_{dim}}\}, \tag{4.1}$$

where $P^k(\Omega_e^{(i)})$ denotes the space of complete polynomials of degree $k \geq 1$.

The finite dimensional subspace $\mathcal{V}_0^{(i)h} \subset \mathcal{V}_0^{(i)}$ of material test functions associated with $\mathcal{C}^{(i)h}$ is defined as

$$\mathcal{V}_0^{(i)h} := \{\eta_0^{(i)h} \in \mathcal{V}_0^{(i)} \ : \ \eta_0^{(i)h} \in [C^0(\Omega^{(i)})]^{n_{dim}} \quad \text{and} \quad \eta_0^{(i)h}|_{\Omega_e^{(i)}} \in [P^k(\Omega_e^{(i)})]^{n_{dim}}\}. \tag{4.2}$$

(A) *Galerkin projection of the frictional contact contribution to the weak form.* The Galerkin projection of the frictional contact contribution to the weak form, given for the continuum case by (3.68), can be written as

$$\boxed{G_c(\varphi^h, \eta_0^h) := \langle t_N^h, \delta g_N^h \rangle_{\Gamma^{(1)h}} + \langle t_{T\alpha}^h, \delta \bar{\xi}^{\alpha h} \rangle_{\Gamma^{(1)h}}} \tag{4.3}$$

where $(\cdot)^h$ denotes the Galerkin projection of $(\cdot)$. In particular, using the short hand notation introduced in (3.68), φ^h and η_0^h refers to the discrete collection of mappings $\varphi^{(i)h}$ and $\eta_0^{(i)h}$, $i = 1, 2$, such that the restriction of each of the maps φ^h and η_0^h to the domain $\bar{\Omega}^{(i)h}$ gives identically $\varphi^{(i)h}$ and $\eta_0^{(i)h}$, respectively.

The projections δg_N^h and $\delta \bar{\xi}^{\alpha h}$ are given by (3.64) and (3.68), with discrete quantities replacing their continuous counterparts.

(B) *Linearization.* The linearization of the frictional contact contribution to the weak form given by (4.3), yield the following bilinear form

$$\boxed{B_{\varphi_t^h}(\eta_0^h, \Delta\varphi^h) := B_{\varphi_t^h}^{geo}(\eta_0^h, \Delta\varphi^h) + B_{\varphi_t^h}^{mat}(\eta_0^h, \Delta\varphi^h)} \tag{4.4}$$

Here $B_{\varphi_t^h}^{geo}(\cdot, \cdot)$ is the *geometric term* defined for fixed (nominal) contact pressure t_N^h and (nominal) frictional tangent traction $t_{T\alpha}^h$ at given configuration $\varphi_t^h \in \mathcal{C}^h$, by the bilinear form:

$$\boxed{B_{\varphi_t^h}^{geo}(\eta_0^h, \Delta\varphi^h) := \langle t_N^h, \Delta(\delta g_N^h) \rangle_{\Gamma^{(1)h}} + \langle t_{T\alpha}^h, \Delta(\delta \bar{\xi}^{\alpha h}) \rangle_{\Gamma^{(1)h}}} \tag{4.5}$$

and $B_{\varphi_t^h}^{mat}(\cdot, \cdot)$ is the *material term* defined for fixed configuration $\varphi_t^h \in \mathcal{C}^h$, by the bilinear form:

$$\boxed{B_{\varphi_t^h}^{mat}(\eta_0^h, \Delta\varphi^h) := \langle \Delta t_N^h, \delta g_N^h \rangle_{\Gamma^{(1)h}} + \langle \Delta t_{T\alpha}^h, \delta \bar{\xi}^{\alpha h} \rangle_{\Gamma^{(1)h}}} \tag{4.6}$$

4.2. Temporal discretization. Frictional return mapping.

Consider the time interval of interest $I = [0, T]$ discretized into a series of non-overlapping subintervals $I := \cup_{n=0}^{N}[t_n, t_{n+1}]$. The incremental solution to the IBVP is obtained applying a time stepping algorithm to integrate the evolution equations within a typical time step $[t_n, t_{n+1}]$, with given nodal and internal variables at time t_n, as initial conditions at the nodal and quadrature points of a typical element $\Omega_e^{(i)}$, respectively.

Following a standard convention, we shall denote by either $(\cdot)_n$ or $(\cdot)_{n+1}$ the algorithmic approximations at times t_n and t_{n+1} to the continuum (time dependent) variable $(\cdot)_t$.

(A) *Frictional time-stepping algorithms.* Most of the usual time-stepping algorithms will require the evaluation of the weak form and internal variables at some time $t_{n+\vartheta}$, where $\vartheta \in (0,1]$. Here, attention will be restricted to the Backward-Euler algorithm, obtained for $\vartheta = 1$. A class of time-stepping algorithms for dynamic plasticity, including Linear Multistep (LMS) methods and amongst them, the so-called Backward Difference (BD) methods, and Implicit Runge-Kutta (IRK) methods, are shown in SIMO [1992,1994]. Here, we will focussed on two algorithms for the time integration of the constrained frictional evolution problem defined by (3.38) and (3.39): the lowest order BD method called Backward-Euler (BE) method and the generalized Projected Mid-Point (PMP) Implicit Runge-Kutta (IRK) method.

(A1) *Backward-Euler (BE) method.* Consider the approximation of (3.41) and (3.42) by the lowest order BD method, the BE scheme, to obtain the algebraic equation

$$\begin{aligned} t_{T\,n+1\,\alpha} &= t_{T\,n\alpha} + \epsilon_T \left[M_{\alpha\beta} (\bar{\xi}^{\beta}_{n+1} - \bar{\xi}^{\beta}_{n}) - \gamma_{n+1}\; p_{n+1\,\alpha} \right] \\ \alpha_{n+1} &= \alpha_n + \gamma_{n+1} [(1-w) + w \| \boldsymbol{t}^{\flat}_{T\,n+1} \|] \end{aligned} \tag{4.7}$$

subjected to the discrete complementary Kuhn-Tucker conditions

$$\begin{aligned} \Phi_{n+1} := \| \boldsymbol{t}^{\flat}_{T\,n+1} \| - \mu(\alpha_{n+1})\; t_{N\,n+1} \leq 0 \\ \gamma_{n+1} \geq 0 \\ \gamma_{n+1}\; \Phi_{n+1} = 0 \end{aligned} \tag{4.8}$$

The solution to the constrained incremental algebraic problem defined by (4.7) and (4.8) is obtained through the introduction of a *trial state*, obtained by freezing the irreversible-slip response, and subsequent *return mapping* algorithm to enforce the constraints.

Step **1.** *Trial state.* The frictional trial state is obtained by freezing the irreversible-slip response, i.e. assuming $\gamma_{n+1} = 0$ and that no constraints are present. Then the trial state is defined as

$$\begin{aligned} t^{trial}_{T_{n+1}\,\alpha} &:= t_{T_n\,\alpha} + \epsilon_T M_{\alpha\beta} (\bar{\xi}^{\beta}_{n+1} - \bar{\xi}^{\beta}_{n}) \\ \alpha^{trial}_{n+1} &:= \alpha_n \\ \Phi^{trial}_{n+1} &:= \| \boldsymbol{t}^{\flat\,trial}_{T_{n+1}} \| - \mu(\alpha^{trial}_{n+1})\; t_{N_{n+1}} \end{aligned} \tag{4.9}$$

where $t_{N\,n+1} = \epsilon_N \langle g_{N\,n+1} \rangle$ is the normal contact pressure at t_{n+1}.

Step **2.** *Return mapping.* The return mapping defines the final state as the solution of the discrete constrained incremental algebraic problem:

$$\begin{aligned} t_{T_{n+1}\,\alpha} &= t^{trial}_{T_{n+1}\,\alpha} - \epsilon_T\; \gamma_{n+1}\; p_{T_{n+1}\,\alpha} \\ \alpha_{n+1} &= \alpha^{trial}_{n+1} + \gamma_{n+1}\; [(1-w) + w \| \boldsymbol{t}^{\flat}_{T\,n+1} \|] \end{aligned} \tag{4.10}$$

$$\begin{aligned} \Phi_{n+1} = \|\boldsymbol{t}^{\flat}_{T\,n+1}\| - \mu(\alpha_{n+1})\; t_{N\,n+1} \leq 0 \\ \gamma_{n+1} \geq 0 \\ \gamma_{n+1}\; \Phi_{n+1} = 0 \end{aligned} \tag{4.11}$$

Assuming that $\Phi^{trial}_{n+1} > 0$, otherwise $\gamma_{n+1} = 0$ and the trial state actually is the final state, the discrete consistency parameter γ_{n+1} can be computed by enforcing the discrete counterpart of the consistency condition $\Phi_{n+1} = 0$.

Introducing $\boldsymbol{p}^{\flat}_{T_{n+1}} := \boldsymbol{t}^{\flat}_{T_{n+1}} / \|\boldsymbol{t}^{\flat}_{T_{n+1}}\|$ into the intrinsic expression of the frictional traction

$$\boldsymbol{t}^{\flat}_{T_{n+1}} = \boldsymbol{t}^{\flat trial}_{T_{n+1}} - \epsilon_T\; \gamma_{n+1}\; \boldsymbol{p}^{\flat}_{T_{n+1}} \tag{4.12}$$

collecting terms, setting $\boldsymbol{p}^{\flat trial}_{T_{n+1}} := \boldsymbol{t}^{\flat trial}_{T_{n+1}} / \|\boldsymbol{t}^{\flat trial}_{T_{n+1}}\|$ and taking norms leads to,

$$\begin{aligned} \boldsymbol{p}^{\flat}_{T_{n+1}} &= \boldsymbol{p}^{\flat trial}_{T_{n+1}} \\ \|\boldsymbol{t}^{\flat}_{T_{n+1}}\| &= \|\boldsymbol{t}^{\flat trial}_{T_{n+1}}\| - \epsilon_T\; \gamma_{n+1} \end{aligned} \tag{4.13}$$

Introducing (4.13) into (4.10)-(4.12), the frictional return mapping takes the form:

$$\begin{aligned} \boldsymbol{t}^{\flat}_{T_{n+1}} &= \Big(1 - \epsilon_T\; \frac{\gamma_{n+1}}{\|\boldsymbol{t}^{\flat trial}_{T_{n+1}}\|}\Big)\; \boldsymbol{t}^{\flat trial}_{T_{n+1}} \\ \alpha_{n+1} &= \alpha^{trial}_{n+1} + \gamma_{n+1}\; [(1-w) + w\|\boldsymbol{t}^{\flat trial}_{T_{n+1}}\| - w\; \epsilon_T\; \gamma_{n+1}] \\ \Phi_{n+1} &:= \|\boldsymbol{t}^{\flat trial}_{T_{n+1}}\| - \epsilon_T\; \gamma_{n+1} - \mu(\alpha_{n+1})\; t_{N\,n+1} = 0 \end{aligned} \tag{4.14}$$

or alternatively, using the consistency condition,

$$\begin{aligned} \boldsymbol{t}^{\flat}_{T_{n+1}} &= \mu(\alpha_{n+1})\; t_{N\,n+1}\; \boldsymbol{p}^{\flat trial}_{T_{n+1}} \\ \alpha_{n+1} &= \alpha^{trial}_{n+1} + \gamma_{n+1}\; [(1-w) + w\; \mu(\alpha_{n+1})\; t_{N\,n+1}] \\ \Phi_{n+1} &:= \|\boldsymbol{t}^{\flat trial}_{T_{n+1}}\| - \epsilon_T\; \gamma_{n+1} - \mu(\alpha_{n+1})\; t_{N\,n+1} = 0 \end{aligned} \tag{4.15}$$

Computation of the consistency parameter γ_{n+1} will require, in general, to solve the nonlinear equation $\Phi_{n+1} = \hat{\Phi}(\gamma_{n+1}) = 0$, were it is implicitly understood that we are looking at α_{n+1} as a function $\alpha_{n+1} = \alpha_{n+1}(\gamma_{n+1})$, using $(4.14)_2$ instead of $(4.15)_2$. Using a Newton-Raphson method the linearization of the slip function yields

$$\Phi^{(k)}_{n+1} + D\Phi^{(k)}_{n+1} \cdot \Delta\gamma^{(k)}_{n+1} = 0 \tag{4.16}$$

with

$$\begin{aligned} \Phi^{(k)}_{n+1} &= \Phi^{trial}_{n+1} - \epsilon_T\; \gamma^{(k)}_{n+1} - [\mu(\alpha^{(k)}_{n+1}) - \mu(\alpha^{trial}_{n+1})]\; t_{N\,n+1} \\ D\Phi^{(k)}_{n+1} &= -\epsilon_T - \partial_\alpha \mu(\alpha^{(k)}_{n+1})\; D\alpha^{(k)}_{n+1}\; t_{N\,n+1} \\ \alpha^{(k)}_{n+1} &= \alpha^{trial}_{n+1} + \gamma^{(k)}_{n+1}\; [(1-w) + w\|\boldsymbol{t}^{\flat trial}_{T_{n+1}}\| - w\; \epsilon_T\; \gamma^{(k)}_{n+1}] \\ D\alpha^{(k)}_{n+1} &= (1-w) + w\|\boldsymbol{t}^{\flat trial}_{T_{n+1}}\| - 2\; w\; \epsilon_T\; \gamma^{(k)}_{n+1} \\ \Delta\gamma^{(k)}_{n+1} &= \gamma^{(k+1)}_{n+1} - \gamma^{(k)}_{n+1} \end{aligned} \tag{4.17}$$

and with the initial condition $\gamma_{n+1}^{(0)} = 0$.

As it is well known, the BE algorithm is consistent and first order accurate. On the other hand, as it was shown by SIMO [1994] within the context of J2 perfect plasticity, in spite of its restriction to first order accuracy, the BE algorithm inherits the dissipative and contractive properties of the continuum problem and becomes optimal for a long-term behavior.

REMARK 4.1. The intrinsic form of the frictional time integration described above can be written as

$$\begin{aligned} \boldsymbol{t}^{\flat}_{T_{n+1}} &:= \boldsymbol{t}^{\flat^{trial}}_{T_{n+1}} - \epsilon_T \, \gamma_{n+1} \, \boldsymbol{p}^{\flat^{trial}}_{T_{n+1}} \\ \boldsymbol{t}^{\flat^{trial}}_{T_{n+1}} &:= \boldsymbol{F}^{-T}_{n+1} \cdot \boldsymbol{t}^{\flat^{ref\ trial}}_{T_{n+1}} \\ \boldsymbol{t}^{\flat^{ref\ trial}}_{T_{n+1}} &:= \boldsymbol{\Lambda}^{n}_{n+1} \cdot \boldsymbol{t}^{\flat^{ref}}_{T_n} + \epsilon_T M_{\alpha\beta}(\bar{\xi}^{\beta}_{n+1} - \bar{\xi}^{\beta}_{n}) \, \boldsymbol{\tau}^{\alpha^{ref}}_{n+1} \end{aligned} \tag{4.18}$$

where the surface deformation gradient $\boldsymbol{F}_{n+1}$ and the surface transport operator $\boldsymbol{\Lambda}^{n}_{n+1}$ are defined as

$$\begin{aligned} \boldsymbol{F}^{-T}_{n+1} &:= \boldsymbol{\tau}^{\alpha}_{n+1} \otimes \boldsymbol{\tau}^{ref}_{\alpha_{n+1}} \\ \boldsymbol{\Lambda}^{n}_{n+1} &:= \boldsymbol{\tau}^{\alpha^{ref}}_{n+1} \otimes \boldsymbol{\tau}^{ref}_{\alpha_n} \end{aligned} \tag{4.19}$$

Here the trial state defined by $\boldsymbol{t}^{\flat^{trial}}_{T_{n+1}} := t^{trial}_{T_{n+1}\alpha} \boldsymbol{\tau}^{\alpha}_{n+1}$ may be interpreted as the result of a two-step algorithm:

i. Time integration of the trial frictional traction on the reference configuration to get $\boldsymbol{t}^{\flat^{ref\ trial}}_{T_{n+1}}$. This time integration consist of two steps. First, the frictional traction in the reference configuration at the last converged time step is *transported* with the operator $\boldsymbol{\Lambda}^{n}_{n+1}$ to the current closest-point projection on the reference configuration, followed by the (trial) slip contribution given by the distance, with respect to the metric $M_{\alpha\beta}$, between the current and last converged closest-point projections on the reference configuration.

ii. Push-forward to the current configuration to get $\boldsymbol{t}^{\flat^{trial}}_{T_{n+1}}$.

Once the trial state has been defined the return mapping is performed on the current configuration, following standard procedures. □

(A2) *Generalized Projected Mid-Point (PMP) Implicit Runge-Kutta (IRK) method.* The Generalized Projected Mid-Point IRK method is constructed via a two-stage product formula algorithm as follows:

Stage I. A BE algorithm is applied to integrate the constrained evolution problem within a time sub-interval $[t_n, t_{n+\vartheta}] \subset [t_n, t_{n+1}]$ where $t_{n+\vartheta} := (1-\vartheta)t_n + \vartheta t_{n+1}$ and $\vartheta \in (0,1]$. Thus, the first stage of the algorithm is identical to the scheme already described above. Explicitly, the following steps are performed for prescibed initial data $\{t^{ref}_{T_{n_\alpha}}\}$ and given relative (parametrized) slip increment $\bar{g}^{\alpha}_{T_{n+\vartheta}} := \bar{\xi}^{\alpha}_{n+\vartheta} - \bar{\xi}^{\alpha}_{n}$:

Step **1.** Define the generalized mid-point trial state according to

$$\begin{aligned} t^{trial}_{T_{n+\vartheta}\alpha} &:= t_{T_n\alpha} + \epsilon_T M_{\alpha\beta}(\bar{\xi}^{\beta}_{n+\vartheta} - \bar{\xi}^{\beta}_{n}) \\ \alpha^{trial}_{n+\vartheta} &:= \alpha_n \\ \Phi^{trial}_{n+\vartheta} &:= \|\boldsymbol{t}^{\flat^{trial}}_{T_{n+\vartheta}}\| - \mu(\alpha^{trial}_{n+\vartheta}) \, t_{N_{n+\vartheta}} \end{aligned} \tag{4.20}$$

Step **2.** The return mapping defines the final state at the generalized mid-point configuration $\mathcal{C}_{n+\vartheta}$ as the solution of the discrete constrained incremental algebraic problem:

$$\begin{aligned} t_{T_{n+\vartheta}\alpha} &= t^{trial}_{T_{n+\vartheta}\alpha} - \epsilon_T\, \gamma_{n+\vartheta}\, p_{T_{n+\vartheta}\alpha} \\ \alpha_{n+\vartheta} &= \alpha^{trial}_{n+\vartheta} + \gamma_{n+\vartheta}\, [(1-w) + w\|t^{\flat}_{T\,n+\vartheta}\|] \end{aligned} \tag{4.21}$$

$$\begin{aligned} \Phi_{n+\vartheta} = \|t^{\flat}_{T\,n+\vartheta}\| - \mu(\alpha_{n+\vartheta})\; t_{N\,n+\vartheta} &\leq 0 \\ \gamma_{n+\vartheta} &\geq 0 \\ \gamma_{n+\vartheta}\; \Phi_{n+\vartheta} &= 0 \end{aligned} \tag{4.22}$$

Stage IIA. Since the trial values $t^{trial}_{T_{n+\vartheta}\,\alpha}$ and the converged values $t_{T_{n+\vartheta}\,\alpha}$ are available from Stage I and within the context of a product formula algorithm, the initial data $t^{*}_{T_{n+\vartheta}\,\alpha}$ and $\alpha^{*}_{n+\vartheta}$ for the second stage are defined using the linear extrapolation:

$$\begin{aligned} t^{*}_{T_{n+\vartheta}\alpha} &:= \frac{1}{\vartheta} t_{T_{n+\vartheta}\alpha} - \frac{1-\vartheta}{\vartheta} t^{trial}_{T_{n+\vartheta}\alpha} \\ \alpha^{*}_{n+\vartheta} &:= \frac{1}{\vartheta} \alpha_{n+\vartheta} - \frac{1-\vartheta}{\vartheta} \alpha^{trial}_{n+\vartheta} \end{aligned} \tag{4.23}$$

Within a finite deformation framework, all the objects involved in the linear extrapolation given by (4.23) should be viewed as objects lying in the *same* generalized mid-point configuration $\mathcal{C}_{n+\vartheta}$. Thus, for the friction Coulomb model this extrapolation is performed on the plane $t_N = t_{N\,n+\vartheta}$ of the tractions space.

Stage IIB. The second part of Stage II is identical to Stage I, where now the initial prescribed data becomes $t^{*}_{T_{n+\vartheta}\,\alpha}$ and the given (parametrized) relative slip increment is $\bar{g}^{\alpha}_{T_{n+1}} := \bar{\xi}^{\alpha}_{n+1} - \bar{\xi}^{\alpha}_{n+\vartheta}$. The steps involved in the update are the following:

Step **1.** Define the trial state according to

$$\begin{aligned} t^{trial}_{T_{n+1}\alpha} &:= t^{*}_{T_{n+\vartheta}\alpha} + \epsilon_T M_{\alpha\beta}(\bar{\xi}^{\beta}_{n+1} - \bar{\xi}^{\beta}_{n+\vartheta}) \\ \alpha^{trial}_{n+1} &:= \alpha^{*}_{n+\vartheta} \\ \Phi^{trial}_{n+1} &:= \|t^{b^{trial}}_{T_{n+1}}\| - \mu(\alpha^{trial}_{n+1})\; t_{N_{n+1}} \end{aligned} \tag{4.24}$$

Step **2.** Perform the return mapping to get the final state at the configuration $\mathcal{C}_{n+1}$ as the solution of the discrete constrained incremental algebraic problem:

$$\begin{aligned} t_{T_{n+1}\alpha} &= t^{trial}_{T_{n+1}\alpha} - \epsilon_T\, \gamma_{n+1}\, p_{T_{n+1}\alpha} \\ \alpha_{n+1} &= \alpha^{trial}_{n+1} + \gamma_{n+1}\, [(1-w) + w\|t^{\flat}_{T\,n+1}\|] \end{aligned} \tag{4.25}$$

$$\begin{aligned} \Phi_{n+1} = \|t^{\flat}_{T\,n+1}\| - \mu(\alpha_{n+1})\; t_{N\,n+1} &\leq 0 \\ \gamma_{n+1} &\geq 0 \\ \gamma_{n+1}\; \Phi_{n+1} &= 0 \end{aligned} \tag{4.26}$$

A rigorous stability and accuracy analysis of the two-stage, implicit, PMP algorithm, within the context of J2 plasticity, was provided by SIMO [1994]. The accuracy and stability analysis show that the generalized PMP algorithm is obviously consistent, second order accurate for the PMP algorithm ($\vartheta = 0.5$), B-stable for $\vartheta \geq 0.5$ and ensures that the final stage is on the admissible domain. Remarkably, in sharp contrast with others second order accurate algorithms, i.e. mid-point rule, second order accuracy is achieved performing a *radial return mapping* in each of the Stages and thus a solution will be always guaranteed to exist for arbitrarily large time-steps. However, the long-term behaviour of this scheme is not optimal when compared with that exhibited by the, less accurate, BE algorithm. In contrast, this scheme becomes optimal for short-term behavior.

(B) *Linearization of the frictional time-stepping algorithm.* The frictional time-stepping algorithms presented above are amenable to exact linearization, leading to the corresponding terms of the *consistent* or *algorithmic* tangent operator. In order to accomodate the linearization of the BE and PMP return mapping algorithms into a single expression, we will derive the linearization of the frictional traction at time $t_{n+\vartheta}$, at the generic configuration $\mathcal{C}_{n+\vartheta}$, where $\vartheta = 1$ for the BE algorithm and $\vartheta \in (0, 1]$ for the PMP algorithm. We point out that the implementation of the PMP IRK algorithm actually requires *only* the linearization of the Stage I, while Stage II can be viewed as an update procedure to provide the initial conditions for the next time step, after convergence has been achieved.

Using the directional derivative, the linearization of the frictional time integration algorithm leads to the following expressions.

Step **1.** *Trial state.* The linearization of the trial state takes the form

$$\begin{aligned} \Delta t_{T_{n+\vartheta}\,\alpha} &:= \Delta t^{trial}_{T_{n+\vartheta}\,\alpha} \\ \Delta \alpha_{n+\vartheta} &:= \Delta \alpha^{trial}_{n+\vartheta} = 0 \end{aligned} \tag{4.27}$$

Step **2.** *Return mapping.* The linearization of the return mapping takes the form

$$\begin{aligned} \Delta t_{T_{n+\vartheta}\,\alpha} &:= \mu(\alpha_{n+\vartheta})\; \Delta t_{N n+\vartheta}\; p^{trial}_{T_{n+\vartheta}\,\alpha} + \mu(\alpha_{n+\vartheta})\; t_{N n+\vartheta}\; \Delta p^{trial}_{T_{n+\vartheta}\,\alpha} \\ &\quad + \partial_\alpha \mu(\alpha_{n+\vartheta})\; \Delta \alpha_{n+\vartheta}\; t_{N n+\vartheta}\; p^{trial}_{T_{n+\vartheta}\,\alpha} \\ \Delta \alpha_{n+\vartheta} &:= \Delta \gamma_{n+\vartheta}\; [(1-w) + w\; \mu(\alpha_{n+\vartheta})\; t_{N n+\vartheta} - w\; \epsilon_T\; \gamma_{n+\vartheta}] \\ &\quad + \gamma_{n+\vartheta}\; w\; \Delta \| \boldsymbol{t}^{b\,trial}_{T_{n+\vartheta}} \| \\ &:= \Delta \gamma_{n+\vartheta}\; [(1-w) + w\; \mu(\alpha_{n+\vartheta})\; t_{N n+\vartheta}] \\ &\quad + \gamma_{n+\vartheta}\; w\; [\partial_\alpha \mu(\alpha_{n+\vartheta})\; t_{N n+\vartheta}\; \Delta \alpha_{n+\vartheta} + \mu(\alpha_{n+\vartheta})\; \Delta t_{N_{n+\vartheta}} \end{aligned} \tag{4.28}$$

with

$$\begin{aligned} \Delta t_{N_{n+\vartheta}} &:= \epsilon_N H(g_{N_{n+\vartheta}})\; \Delta g_{N_{n+\vartheta}} \\ \Delta g_{N_{n+\vartheta}} &:= -\vartheta\; [\Delta \boldsymbol{\varphi}^{(1)h} - \Delta \boldsymbol{\varphi}^{(2)h} \circ \boldsymbol{\psi}^{(2)}_0(\bar{\boldsymbol{\xi}}_{n+\vartheta})] \cdot \boldsymbol{\nu} \\ \Delta t^{trial}_{T_{n+\vartheta}\,\alpha} &:= \Xi_{\alpha\beta}\; \Delta \bar{\xi}^{\beta}_{n+\vartheta} \end{aligned} \tag{4.29a}$$

$$
\begin{aligned}
\Delta p^{trial}_{T_{n+\vartheta}\,\alpha} &:= (\delta^{\beta}_{\alpha} - \pi^{\beta}_{\alpha})\,\frac{\Delta t^{trial}_{T_{n+\vartheta}\,\beta}}{\|t^{b\,trial}_{T_{n+\vartheta}}\|} + \pi^{\beta}_{\alpha}\; p^{b\,trial}_{T_{n+\vartheta}} \cdot [\vartheta\; \Delta\varphi^{(2)h}_{,\beta}(\bar{\xi}) + e_{\beta,\gamma}(\bar{\xi})\; \Delta\bar{\xi}^{\gamma}_{n+\vartheta}] \\
\Delta\|t^{b\,trial}_{T_{n+\vartheta}}\| &:= p^{trial\;\alpha}_{T_{n+\vartheta}}\; \Delta t^{trial}_{T_{n+\vartheta}\,\alpha} - p^{trial\;\alpha}_{T_{n+\vartheta}}\; t^{b\,trial}_{T_{n+\vartheta}} \cdot [\vartheta\; \Delta\varphi^{(2)h}_{,\alpha}(\bar{\xi}) + e_{\alpha,\beta}(\bar{\xi})\; \Delta\bar{\xi}^{\beta}_{n+\vartheta}] \qquad (4.29b) \\
\Delta\bar{\xi}^{\alpha}_{n+\vartheta} &:= \vartheta A^{\alpha\beta}\{[\Delta\varphi^{(1)h} - \Delta\varphi^{(2)h}(\bar{\xi}_{n+\vartheta})] \cdot \tau_{\beta} - g_{N_{n+\vartheta}}\boldsymbol{\nu} \cdot [\Delta\varphi^{(2)h}_{,\beta}(\bar{\xi}_{n+\vartheta})]\} \\
\Delta\gamma_{n+\vartheta} &:= \frac{1}{\epsilon_T}[\Delta\|t^{b\,trial}_{T_{n+\vartheta}}\| - \mu(\alpha_{n+\vartheta})\; \Delta t_{N_{n+\vartheta}}] - \frac{1}{\epsilon_T}\partial_{\alpha}\mu(\alpha_{n+\vartheta})\; t_{N_{n+\vartheta}}\; \Delta\alpha_{n+\vartheta}
\end{aligned}
$$

where,

$$
\begin{aligned}
\Xi_{\alpha\beta} &:= \epsilon_T\,(M_{\alpha\beta} + M_{\alpha\gamma,\beta}\; g^{\gamma}_{T}) \\
g^{\alpha}_{T} &:= \bar{\xi}^{\alpha}_{n+\vartheta} - \bar{\xi}^{\alpha}_{n} \\
\pi^{\beta}_{\alpha} &:= p^{trial}_{T_{n+\vartheta}\,\alpha}\; p^{trial\;\beta}_{T_{n+\vartheta}}
\end{aligned}
\qquad (4.30)
$$

with the, in general, *non-symmetric* operator $\Xi_{\alpha\beta}$ evaluated at $t_{n+\vartheta}$. Here, $\Delta\varphi^{(1)h}$ and $\Delta\varphi^{(2)h}$ refers to the incremental displacements in the whole step, i.e. from t_n to t_{n+1}, and it is implicitly assumed that all the objects involved in the expressions are evaluated at time $t_{n+\vartheta}$.

Introducing $\Delta\gamma_{n+\vartheta}$ into the expression of $\Delta\alpha_{n+\vartheta}$ and collecting terms, leads to

$$
\Delta\alpha_{n+\vartheta} := \beta_1\; \Delta\|t^{b\,trial}_{T_{n+\vartheta}}\| - \beta_2\; \mu(\alpha_{n+\vartheta})\; \Delta t_{N_{n+\vartheta}} \qquad (4.31)
$$

with

$$
\begin{aligned}
\beta_1 &:= \frac{\partial\alpha/\partial\gamma|_{n+\vartheta} + w\;\epsilon_T\;\gamma_{n+\vartheta}}{\epsilon_T + \partial\alpha/\partial\gamma|_{n+\vartheta}\;\partial_{\alpha}\mu(\alpha_{n+\vartheta})\;t_{N_{n+\vartheta}}} \\
\beta_2 &:= \frac{\partial\alpha/\partial\gamma|_{n+\vartheta}}{\epsilon_T + \partial\alpha/\partial\gamma|_{n+\vartheta}\;\partial_{\alpha}\mu(\alpha_{n+\vartheta})\;t_{N_{n+\vartheta}}}
\end{aligned}
\qquad (4.32)
$$

where

$$
\partial\alpha/\partial\gamma|_{n+\vartheta} := (1-w) + w\;\mu(\alpha_{n+\vartheta})\;t_{N\,n+\vartheta} - w\;\epsilon_T\;\gamma_{n+\vartheta} \qquad (4.33)
$$

REMARK 4.2. As it is clear from (4.30) the lack of symmetry of $\Xi_{\alpha\beta}$ arises from the variation of the surface metric in the reference configuration as the closest-point projection varies. As it was pointed out by LAURSEN & SIMO [1993,1994], a simple procedure to remove this non-symmetry is to use the metric at the center of the master element rather than at the reference placement of the current closest-point projection. □

4.3. FE-implementation. Matrix form of the residual and tangent operator.

In what follows, attention will be restricted to the finite element discretization of the contact surfaces, leading to the matrix form of the frictional contact residual and tangent operators.

Let n_{sele} and n_{mele} the total number of slave and master elements, n_{snod} and n_{mnod} the total number of slave and master nodes in a triangularization of the slave and master contact surfaces, respectively, and n^{e}_{snod} and n^{e}_{mnod} the number of nodes in a generic slave

and master surface elements $\Gamma_e^{(1)h}$ and $\Gamma_e^{(2)h}$, labeled as $\{\boldsymbol{X}_a^e \in \mathbb{R}^{n_{dim}} : a = 1, \ldots, n_{snod}^e\}$ and $\{\boldsymbol{Y}_a^e \in \mathbb{R}^{n_{dim}} : a = 1, \ldots, n_{mnod}^e\}$, respectively.

This local numbering system is related to the global numbering system via the following standard convention:

$$\begin{aligned} \boldsymbol{X}_A &= \boldsymbol{X}_a^e \quad \text{with } A = ID_s^{(1)}(e,a),\ e = 1, \ldots, n_{sele},\quad A = 1, \ldots, n_{snod} \\ \boldsymbol{Y}_A &= \boldsymbol{Y}_a^e \quad \text{with } A = ID_s^{(2)}(e,a),\ e = 1, \ldots, n_{mele},\quad A = 1, \ldots, n_{mnod} \end{aligned} \tag{4.34}$$

where the $n_{sele} \times n_{snod}^e$ array $ID_s^{(1)}(\cdot,\cdot)$ and the $n_{mele} \times n_{mnod}^e$ array $ID_s^{(2)}(\cdot,\cdot)$ are defined by the geometry of the triangularization $\mathcal{T}^{(i)h}$. A rather convenient formulation of the Galerkin projection is achieved by writing the local polynomial basis as $\{N^a(\zeta)\}$, where $\zeta = (\zeta_1, \ldots, \zeta_{n_{dim}-1})$ are normalized coordinates with domain the unit square $\square$ in $\mathbb{R}^{n_{dim}-1}$ and introducing the isoparametric map:

$$\begin{aligned} \zeta \in \square \mapsto \boldsymbol{X}^h &:= \psi_0^{e(1)}(\zeta) = \sum_{a=1}^{n_{snod}^e} N^a(\zeta) \boldsymbol{X}_a^e \in \Gamma_e^{(1)} \\ \zeta \in \square \mapsto \boldsymbol{Y}^h &:= \psi_0^{e(2)}(\zeta) = \sum_{a=1}^{n_{mnod}^e} N^a(\zeta) \boldsymbol{Y}_a^e \in \Gamma_e^{(2)} \end{aligned} \tag{4.35}$$

where the local polynomial basis functions $N^a : \square \to \mathbb{R}$ are referred to as the local element shape functions and satisfy the completeness condition $N^a(\zeta_b) = \delta_b^a$, where $\zeta_a = (\zeta_{1\,a}, \ldots, \zeta_{n_{dim}-1\,a})$ are the vertices of the bi-unit square.

The Galerkin projection of the frictional contact contribution to the weak form given by (4.3) and to the bilinear form given by (4.4)-(4.6), can be written as the assembly of integrals over the n_{sele} slave surface elements of $\Gamma^{(1)h}$ as:

$$\begin{aligned} G_c(\varphi^h, \eta_0^h) &:= \bigcup_{e=1}^{n_{sele}} G_c^e(\varphi^h, \eta_0^h) \\ B_{\varphi_t^h}(\eta_0^h, \Delta\varphi^h) &:= \bigcup_{e=1}^{n_{sele}} B_{\varphi_t^h}^e(\eta_0^h, \Delta\varphi^h) \end{aligned} \tag{4.36}$$

where $G_c^e(\varphi^h, \eta_0^h)$ and $B_{\varphi_t^h}^e(\eta_0^h, \Delta\varphi^h)$ represent the frictional contact contribution to the weak form and bilinear form, over a typical slave element surface $\Gamma_e^{(1)h} \subset \Gamma^{(1)h}$, given by (4.3) and (4.4)-(4.6) with L_2-inner products over the element domain.

Numerical integration of these element frictional contact contributions leads to the following expressions:

$$\boxed{\begin{aligned} G_c^e(\varphi_e^h, \eta_{0\,e}^h) &:= -\sum_{i=1}^{n_{int}} W_i\ j(\zeta_i)\ \delta\boldsymbol{\Phi}_c^{e,i} \cdot \boldsymbol{R}_c^{e,i} \\ B_{\varphi_t^h}^e(\eta_0^h, \Delta\varphi^h) &:= \sum_{i=1}^{n_{int}} W_i\ j(\zeta_i)\ \delta\boldsymbol{\Phi}_c^{e,i} \cdot \boldsymbol{K}_c^{e,i} \cdot \Delta\boldsymbol{\Phi}_c^{e,i} \end{aligned}} \tag{4.37}$$

where n_{int} is the number of integration points to be used in the quadrature rule over the domain $\Gamma_e^{(1)h}$, W_i is the weight of the quadrature point ζ_i, $j(\zeta_i) = \|\boldsymbol{X}_{,1}(\zeta_i) \times \boldsymbol{X}_{,2}(\zeta_i)\|$, where $\boldsymbol{X}_{,\alpha} = d\boldsymbol{X}/d\zeta^\alpha$, $\alpha = 1, 2$, is the jacobian of the isoparametric map at the quadrature point ζ_i, $\delta\boldsymbol{\Phi}_c^{e,i}$ and $\Delta\boldsymbol{\Phi}_c^{e,i}$ are vectors of involved nodal variations corresponding to the quadrature point i of element e, and $\boldsymbol{R}_c^{e,i}$ and $\boldsymbol{K}_c^{e,i}$ are the frictional contact local element residual vector and tangent matrix corresponding to the quadrature point i, respectively.

REMARK 4.3. As it is evident from (4.37), the element residual and tangent finite element operators have been organized by (slave) quadrature point rather than by (slave) element. This scheme proves to be more convenient, taking into account that each (slave) quadrature point may involve degrees-of-freedom of (master) nodes of different (master) elements. Finite element operators associated to a typical (slave) quadrature point in a typical (slave) element, will involve the dof's of the (slave) nodes of its (slave) element and the dof's of the (master) nodes of the (master) element containing the contact point. On the other hand, finite element operators associated to a typical (slave) element, will involve the dof's of the (slave) nodes of its (slave) element and the dof's of the (master) nodes of the, possibly different, (master) elements containing each one of the contact points associated to each (slave) quadrature point. □

REMARK 4.4. Associated to each (slave) quadrature point we define a *contact element* involving degrees-of-freedom of the slave and master surface elements. When nodal quadrature points are used, the contact element will involves the degrees-of-freedom of the slave node and the degrees-of-freedom of the master element surface containing the closest-point projection. When a different quadrature rule is used, the contact element will involves all the degrees-of-freedom of the slave and master surface elements. □

(A) *Application: Residual and tangent operator for a n-node 3D surface element discretization.* In this section we will present the finite element implementation of the frictional contact model, assuming an arbitrary n-node finite element 3D spatial discretization of contact (master) surfaces. Furthermore, we will assume that nodal quadrature is used to define (4.37).

In what follows, we will restrict our attention to a typical slave quadrature point, i.e. a slave node using nodal quadrature, with current placement denoted as $\boldsymbol{x}$ and to the n-node master element surface containing its projection $\bar{\boldsymbol{y}} \in \gamma^{(2)h}$, denoted as $\gamma_e^{(2)h}$. It is assumed that the projection point $\bar{\boldsymbol{y}}$ lies in the interior domain of the surface element $\gamma_e^{(2)h}$.

We will denote as *contact element* the set of nodes consisting of the slave node (playing the role of quadrature point) and the n-master nodes defining the surface element $\gamma_e^{(2)h}$. Associated to each contact element we define the vectors of nodal variations $\delta\boldsymbol{\Phi}_c$ and $\Delta\boldsymbol{\Phi}_c$ containing the variation of the slave (quadrature) node, denoted as $\delta\boldsymbol{d}_s$ and $\Delta\boldsymbol{d}_s$ respectively, and those of the n-master nodes in $\gamma_e^{(2)h}$, denoted as $\delta\boldsymbol{d}_a$ and $\Delta\boldsymbol{d}_a$,

$a = 1, \ldots, n$, respectively, as

$$\delta \boldsymbol{\Phi}_c := \left\{ \begin{array}{c} \delta \boldsymbol{d}_s \\ \delta \boldsymbol{d}_1 \\ \cdot \\ \cdot \\ \delta \boldsymbol{d}_n \end{array} \right\}, \qquad \Delta \boldsymbol{\Phi}_c := \left\{ \begin{array}{c} \Delta \boldsymbol{d}_s \\ \Delta \boldsymbol{d}_1 \\ \cdot \\ \cdot \\ \Delta \boldsymbol{d}_n \end{array} \right\} \tag{4.38}$$

Furthermore we introduce the following operators

$$\boldsymbol{N} = \left\{ \begin{array}{c} \boldsymbol{\nu} \\ -N_1(\bar{\xi})\, \boldsymbol{\nu} \\ \cdot \\ \cdot \\ -N_n(\bar{\xi})\, \boldsymbol{\nu} \end{array} \right\}, \quad \boldsymbol{T}_\alpha = \left\{ \begin{array}{c} \boldsymbol{\tau}_\alpha \\ -N_1(\bar{\xi})\, \boldsymbol{\tau}_\alpha \\ \cdot \\ \cdot \\ -N_n(\bar{\xi})\, \boldsymbol{\tau}_\alpha \end{array} \right\}, \quad \boldsymbol{N}_\alpha = \left\{ \begin{array}{c} 0 \\ -N_{1,\alpha}(\bar{\xi})\, \boldsymbol{\nu} \\ \cdot \\ \cdot \\ -N_{n,\alpha}(\bar{\xi})\, \boldsymbol{\nu} \end{array} \right\}, \tag{4.39}$$

where $\alpha = 1, 2$, and N_a, $a = 1, \ldots, n$ are the standard isoparametric shape functions of the arbitrary n-node element. Using the operators introduced above, we also define:

$$\begin{aligned} \boldsymbol{D}^\alpha &:= A^{\alpha\beta}(\boldsymbol{T}_\beta + g_N \boldsymbol{N}_\beta) \\ \bar{\boldsymbol{N}}_\alpha &:= \boldsymbol{N}_\alpha - \kappa_{\alpha\beta} \boldsymbol{D}^\beta \end{aligned} \tag{4.40}$$

where the indices α and β ranges from 1 to 2 and the summatory on repeated indices is assumed. Here, $A^{\alpha\beta}$ are the components of the inverse of matrix $\boldsymbol{A}$ defined in (3.67).

With the preceding notation in hand, and using the key discrete relations,

$$\begin{aligned} \delta g_N^h &:= -\boldsymbol{N} \cdot \delta \boldsymbol{\Phi}_c \\ \delta \bar{\xi}^{\alpha h} &:= \boldsymbol{D}^\alpha \cdot \delta \boldsymbol{\Phi}_c \end{aligned} \tag{4.41}$$

the frictional contact residual $\boldsymbol{R}_c$ takes the expression,

$$\boxed{\boldsymbol{R}_c := t_N\, \boldsymbol{N} - t_{T\alpha} \boldsymbol{D}^\alpha} \tag{4.42}$$

where $\alpha = 1, 2$.

The frictional contact tangent operator can be split into the *normal* and *tangent* contributions.

$$\boldsymbol{K}_c := \boldsymbol{K}_{c_N} + \boldsymbol{K}_{c_T} \tag{4.43}$$

Additionally, from the *material* and *geometric* terms in the bilinear form (4.4), the normal contact and frictional tangent operators, can be split as

$$\begin{aligned} \boldsymbol{K}_{c_N} &:= \boldsymbol{K}_{c_N}^{mat} + \boldsymbol{K}_{c_N}^{geo} \\ \boldsymbol{K}_{c_T} &:= \boldsymbol{K}_{c_T}^{mat} + \boldsymbol{K}_{c_T}^{geo} \end{aligned} \tag{4.44}$$

where $\boldsymbol{K}_{c_N}^{mat}$ and $\boldsymbol{K}_{c_N}^{geo}$ are the material and geometric contributions to the normal contact tangent operator, respectively, and $\boldsymbol{K}_{c_T}^{mat}$ and $\boldsymbol{K}_{c_T}^{geo}$ are the material and geometric contributions to the frictional tangent operator, respectively.

Using the operators defined above, the normal contact tangent operators can be written as

$$\boxed{\begin{aligned} \boldsymbol{K}_{c_N}^{mat} &:= \epsilon_N H(g_N)\ \boldsymbol{N} \otimes \boldsymbol{N} \\ \boldsymbol{K}_{c_N}^{geo} &:= t_N\ [g_N\ m^{\alpha\beta} \bar{\boldsymbol{N}}_\alpha \otimes \bar{\boldsymbol{N}}_\beta - (\boldsymbol{D}^\alpha \otimes \boldsymbol{N}_\alpha + \boldsymbol{N}_\alpha \otimes \boldsymbol{D}^\alpha) + \kappa_{\alpha\beta} \boldsymbol{D}^\alpha \otimes \boldsymbol{D}^\beta] \end{aligned}} \tag{4.45}$$

To define the frictional tangent operators, we introduce first the following operators:

$$\begin{aligned} \boldsymbol{T}_{\alpha\beta} &:= [0^T,\ -N_{1,\beta}(\bar{\xi})\ \boldsymbol{\tau}_\alpha^T,\ \ldots,\ -N_{n,\beta}(\bar{\xi})\ \boldsymbol{\tau}_\alpha^T]^T \\ \boldsymbol{N}_{\alpha\beta} &:= [0^T,\ -N_{1,\alpha\beta}(\bar{\xi})\boldsymbol{\nu}^T,\ \ldots,\ -N_{n,\alpha\beta}(\bar{\xi})\boldsymbol{\nu}^T]^T \\ \boldsymbol{P}_\alpha &:= [0^T,\ -N_{1,\alpha}(\bar{\xi})\ \boldsymbol{p}_T^{\flat T},\ \ldots,\ -N_{n,\alpha}(\bar{\xi})\ \boldsymbol{p}_T^{\flat T}]^T \end{aligned} \tag{4.46}$$

where $\alpha, \beta = 1, 2$, and the shape functions are evaluated at $\bar{\xi}$. Based on the definitions (4.34),(4.35) and (4.41), we introduce the additional operators

$$\begin{aligned} \bar{\boldsymbol{T}}_{\alpha\beta} &:= \boldsymbol{T}_{\alpha\beta} - (e_{\beta,\gamma}(\bar{\xi}) \cdot \boldsymbol{\tau}_\alpha)\boldsymbol{D}^\gamma \\ \bar{\boldsymbol{P}}_\alpha &:= \boldsymbol{P}_\alpha\ - (e_{\alpha,\gamma}(\bar{\xi}) \cdot \boldsymbol{p}_T^\flat)\boldsymbol{D}^\gamma \\ \hat{\boldsymbol{T}}_{\alpha\beta} &:= \boldsymbol{T}_{\alpha\beta} + g_N \boldsymbol{N}_{\alpha\beta} \\ \hat{\boldsymbol{D}}^\alpha &:= \boldsymbol{D}^\alpha - m^{\alpha\beta}\boldsymbol{T}_\beta \end{aligned} \tag{4.47}$$

where $\alpha, \beta = 1, 2$

With the preceding definitions in hand, using (4.37) and the key expressions

$$\begin{aligned} (\delta\boldsymbol{\varphi}^{(1)h} - \delta\boldsymbol{\varphi}^{(2)h}) \cdot \boldsymbol{\tau}_\alpha &:= \boldsymbol{T}_\alpha \cdot \delta\boldsymbol{\Phi}_c \\ \delta\boldsymbol{\varphi}_{,\alpha}^{(2)h} \cdot \boldsymbol{\nu} &:= -\boldsymbol{N}_\alpha \cdot \delta\boldsymbol{\Phi}_c \\ \delta\boldsymbol{\varphi}_{,\alpha}^{(2)h} \cdot \boldsymbol{\tau}_\beta &:= -\boldsymbol{T}_{\beta\alpha} \cdot \delta\boldsymbol{\Phi}_c \\ \delta\boldsymbol{\varphi}_{,\alpha\beta}^{(2)h} \cdot \boldsymbol{\nu} &:= -\boldsymbol{N}_{\alpha\beta} \cdot \delta\boldsymbol{\Phi}_c \end{aligned} \tag{4.48}$$

the geometric part of the frictional tangent operator can be written as

$$\boxed{\begin{aligned} \boldsymbol{K}_{c_T}^{geo} &:= t_{T_\alpha} A^{\alpha\beta} \boldsymbol{K}_{c_{T\beta}}^{geo} \\ \boldsymbol{K}_{c_{T\alpha}}^{geo} &:= \hat{\boldsymbol{T}}_{\alpha\beta} \otimes \boldsymbol{D}^\beta + \boldsymbol{D}^\beta \otimes \hat{\boldsymbol{T}}_{\alpha\beta} \\ &\quad + \hat{\boldsymbol{D}}^\beta \otimes \bar{\boldsymbol{T}}_{\beta\alpha} + \bar{\boldsymbol{T}}_{\beta\alpha} \otimes \hat{\boldsymbol{D}}^\beta \\ &\quad - (\boldsymbol{N} \otimes \bar{\boldsymbol{N}}_\alpha + \bar{\boldsymbol{N}}_\alpha \otimes \boldsymbol{N}) \\ &\quad - (e_{\beta,\gamma}(\bar{\xi}) \cdot \boldsymbol{\tau}_\alpha + g_N\ e_{\alpha,\beta\gamma}(\bar{\xi}) \cdot \boldsymbol{\nu})\ \boldsymbol{D}^\beta \otimes \boldsymbol{D}^\gamma \end{aligned}} \tag{4.49}$$

The material part of the frictional tangent operator will depend of the slip/stick frictional state. Using the above definitions, the *stick* material frictional tangent operator, denoted

as $\boldsymbol{K}_{c_T}^{mat,stick}$ and the *slip* material frictional tangent operator, denoted as $\boldsymbol{K}_{c_T}^{mat,slip}$, can be written as

$$\boxed{\begin{aligned}\boldsymbol{K}_{c_T}^{mat,stick} &:= \Xi_{\alpha\beta}\ \boldsymbol{D}^{\alpha}\otimes\boldsymbol{D}^{\beta}\\ \boldsymbol{K}_{c_T}^{mat,slip} &:= -(1-\bar{\beta}_2)\ \mu(\alpha)\ \epsilon_N\ H(g_N)\ p_{T_\alpha}\ \boldsymbol{D}^{\alpha}\otimes\boldsymbol{N}\\ &\quad+[\frac{\mu(\alpha)\ t_N}{\|\boldsymbol{t}_T^{trial}\|}(\delta_\alpha^\gamma-\pi_\alpha^\gamma)+\bar{\beta}_1\ \pi_\alpha^\gamma]\ \Xi_{\gamma\beta}\ \boldsymbol{D}^{\alpha}\otimes\boldsymbol{D}^{\beta}\\ &\quad-[\mu(\alpha)\ t_N-\frac{\bar{\beta}_1}{\|\boldsymbol{t}_T^{trial}\|}]\ \pi_\alpha^\beta\ \boldsymbol{D}^{\alpha}\otimes\bar{\boldsymbol{P}}_{\beta}\end{aligned}} \tag{4.50}$$

where $\bar{\beta}_1 := \beta_1\ \partial_\alpha\mu(\alpha)\ t_N$ and $\bar{\beta}_2 := \beta_2\ \partial_\alpha\mu(\alpha)\ t_N$ and β_1 and β_2 are given in (4.32).

REMARK 4.5. *Bi-linear surface elements.* Note that for the particular case of 4-node bi-linear surface finite elements, $\boldsymbol{N}_{\alpha\beta}=0$ for $\alpha=\beta$, $\boldsymbol{e}_{\alpha,\beta}=0$ for $\alpha=\beta$, $\boldsymbol{e}_{\alpha,\beta\gamma}=0$ for any α,β,γ, $\boldsymbol{E}_{\alpha,\beta}=0$ for $\alpha=\beta$ and the components of the *non-symmetric* operator $\Xi_{\alpha\beta}$ $(4.30)_1$ take the form:

$$\begin{aligned}\Xi_{11} &:= \epsilon_T\ (M_{11}+\lambda_1 g_T^2)\\ \Xi_{12} &:= \epsilon_T\ (M_{12}+2\lambda_1 g_T^1+\lambda_2 g_T^2)\\ \Xi_{21} &:= \epsilon_T\ (M_{21}+\lambda_1 g_T^1+2\lambda_2 g_T^2)\\ \Xi_{22} &:= \epsilon_T\ (M_{22}+\lambda_2 g_T^1)\end{aligned} \tag{4.51}$$

where the short hand notation $\lambda_\alpha := \boldsymbol{E}_{1,2}(\bar{\boldsymbol{\xi}})\cdot\boldsymbol{\tau}_\alpha^{ref}$ and $g_T^\alpha := \bar{\xi}_{n+\vartheta}^\alpha - \bar{\xi}_n^\alpha$ has been introduced. In the above expressions, greek indices α,β,γ varies from 1 to 2. □

(B) *Application: Residual and tangent operator for a n-node 2D surface element discretization.* Here we will present the finite element implementation of the frictional contact model, assuming an arbitrary n-node finite element 2D spatial discretization of contact (master) surfaces. Furthermore, we will assume that nodal quadrature is used to define (4.37).

In what follows, we will restrict our attention to a typical slave quadrature point, i.e. a slave node using nodal quadrature, with current placement denoted as $\boldsymbol{x}$ and to the n-node master element surface containing its projection $\bar{\boldsymbol{y}}\in\gamma^{(2)h}$, denoted as $\gamma_e^{(2)h}$. It is assumed that the projection point $\bar{\boldsymbol{y}}$ lies in the interior domain of the surface element $\gamma_e^{(2)h}$.

We will denote as *contact element* the set of nodes consisting of the slave node (playing the role of quadrature point) and the n-master nodes defining the surface element $\gamma_e^{(2)h}$. Associated to each contact element we define the vectors of nodal variations $\delta\boldsymbol{\Phi}_c$ and $\Delta\boldsymbol{\Phi}_c$ containing the variation of the slave (quadrature) node, denoted as $\delta\boldsymbol{d}_s$ and $\Delta\boldsymbol{d}_s$ respectively, and those of the n-master nodes in $\gamma_e^{(2)h}$, denoted as $\delta\boldsymbol{d}_a$ and $\Delta\boldsymbol{d}_a$,

$a = 1, \ldots, n$, respectively, as

$$\delta \boldsymbol{\Phi}_c := \begin{Bmatrix} \delta \boldsymbol{d}_s \\ \delta \boldsymbol{d}_1 \\ \cdot \\ \cdot \\ \delta \boldsymbol{d}_n \end{Bmatrix}, \qquad \Delta \boldsymbol{\Phi}_c := \begin{Bmatrix} \Delta \boldsymbol{d}_s \\ \Delta \boldsymbol{d}_1 \\ \cdot \\ \cdot \\ \Delta \boldsymbol{d}_n \end{Bmatrix} \tag{4.52}$$

Furthermore we introduce the following operators

$$\boldsymbol{N} = \begin{Bmatrix} \boldsymbol{\nu} \\ -N_1(\bar{\xi})\ \boldsymbol{\nu} \\ \cdot \\ \cdot \\ -N_n(\bar{\xi})\ \boldsymbol{\nu} \end{Bmatrix}, \quad \boldsymbol{T}_1 = \begin{Bmatrix} \boldsymbol{\tau}_1 \\ -N_1(\bar{\xi})\ \boldsymbol{\tau}_1 \\ \cdot \\ \cdot \\ -N_n(\bar{\xi})\ \boldsymbol{\tau}_1 \end{Bmatrix}, \quad \boldsymbol{N}_1 = \begin{Bmatrix} 0 \\ -N_{1,1}(\bar{\xi})\ \boldsymbol{\nu} \\ \cdot \\ \cdot \\ -N_{n,1}(\bar{\xi})\ \boldsymbol{\nu} \end{Bmatrix}, \tag{4.53}$$

where N_a, $a = 1, \ldots, n$, are the standard isoparametric shape functions of the arbitrary n-node element. Using the operators introduced above, we also define:

$$\begin{aligned} \boldsymbol{D}^1 &:= A^{11}(\boldsymbol{T}_1 + g_N \boldsymbol{N}_1) \\ \bar{\boldsymbol{N}}_1 &:= \boldsymbol{N}_1 - \kappa_{11} \boldsymbol{D}^1 \end{aligned} \tag{4.54}$$

were, A^{11} is the inverse of $A_{11} = m_{11} + g_N\ \kappa_{11}$.

With the preceding notation in hand, and using the key discrete relations,

$$\begin{aligned} \delta g_N^h &:= -\boldsymbol{N} \cdot \delta \boldsymbol{\Phi}_c \\ \delta \bar{\xi}^{1h} &:= \boldsymbol{D}^1 \cdot \delta \boldsymbol{\Phi}_c \end{aligned} \tag{4.55}$$

the frictional contact residual $\boldsymbol{R}_c$ takes the expression,

$$\boxed{\boldsymbol{R}_c := t_N\ \boldsymbol{N} - t_{T_1} \boldsymbol{D}^1} \tag{4.56}$$

The frictional contact tangent operator can be split into the *normal* and *tangent* contributions.

$$\boldsymbol{K}_c := \boldsymbol{K}_{c_N} + \boldsymbol{K}_{c_T} \tag{4.57}$$

Additionally, from the *material* and *geometric* terms in the bilinear form (4.4), the normal contact and frictional tangent operators, can be split as

$$\begin{aligned} \boldsymbol{K}_{c_N} &:= \boldsymbol{K}_{c_N}^{mat} + \boldsymbol{K}_{c_N}^{geo} \\ \boldsymbol{K}_{c_T} &:= \boldsymbol{K}_{c_T}^{mat} + \boldsymbol{K}_{c_T}^{geo} \end{aligned} \tag{4.58}$$

where $\boldsymbol{K}_{c_N}^{mat}$ and $\boldsymbol{K}_{c_N}^{geo}$ are the material and geometric contributions to the normal contact tangent operator, respectively, and $\boldsymbol{K}_{c_T}^{mat}$ and $\boldsymbol{K}_{c_T}^{geo}$ are the material and geometric contributions to the frictional tangent operator, respectively.

Using the operators defined above, the normal contact tangent operators can be written as

$$\boxed{\begin{aligned} \boldsymbol{K}_{c_N}^{mat} &:= \epsilon_N H(g_N)\ \boldsymbol{N} \otimes \boldsymbol{N} \\ \boldsymbol{K}_{c_N}^{geo} &:= t_N\ [g_N\ m^{11} \bar{\boldsymbol{N}}_1 \otimes \bar{\boldsymbol{N}}_1 - (\boldsymbol{D}^1 \otimes \boldsymbol{N}_1 + \boldsymbol{N}_1 \otimes \boldsymbol{D}^1) + \kappa_{11} \boldsymbol{D}^1 \otimes \boldsymbol{D}^1] \end{aligned}} \tag{4.59}$$

To define the frictional tangent operators, we introduce first the following operators:

$$\begin{aligned} \boldsymbol{T}_{11} &:= [0^T,\ -N_{1,1}(\bar{\xi})\ \boldsymbol{\tau}_1^T,\ \ldots,\ -N_{n,1}(\bar{\xi})\ \boldsymbol{\tau}_1^T]^T \\ \boldsymbol{N}_{11} &:= [0^T,\ -N_{1,11}(\bar{\xi}) \boldsymbol{\nu}^T,\ \ldots,\ -N_{n,11}(\bar{\xi}) \boldsymbol{\nu}^T]^T \\ \boldsymbol{P}_1 &:= [0^T,\ -N_{1,1}(\bar{\xi})\ \boldsymbol{p}_T^{\flat T},\ \ldots,\ -N_{n,1}(\bar{\xi})\ \boldsymbol{p}_T^{\flat T}]^T \end{aligned} \tag{4.60}$$

where the shape functions are evaluated at $\bar{\xi}$. Based on the definitions (4.34),(4.35) and (4.55), we introduce the additional operators

$$\begin{aligned} \bar{\boldsymbol{T}}_{11} &:= \boldsymbol{T}_{11} - (\boldsymbol{e}_{1,1}(\bar{\xi}) \cdot \boldsymbol{\tau}_1) \boldsymbol{D}^1 \\ \bar{\boldsymbol{P}}_1 &:= \boldsymbol{P}_1 - (\boldsymbol{e}_{1,1}(\bar{\xi}) \cdot \boldsymbol{p}_T^{\flat}) \boldsymbol{D}^1 \\ \hat{\boldsymbol{T}}_{11} &:= \boldsymbol{T}_{11} + g_N \boldsymbol{N}_{11} \\ \hat{\boldsymbol{D}}^1 &:= \boldsymbol{D}^1 - m^{11} \boldsymbol{T}_1 \end{aligned} \tag{4.61}$$

With the preceding notation in hand, and using the key discrete relations,

$$\begin{aligned} (\delta\varphi^{(1)h} - \delta\varphi^{(2)h}) \cdot \boldsymbol{\tau}_1 &:= \boldsymbol{T}_1 \cdot \delta\boldsymbol{\Phi}_c \\ \delta\varphi_{,1}^{(2)h} \cdot \boldsymbol{\nu} &:= -\boldsymbol{N}_1 \cdot \delta\boldsymbol{\Phi}_c \\ \delta\varphi_{,1}^{(2)h} \cdot \boldsymbol{\tau}_1 &:= -\boldsymbol{T}_{11} \cdot \delta\boldsymbol{\Phi}_c \\ \delta\varphi_{,11}^{(2)h} \cdot \boldsymbol{\nu} &:= -\boldsymbol{N}_{11} \cdot \delta\boldsymbol{\Phi}_c \end{aligned} \tag{4.62}$$

the geometric part of the frictional tangent operator can be written as

$$\boxed{\begin{aligned} \boldsymbol{K}_{c_T}^{geo} &:= t_{T_1} A^{11} \boldsymbol{K}_{c_{T1}}^{geo} \\ \boldsymbol{K}_{c_{T1}}^{geo} &:= \hat{\boldsymbol{T}}_{11} \otimes \boldsymbol{D}^1 + \boldsymbol{D}^1 \otimes \hat{\boldsymbol{T}}_{11} \\ &\quad + \hat{\boldsymbol{D}}^1 \otimes \bar{\boldsymbol{T}}_{11} + \bar{\boldsymbol{T}}_{11} \otimes \hat{\boldsymbol{D}}^1 \\ &\quad - (\boldsymbol{N} \otimes \bar{\boldsymbol{N}}_1 + \bar{\boldsymbol{N}}_1 \otimes \boldsymbol{N}) \\ &\quad - (\boldsymbol{e}_{1,1}(\bar{\xi}) \cdot \boldsymbol{\tau}_1 + g_N\ \boldsymbol{e}_{1,11}(\bar{\xi}) \cdot \boldsymbol{\nu})\ \boldsymbol{D}^1 \otimes \boldsymbol{D}^1 \end{aligned}} \tag{4.63}$$

The material part of the frictional tangent operator will depend of the slip/stick frictional state. Using the above definitions, the *stick* material frictional tangent operator, denoted

as $\boldsymbol{K}_{c_T}^{mat,stick}$ and the *slip* material frictional tangent operator, denoted as $\boldsymbol{K}_{c_T}^{mat,slip}$, can be written as

$$\boxed{\begin{aligned}\boldsymbol{K}_{c_T}^{mat,stick} &:= \Xi_{11}\ \boldsymbol{D}^1 \otimes \boldsymbol{D}^1 \\ \boldsymbol{K}_{c_T}^{mat,slip} &:= -(1-\bar{\beta}_2)\ \mu(\alpha)\ \epsilon_N\ H(g_N)\ p_{T_1}\ \boldsymbol{D}^1 \otimes \boldsymbol{N} \\ &\quad + \bar{\beta}_1\ \Xi_{11}\ \boldsymbol{D}^1 \otimes \boldsymbol{D}^1 \\ &\quad - [\mu(\alpha)\ t_N - \frac{\bar{\beta}_1}{\|\boldsymbol{t}_T^{trial}\|}]\ \boldsymbol{D}^1 \otimes \bar{\boldsymbol{P}}_1\end{aligned}} \tag{4.64}$$

where $\bar{\beta}_1 := \beta_1\ \partial_\alpha \mu(\alpha)\ t_N$ and $\bar{\beta}_2 := \beta_2\ \partial_\alpha \mu(\alpha)\ t_N$ and β_1 and β_2 are given in (4.32).

REMARK 4.6. *Linear surface elements.* Note that for the particular case of 2-node linear surface finite elements, $N_{11} = 0$, $e_{1,1} = 0$, $\kappa_{11} = 0$, $e_{1,11} = 0$, $E_{1,1} = 0$, $A^{11} = m^{11}$ and $\Xi_{11} := \epsilon_T\ M_{11}$. □

5. Numerical Simulations.

The formulation presented in the preceding sections is illustrated below in a number of numerical simulations. The goals are to provide a practical accuracy assessment of the frictional wear model and to demonstrate the robustness of the overall frictional contact formulation in different numerical simulations and particularly in metal forming operations. The calculations are performed with an enhanced version of the finite element program FEAP developed by R.L. Taylor and J.C. Simo and documented in ZIENKIEWICZ & TAYLOR [1991].

(A) *Draw Bead Simulator.* This example is concerned with the simulation of a draw bead in a deep drawing sheet metal forming process. An initially flat Galvannealed (GA) sheet metal strip will be draw through a set of rollers. The material properties for the GA sheet metal strip were taken as bulk modulus $K = 171.6$ GPa, shear modulus $G = 79.2$ GPa and a power hardening law given by the Swift equation

$$\sigma_Y = 536.0\ (0.0033 + \bar{\varepsilon}^p)^{0.21}\ \text{MPa} \tag{5.1}$$

The rollers were considered as rigid surfaces. Frictional wear phenomena at the interfaces, between the GA metal sheet and the rigid rollers, was modeled using a frictional softening curve defined in terms of the frictional dissipation α as

$$\mu = 0.078 - 0.666 \cdot 10^{-2}\ \alpha \tag{5.2}$$

where α is measured in KN/cm. The strip was 1 mm thick and measured 70 mm length. The three main rollers and the two guide rollers were of radius 5 and 2 mm, respectively. The separation between the three main rollers was 11 mm and the upper main roller was positioned at a distance of 20 mm from the right edge of the strip. The distance between the upper main roller and the two guide rollers was 14 and 24 mm, respectively. FIGURE

5.1 shows the initial geometry of the test. Plane strain conditions have been assumed and only a half part of each roller has been discretized. The loading process consist of two phases. In the first phase, the main upper roller goes down up to a distance of 6.35 mm while the right edge of the strip is kept fixed, creating a situation of three point bending load. This first phase simulates the clamping of the sheet by the blankholder at the beginning of a deep drawing process. In the second phase, the rollers are kept fixed and the strip is pulled out from the right edge up to a final distance of 15 mm.

The geometry of the problem was modeled with 140 continuum elements being utilized for the discretization of the strip, using 2 elements accros the thickness, and 20 elements being used for the discretization of each of the rollers. A mixed Q1/P0 finite element formulation at finite strains was used for the discretization of the strip. Frictional contact constraints were regularized by means of penalty method and the normal and tangential penalty parameters were taken as $\varepsilon_N = 5 \cdot 10^{11}$ N/m^3 and $\varepsilon_T = 1 \cdot 10^{10}$ N/m^3, respectively. The loading process was achieved in 170 time steps, 20 steps for the first phase and 150 time steps for the second phase, through displacement control of the upper main roller and the right edge of the strip. The Newton-Raphson method, combined with a line search optimization procedure, was used to solve the nonlinear system of equations arising form the spatial and temporal discretization of the weak form of the momentum balance equation. Convergence of the incremental iterative solution procedure was monitored by requiring a tolerance of 10^{-18} in the energy norm.

The analysis was performed in a Silicon Graphics Power Challenge L Workstation and it was accomplished in 34 min CPU time. Table V.1 shows the Euclidean norm of the residual at four typical time steps.

Table V.1. Draw bead simulator. Euclidean norm of the residual for four typical time steps.

Step 20	*Step* 70	*Step* 120	*Step* 170
1.86289E+07	1.88299E+07	1.88303E+07	1.88302E+07
2.75317E+05	2.27117E+05	2.26716E+05	2.26222E+05
5.26603E+04	1.18516E+04	4.50492E+04	4.29461E+04
3.24054E+04	2.99176E+03	2.21042E+04	1.07448E+04
2.23963E+03	2.33671E+01	1.70857E+03	1.09379E+03
8.16929E+02	2.15757E-04	2.32598E+02	9.72306E+00
3.16493E+02		1.21763E+02	9.63659E-04
1.18062E+02		1.97021E-01	
4.87770E-01		4.51680E-06	
1.00563E-05			

FIGURE 5.1 shows the initial geometry and deformed shapes of the strip at different stages of the process, corresponding to the end of the first phase, for a vertical displacement of 6.35 mm of the upper main roller, and to different prescribed displacements of 5, 10 and 15 of the right edge of the strip, during the second phase.

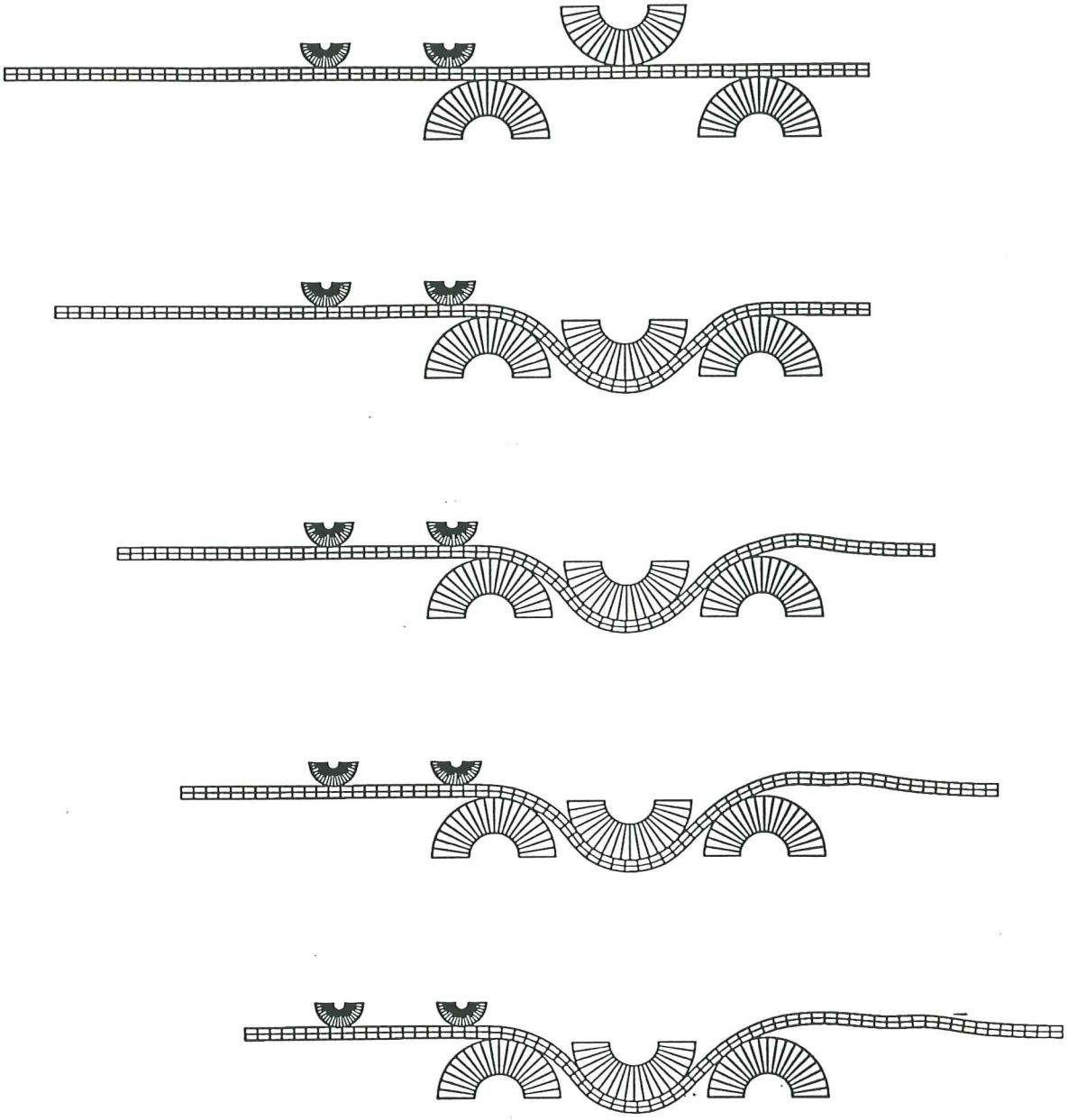

FIGURE 5.1. Draw Bead Simulator. Initial configuration and deformed shapes of the strip at five different stages of the process, corresponding to a displacement of the upper main roller of 6.350 mm, at the end of the first phase, and to prescribed displacements of 5, 10 and 15 mm of the right edge of the strip, during the second phase, respectively.

FIGURE 5.2 shows the evolution of the horizontal displacement of the left edge of the strip and the horizontal reaction at the right edge of the strip, during the loading process. FIGURE 5.3 shows the wear profiles on the main rollers at the same selected stages of the analysis of FIGURE 5.1.

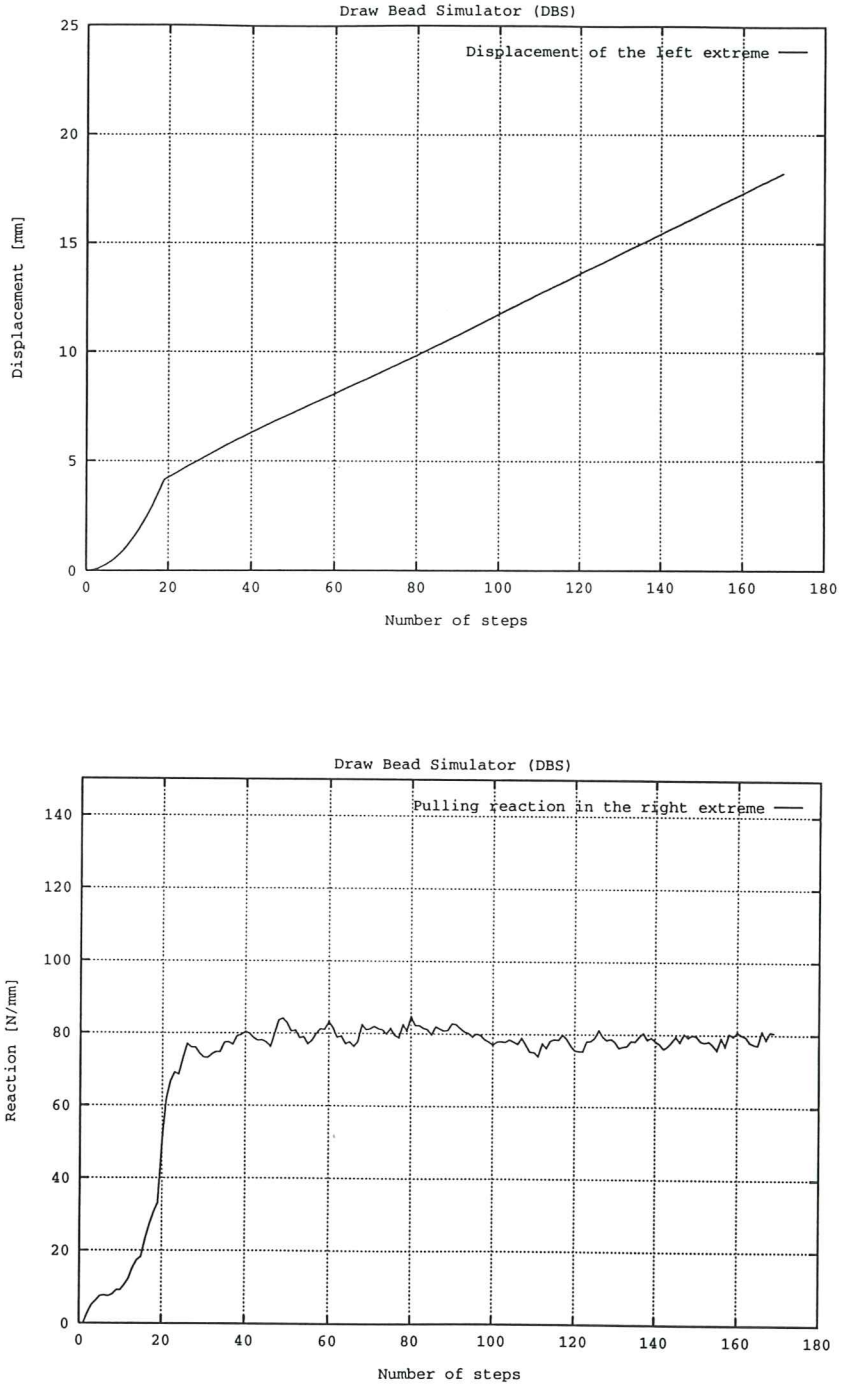

FIGURE 5.2. Draw Bead Simulator. Evolution of the horizontal displacement at the left edge of the strip and the horizontal reaction at the right edge of the strip, during the loading process.

FIGURE 5.3. Draw Bead Simulator. Wear profiles on the main rollers at different stages of the analysis. (a) At the end of the first phase for an upper main roller displacement of 6.350 mm. (b) For a right edge prescribed horizontal displacement of 5 mm, (c) 10 mm and (c) 15 mm, during the second phase.

(B) *Flat Sheet Sliding tests.* This example is taken from DE SOUZA NETO *et al.* [1995] and is concerned with the numerical simulation of flat sheet sliding tests. The experimental tests are as follows. A steel flat sheet is clamped to the sliding table. A precribed normal force is then applied to the tip of the tool material (SKD-11). The tip

is kept fixed during the experiment to avoid rotation and ensure high precision in the measurement of the friction coefficient. Once the normal force has been applied, the table slides 300 mm driven by a hydraulic cylinder. After sliding, the normal force is released and the table returns to its initial position. The normal force is then reapplied and the cycle is repeated a number of times.

Two zinc coated sheet metals, typically employed in the manufacture of automotive body shells, have been considered: Galvannealed (GA) and Electrogalvanised (EG) steel sheets. The mechanical properties for the GA and EG steel sheets are shown in Table V.2, where K is the bulk modulus, G is the shear modulus, YP is the initial yield stress, TS is the maximum tensile strength, EL is the elongation at rupture and n is the exponent of the power law hardening for plasticity. FIGURE 5.4 shows the hardening power law curves for the GA and EG steel sheets:

$$\begin{aligned} \sigma_Y &= 374.0 \cdot (0.054 + \bar{\varepsilon}^p)^{0.216} \quad \text{MPa} \quad \text{for the GA steel} \\ \sigma_Y &= 367.6 \cdot (0.041 + \bar{\varepsilon}^p)^{0.243} \quad \text{MPa} \quad \text{for the EG steel} \end{aligned} \tag{5.3}$$

Table V.2. Flat Sheet Sliding tests.
Mechanical properties for the GA and EG steel sheets.

Material	K (GPa)	G (GPa)	YP (MPa)	TS (MPa)	EL (%)	n
GA	171.6	79.2	199.1	319.3	42.7	0.216
EG	171.6	79.2	169.2	310.0	45.4	0.243

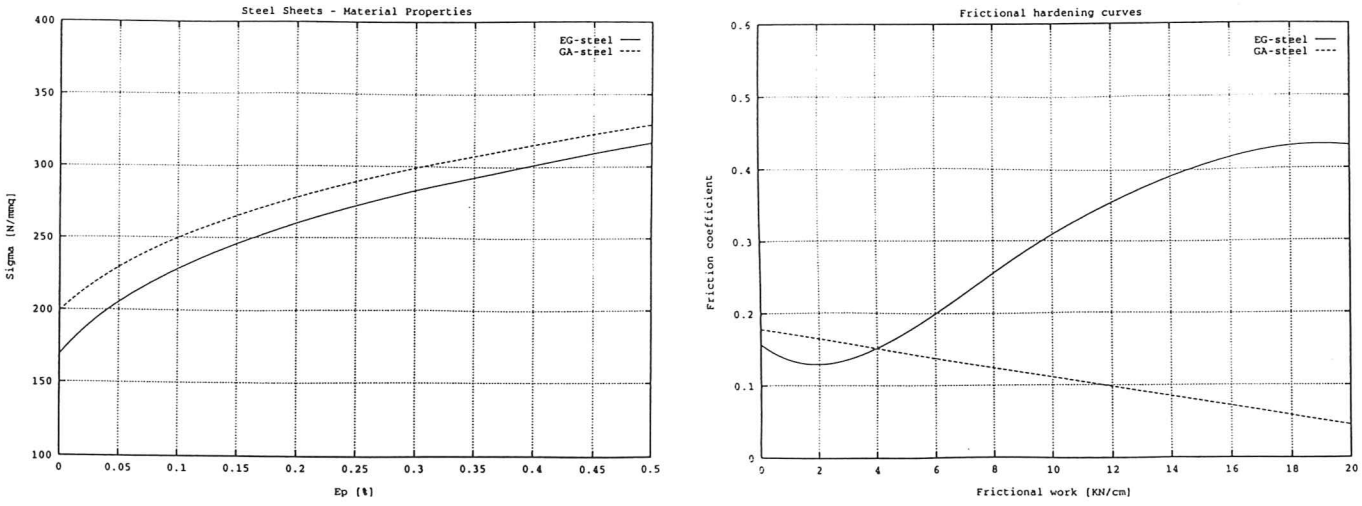

FIGURE 5.4. Flat Sheet Sliding tests. (a) Hardening plasticity laws for the GA and EG steel materials. (b) Frictional hardening laws for the GA and EG steel materials.

Frictional behavior was modeled as a polynomial function of the frictional dissipation α given by

$$\mu(\alpha) = a_0 + a_1\ \alpha + a_2\ \alpha^2 + \ldots + a_p\ \alpha^p \tag{5.4}$$

The presence of a hard surface coating, difficult to remove, in the GA steel sheet leads to a progressive softening of the frictional behavior. In contrast with this behavior, the EG steel sheet experiences an initial softening, due to flattening of microasperities, followed by a substantial increase of the friction coefficient, due to the removal of its relatively soft zinc coat. The coefficients of the frictional hardening law, for a frictional dissipation α measured in KN/mm, for the GA and EG steel sheets are shown in Table V.3. Frictional hardening behavior for the GA and EG steel sheets is shown in FIGURE 5.4.

Table V.3. Flat Sheet Sliding tests.
Frictional hardening law for the GA and EG steel sheets.
Coefficients of the polynomial function for frictional dissipation measured in KN/cm.

Material	a_0	a_1	a_2	a_3	a_4	a_5
GA	0.178	$-0.666 \cdot 10^{-2}$				
EG	0.157	$-0.315 \cdot 10^{-1}$	$0.104 \cdot 10^{-1}$	$-0.821 \cdot 10^{-3}$	$0.289 \cdot 10^{-4}$	$-0.410 \cdot 10^{-6}$

The sheet initially measured 400 mm long, 100 mm wide and 0.8 mm thick. The tip of the tool measured 10 mm long and 10 mm wide, with an inner radius of 2.5 mm at the bottom corner of the right edge. Then the tested surface at the experiment measured 300 mm long and 10 mm wide.

For simplicity, only 30 mm of the sheet length has been considered in the numerical simulation and a plane strain state has been assumed. The sliding cycle has been repeated 20 times for different compressive constant normal forces of 3.92, 2.94, 1.96 and 0.98 KN applieds to the tip of the tool.

A mesh of 111 four noded quadrilateral elements has been used for the discretization of the tool. The sheet has been discretized by two layers of 60 continuum elements and the nodes of its left edge have been considered as constrained. A mixed Q1/P0 finite element formulation at finite strain has been used. The table has been considered as rigid.

At the beginning of a sliding cycle, the tip lies at 2.5 mm from the left edge of the sheet. Starting from this initial configuration and after the normal force has been applied, a relative sliding of 20 mm between the table and the tip is incrementally imposed. This ensures an approximately 10 mm long evenly worn region on the sheet surface (between 12.5 mm and 22.5 mm from the left edge). Then the normal force is released, the tip is lifted up and returned to its initial position, thereby closing a cycle. Note that a steady state frictional force will occur when the entire surface of the tip contacts the evenly worn region of the sheet. The finite element mesh as well as the description of a sliding cycle is shown in FIGURE 5.5.

Frictional contact constraints were regularized by means of penalty method and the normal and tangential penalty parameters were taken as $\varepsilon_N = 5 \cdot 10^{11}$ N/m^3 and $\varepsilon_T =$

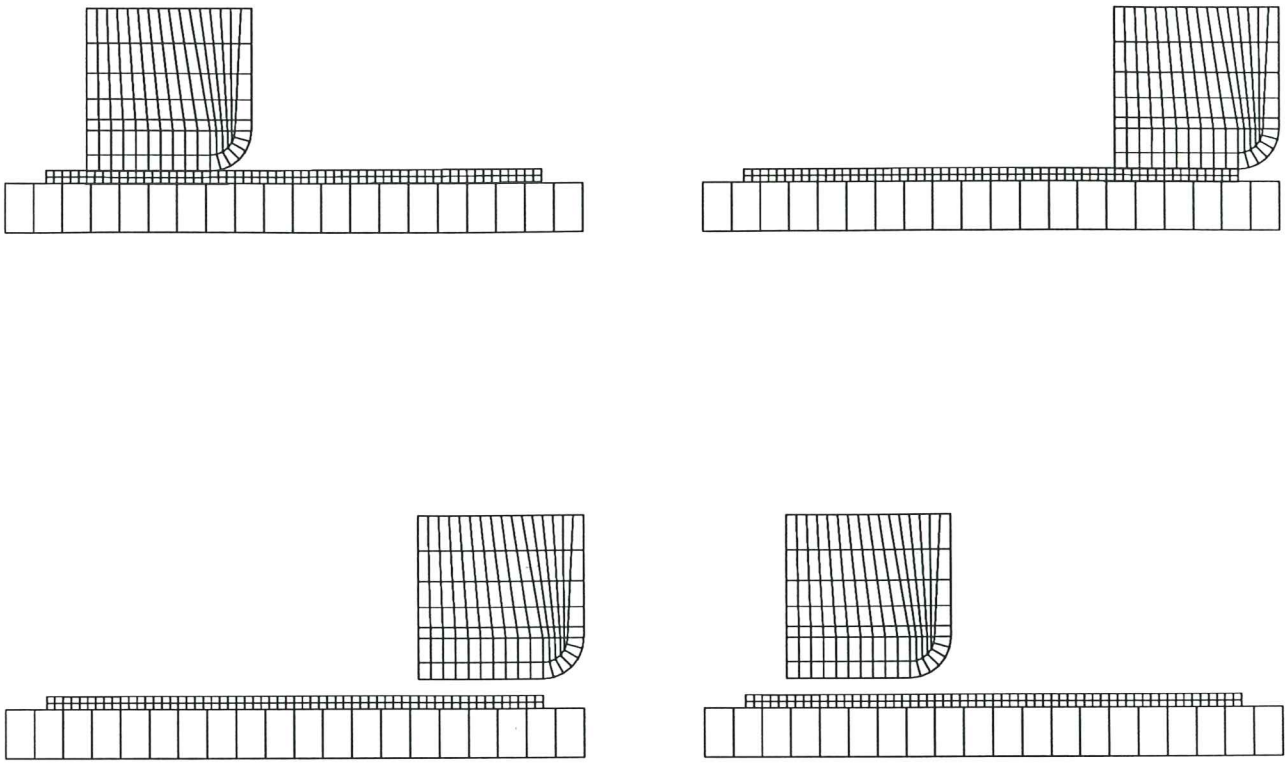

FIGURE 5.5. Flat Sheet Sliding tests. Finite element mesh and sliding cycle. (a) Initial configuration and application of normal force; (b) Sliding; (c) Release normal force, and (d) Return to initial configuration.

$1 \cdot 10^{10}$ N/m^3, respectively. A typical loading cycle was achieved in 30 time steps: 5 steps to applied the normal force, 20 steps for sliding and 5 steps to remove the normal force.

The Newton-Raphson method, combined with a line search optimization procedure, was used to solve the nonlinear system of equations arising form the spatial and temporal discretization of the weak form of the momentum balance equation. Convergence of the incremental iterative solution procedure was monitored by requiring a tolerance of 10^{-18} in the energy norm.

The analysis was performed in a Silicon Graphics Power Challenge L Workstation and a typical case, GA steel sheet using a normal force of 0.98 KN, was accomplished in 23 min CPU time. Table V.4 shows the Euclidean norm of the residual at four typical time steps, using a GA steel and a normal force of 0.98 KN. A typical intermediate step at different passes has been selected.

FIGURES 5.6 and 5.7 show the tangential forces obtained in the numerical analysis of the sliding tests, using GA steel and EG steel sheets, respectively, at different constant normal forces. In order to compare the results obtained in this work with the (average) experimental and numerical results given by DE SOUZA NETO *et al.* [1995], it is important to observe that one must consider only an average value within the central part of the sheet for each pass, in the evenly worn region, disregarding the values at the beginning and at

Table V.4. Flat Sheet Sliding tests.
Euclidean norm of the residual for four typical time steps.
GA steel sheet. Normal force of 0.98 KN.

Pass 1	*Pass* 5	*Pass* 10	*Pass* 15
1.23075E+09	1.23075E+09	1.23075E+09	1.23075E+09
4.70945E+04	4.70696E+04	4.70458E+04	4.70230E+04
1.23677E+04	1.23583E+04	1.23494E+04	1.23408E+04
8.04745E+02	8.01015E+02	7.97387E+02	7.93858E+02
1.21043E+02	1.22529E+02	1.23987E+02	1.25417E+02
2.20370E+00	2.26997E+00	2.33562E+00	2.40061E+00
7.13569E-06	6.83974E-06	6.70814E-06	8.21763E-06

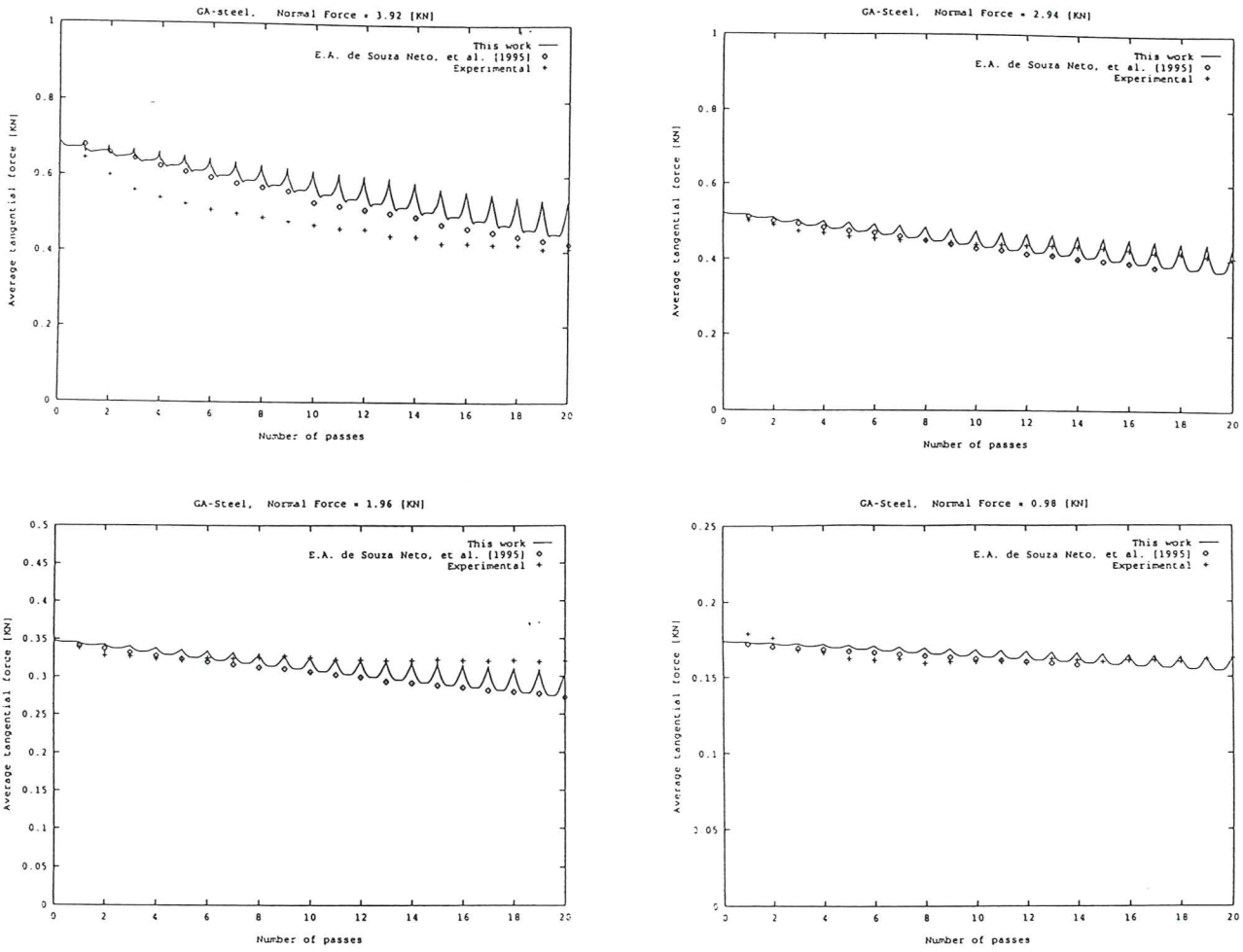

FIGURE 5.6. Flat Sheet Sliding tests. Tangential force versus number of passes during the sliding tests using a GA steel sheet at different constant normal forces: (a) Normal force = 3.92 KN; (b) Normal force = 2.94 KN; (c) Normal force = 1.96 KN; (d) Normal force = 0.98 KN.

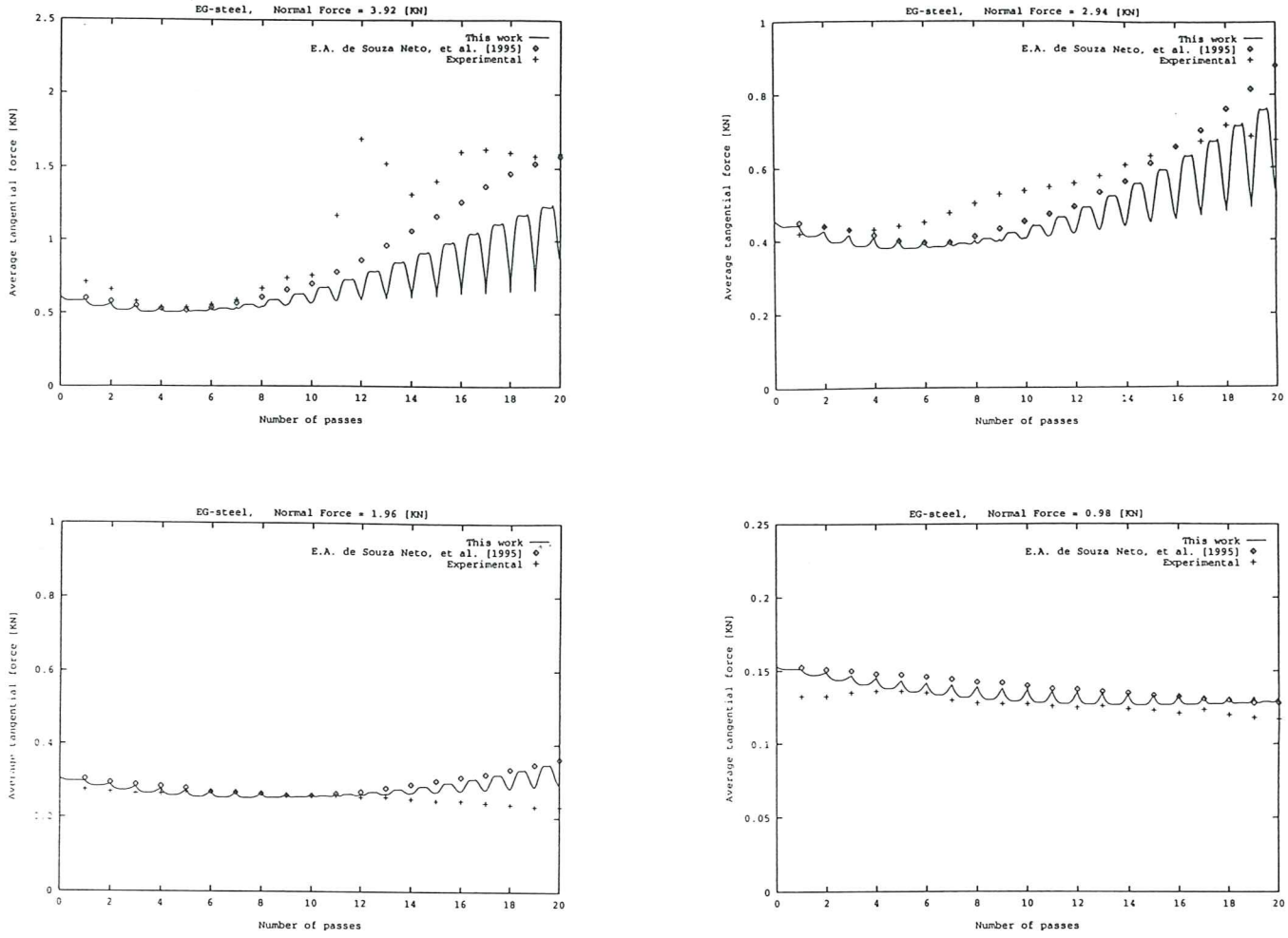

FIGURE 5.7. Flat Sheet Sliding tests. Tangential force versus number of passes during the sliding tests using a EG steel sheet at different constant normal forces: (a) Normal force = 3.92 KN; (b) Normal force = 2.94 KN; (c) Normal force = 1.96 KN; (d) Normal force = 0.98 KN.

the end of each pass, where the distribution of the friction coefficient is not uniform. A detail of the wear profile in the sheet is depicted in FIGURE 5.8, for the GA steel and for a normal force of 0.98 KN. The figure clearly shows an evenly worn region in the central part of the sheet, between 12.5 and 22.5 mm from the left edge, while the wear at the edges is not uniform.

In FIGURES 5.6 and 5.7, it is clearly evident the different wear evolution experimented by the GA and EG steel sheets. For the GA steel, due to the softening of the friction coefficient law, the tangential force presents a local minimum within a pass at the central part of the sheet, in the evenly worn region. In contrast, for the EG steel, particularly for high normal pressures, the tangential force at the central part of the sheet moves from a local minimum towards a local maximum within a pass, according to the frictional softening/hardening behavior. Remarkably, a significant hardening is observed for the EG

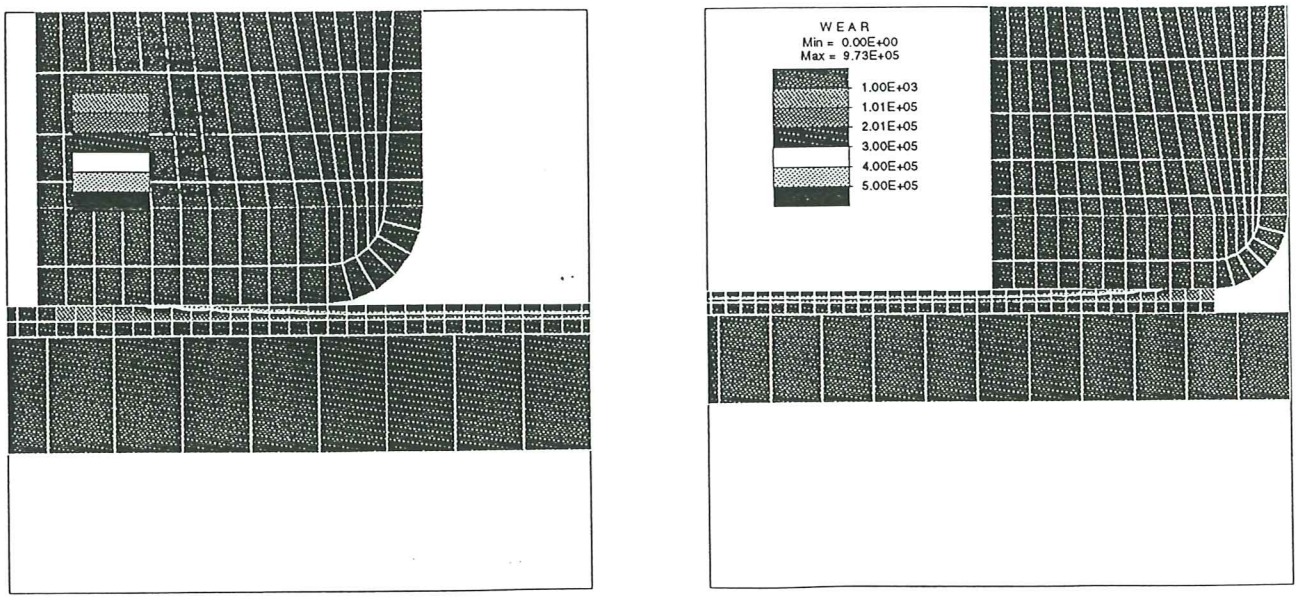

FIGURE 5.8. Flat Sheet Sliding tests. Wear profiles at the GA steel sheet for a normal force of 0.98 KN.

steel at high normal pressures, while a slight softening appears at low normal pressures. These results clearly show that a classical frictional Coulomb law, using a constant friction coefficient, would not be able to capture this behavior, leading to useless inaccurate predictions.

The tangential forces predicted by the numerical analyses, for both GA and EG steel sheets and for all levels of constant normal force, agree well with the experimental and numerical (average) results given by DE SOUZA NETO *et al.* [1995].

6. Concluding Remarks.

Wear related phenomena have an important impact on the economy of industrial metal forming processes. Wear is the dominant die failure mechanism for both bulk and sheet forming operations. The inclusion of wear phenomena model into available decision support systems used in industrial design and optimization practice, would improve die design and service life considerably, leading to an important reduction of manufacturing costs.

Adhesive and abrasive wear have been identified as the main wear mechanisms. Archard's wear law provides an estimate of both wear mechanisms arising in metal forming operations.

Clearly, wear affects the frictional conditions between contact surfaces. A frictional wear contact model has been proposed, taking the frictional coefficient as a function of a wear related internal variable, to be chosen as the frictional dissipation or the slip amount. This frictional wear model has been incorporated to a continuum-based multi-body frictional contact formulation at finite strains.

Within the context of the displacement-driven formulation of frictional contact problems, exploiting the computational framework developed for plasticity, two frictional return mapping algorithms have been considered: the BE and the implicit PMP rules. An exact linearization of the algorithms allows to derive the consistent frictional contact tangent operator.

Numerical simulations shown the suitability of the proposed model to predict wear phenomena in large scale computations. A good agreement has been observed between the numerical results and the experimental ones obtained for the sliding tests. These results, allows to suggest that the adoption of the frictional dissipation as the internal variable associated to the frictional behavior has captured the essential features of the wear phenomena.

Acknowledgement

Support for this work was provided by the European Commission through the BRITE-EURAM Project no. BE-5248-92, under contract no. BRE2-CT92-0180. This support is gratefully acknowledged.

References

AGELET DE SARACIBAR, C. [1995], "A New Frictional Time Integration Algorithm for Multi-Body Large Slip Frictional Contact Problems", submitted to *Computer Methods in Applied Mechanics and Engineering.*

AGELET DE SARACIBAR, C. [1995], "Numerical Analysis of Frictional Contact Problems", *Lecture notes of Short Course on Computational Techniques for Plasticity*, International Center for Numerical Methods in Engineering, Barcelona, Spain.

ARCHARD, J.F. [1953], "Contact and Rubbing of Flat Surfaces", *Journal of Applied Physics*, **24**, 981-988.

BATHE, K.-J. & A. CHAUDHARY [1985], "A Solution Method for Planar and Axisymmetric Contact Problems", *International Journal for Numerical Methods in Engineering*, **21**, 65-88.

BELYTSCHKO, T. & M.O. NEAL [1991], "Contact-Impact by the Pinball Algorithm with Penalty and Lagrangian Methods", *International Journal for Numerical Methods in Engineering*, to appear.

BENSON, D.J. & J.O. HALLQUIST [1990], "A Single Surface Contact Algorithm for the Post-Buckling Analysis of Shell Structures", *Computer Methods in Applied Mechanics and Engineering*, **78**, 141-163.

CAMPOS, L.T., J.T. ODEN & N. KIKUCHI [1982], "A Numerical Analysis of a Class of Contact Problems with Friction in Elastostatics", *Computer Methods in Applied Mechanics and Engineering*, **34**, 821-845.

CARPENTER, N.J., R.L. TAYLOR & M.G. KATONA [1991], "Lagrange Constraints for Transient Finite Element Surface Contact", *International Journal for Numerical Methods in Engineering*, **32**, 103-128.

CHENG, J.-H. & N. KIKUCHI [1985], "An Analysis of Metal Forming Processes Using Large Deformation Elastic-Plastic Formulations", *Computer Methods in Applied Mechanics and Engineering*, **49**, 71-108.

CIARLET, P.G. [1988], *Mathematical Elasticity. Volume 1: Three-Dimensional Elasticity*, North-Holland, Amsterdam.

CURNIER, A. [1984], "A theory of friction", *International Journal of Solids and Structures*, **20**, 637-647.

CURNIER, A. & P. ALART [1988], "A Generalized Newton Method for Contact Problems with Friction", *Journal de Mecanique Theorique et Appliquee*, supplement no. 1 to **7**, 67-82.

DUVAUT, G. & J.L. LIONS [1972], *Les Inequations en Mecanique et en Physique*, Dunod, Paris.

GALLEGO, F.J. & J.J. ANZA [1989], "A Mixed Finite Element Model for the Elastic Contact Problem", *International Journal for Numerical Methods in Engineering*, **28**, 1249-1264.

GIANNAKOPOULOS, A.E. [1989], "The Return Mapping Method for the Integration of Friction Constitutive Relations", *Computers and Structures*, **32**, 157-167.

HALLQUIST, J.O., G.L. GOUDREAU & D.J. BENSON [1985], "Sliding Interfaces with Contact-Impact in Large-Scale Lagrangian Computations", *Computer Methods in Applied Mechanics and Engineering*, **51**, 107-137.

HUGHES, T.J.R. [1987], *The Finite Element Method: Linear Static and Dynamic Finite Element Analysis*, Prentice-Hall, Englewood Cliffs, NJ.

JU, J.-W. & R.L. TAYLOR [1988], "A Perturbed Lagrangian Formulation for the Finite Element Solution of Nonlinear Frictional Contact Problems", *Journal de Mecanique Theorique et Appliquee*, supplement no. 1 to volume **7**, 1-14.

JU, J.-W., R.L. TAYLOR & L.Y. CHENG [1987], "A Consistent Finite Element Formulation of Nonlinear Frictional Contact Problems", *Proceedings of the International Conference NUMETA'87*, J. Middleton et al., eds., A.A. Balkema, Rotterdam.

KIKUCHI, N. & J.T. ODEN [1988], *Contact Problems in Elasticity: A Study of Variational Inequalities and Finite Element Methods*, SIAM, Philadelphia.

KLARBRING, A. & G. BJÖRKMAN [1992], "Solution of Large Displacement Contact Problems with Friction Using Newton's Method for Generalized Equations", *International Journal for Numerical Methods in Engineering*, **34**, 249-269.

LAURSEN, T.A. [1992], "Formulation and Treatment of Frictional Contact Problems Using Finite Elements", *Ph.D. Dissertation*, Stanford University, Division of Applied Mechanics, Report no. 92-6.

LAURSEN, T.A. & S. GOVINDJEE [1994], "A Note on the Treatment of Frictionless Contact Between Non-smooth Surfaces in Fully Non-linear Problems", *Communications in Applied Numerical Methods*, **10**, 869-878

LAURSEN, T.A. & J.C. SIMO [1991], "On the Formulation and Numerical Treatment of Finite Deformation Frictional Contact Problems", in *Nonlinear Computational Mechanics–State of the Art*, P. Wriggers & W. Wagner, eds., Springer-Verlag, Berlin, pp. 716-736.

LAURSEN, T.A. & J.C. SIMO [1992], "Formulation and Regularization of Frictional Contact Problems for Lagrangian Finite Element Computations", in *Proc. of The Third International Conference on Computational Plasticity: Fundamentals and Applications, COMPLAS III*, D.R.J. Owen, E. Onate & E. Hinton, eds., Pineridge Press, Swansea, pp. 395-407.

LAURSEN, T.A. & J.C. SIMO [1993], "A Continuum-Based Finite Element Formulation for the Implicit Solution of Multi-Body, Large Deformation Frictional Contact Problems", *International Journal for Numerical Methods in Engineering*, **36**, 3451-3485.

LAURSEN, T.A. & J.C. SIMO [1994], "Algorithmic Symmetrization of Coulomb Frictional Problems Using Augmented Lagrangians", *Computer Methods in Applied Mechanics and Engineering*, to appear.

LUENBERGER, D.G. [1984], *Linear and Nonlinear Programming*, Addison-Wesley, Reading, Massachusetts.

MARSDEN, J.E. & T.J.R. HUGHES [1983], *Mathematical Foundations of Elasticity*, Prentice-Hall, Inc., Englewood Cliffs, New Jersey.

ODEN, J.T. & J.A.C. MARTINS [1985], "Models and Computational Methods for Dynamic Friction Phenomena", *Computer Methods in Applied Mechanics and Engineering*, **52**, 527-634.

OWEN, D.R.J., D. PERIĆ, A.J.L. CROOK, E.A. DE SOUZA NETO, J. YU & M. DUTKO [1995], "Advanced Computational Strategies for 3D Large Scale Metal Forming Simulations", *Proceedings of the Fifth International Conference on Numerical Methods in Industrial Forming Processes*, to appear

PAPADOPOULOS, P. & R.L. TAYLOR [1990], "A Mixed Formulation for the Finite Element Solution of Contact Problems", *UCB/SEMM Report*, 90/18, University of California at Berkeley.

PARISCH, H. [1989], "A Consistent Tangent Stiffness Matrix for Three-Dimensional Non-Linear Contact Analysis", *International Journal for Numerical Methods in Engineering*, **28**, 1803-1812.

SIMO, J.C. [1988], "A Framework for Finite Strain Elastoplasticity Based on the Multiplicative Decomposition and Hyperelastic Relations. Part II: Computational Aspects", *Computer Methods in Applied Mechanics and Engineering*, **68**, 1-31.

SIMO, J.C. [1992], "Algorithms for Static and Dynamic Multiplicative Plasticity that Preserve the Classical Return Mapping Schemes of the Infinitesimal Theory", submitted to *Computer Methods in Applied Mechanics and Engineering.*

SIMO, J.C. [1994], "Numerical Analysis Aspects of Plasticity", in *Handbook of Numerical Analysis, Volume IV*, P.G. Ciarlet and J.J. Lions, eds., Nort-Holland.

SIMO, J.C. & T.J.R. HUGHES [1994], "Elastoplasticity and Viscoplasticity: Computational Aspects", to be published by Springer-Verlag, Berlin.

SIMO, J.C. & T.A. LAURSEN [1992], "An Augmented Lagrangian Treatment of Contact Problems Involving Friction", *Computers and Structures*, **42**, 97-116.

SIMO, J.C., P. WRIGGERS, K. SCHWEIZERHOF & R.L. TAYLOR [1986], "Finite Deformation Postbuckling Analysis Involving Inelasticity and Contact Constraints", *International Journal for Numerical Methods in Engineering*, **23**, 779-800.

SIMO, J.C., P. WRIGGERS & R.L. TAYLOR [1985], "A Perturbed Lagrangian Formulation for the Finite Element Solution of Contact Problems", *Computer Methods in Applied Mechanics and Engineering*, **50**, 163-180.

DE SOUZA NETO, K. HASHIMOTO, D. PERIĆ & D.R.J. OWEN [1995], "A Phenomenological Model for Frictional Contact of Coated Steel Sheets Accounting for Wear Effects: Theory, Experiments and Numerical Simulation", *International Journal for Numerical Methods in Engineering*, to appear.

WRIGGERS, P. [1987], "On Consistent Tangent Matrices for Frictional Contact Problems", in *Proceedings of the International Conference NUMETA'87*, J. Middleton et al., eds., A.A. Balkema, Rotterdam.

WRIGGERS, P. & C. MIEHE [1992], "Recent Advances in the Simulation of Thermomechanical Contact Processes", in *Proc. of The Third International Conference on Computational Plasticity: Fundamentals and Applications, COMPLAS III*, D.R.J. Owen, E. Onate & E. Hinton, eds., Pineridge Press, Swansea, pp. 325-347.

WRIGGERS, P. & C. MIEHE [1994], "Contact Constraints within Coupled Thermomechanical Analysis. A Finite Element Model", *Computer Methods in Applied Mechanics and Engineering*, **113**, 301-319.

WRIGGERS, P. & J.C. SIMO [1985], "A Note on Tangent Stiffness for Fully Nonlinear Contact Problems", *Communications in Applied Numerical Methods*, **1**, 199-203.

WRIGGERS, P., J.C. SIMO & R.L. TAYLOR [1985], "Penalty and Augmented Lagrangian Formulations for Contact Problems", *Proceedings of the International Conference NUMETA'85*, J. Middleton& G.N. Pande, eds., A.A. Balkema, Rotterdam.

WRIGGERS, P., T. VU VAN & E. STEIN [1990], "Finite Element Formulation of Large Deformation Impact-Contact Problems with Friction", *Computers and Structures*, **37**, 319-331.

WRIGGERS, P. & G. ZAVARISE [1993], "Application of Augmented Lagrangian Techniques for Non-linear Constitutive Laws in Contact Interface", *Communications in Applied Numerical Methods*, **9**, 815-824.

WRIGGERS, P. & G. ZAVARISE [1993], "Thermomechanical Contact. A Rigorous but Simple Numerical Approach", *Computers and Structures*, **46**, 47-53.

ZIENKIEWICZ, O.C. & R.L. TAYLOR [1991], *The Finite Element Method, 4th ed., Volume 2: Solid and Fluid Mechanics, Dynamics and Non-linearity*, McGraw-Hill, London.

List of Tables

List of Figures